Fall 1-31-2002

Inelastic seismic behavior of stiffening systems : multi-span simply-supported (MSSS) bridges

Alireza Yazdani-Motlagh
New Jersey Institute of Technology

ABSTRACT

INELASTIC SEISMIC BEHAVIOR OF STIFFENING SYSTEMS: MULTI-SPAN SIMPLY-SUPPORTED (MSSS) BRIDGES

by
Alireza Yazdani-Motlagh

Stiffening behavior can result from interaction between a structure (base system) and its surrounding environment as in the MSSS bridge soil-structure interaction. In this study, three MSSS bridge cases are parametrically analyzed and their dynamic characteristics and behavior are presented and discussed. Later, for investigating stiffening behavior, a simplified stiffening model is introduced and an extensive parametric study with more than 367,000 analyzed cases is performed. In the parametric study, different stiffening parameters (i.e., stiffness, strength, gap size, and mass), 41 strong motion records, and several damage criteria are considered and effects of the stiffening parameters variations on the dynamic response of simple stiffening systems are presented. It is shown that on the average the displacement response is lower for stiffening systems, consistent with pushover analysis based on the seismic codes. However, considering many other damage indices like dissipated hysteretic energy and low-cycle fatigue damage index, it is quite likely that a stiffening system would sustain more damage than an elastic-plastic system. At the end, suitable design response spectra for stiffening systems are developed and their practical implications for MSSS bridges are demonstrated.

INELASTIC SEISMIC BEHAVIOR OF STIFFENING SYSTEMS: MULTI-SPAN SIMPLY-SUPPORTED (MSSS) BRIDGES

by
Alireza Yazdani-Motlagh

A Dissertation
Submitted to the Faculty of
New Jersey Institute of Technology
in Partial Fulfillment of the Requirements for the Degree of
Doctor of Philosophy in Civil Engineering

Department of Civil And Environmental Engineering

January 2002

APPROVAL PAGE

INELASTIC SEISMIC BEHAVIOR OF STIFFENING SYSTEMS: MULTI-SPAN SIMPLY-SUPPORTED (MSSS) BRIDGES

Alireza Yazdani-Motlagh

M. Ala Saadeghvaziri, Dissertation Advisor — Date
Professor of Civil and Environmental Engineering
New Jersey Institute of Technology

William R. Spillers, Committee Member — Date
Distinguished Professor of Civil and Environmental Engineering
New Jersey Institute of Technology

C.T. Thomas Hsu, Committee Member — Date
Professor of Civil and Environmental Engineering
New Jersey Institute of Technology

Methi Wecharatana, Committee Member — Date
Professor of Civil and Environmental Engineering
New Jersey Institute of Technology

Bala Sivakumar, Committee Member — Date
Chief Engineer of Lichtenstein Consulting Engineers
Paramus, NJ

Ali M. Memari, Committee Member — Date
Assistant Professor of Architectural Engineering
The Pennsylvania State University

BIOGRAPHICAL SKETCH

Author: Alireza Yazdani-Motlagh

Degree: Doctor of Philosophy

Date: January 2002

Undergraduate and Graduate Education:

- Doctor of Philosophy in Civil Engineering,
  New Jersey Institute of Technology, Newark, NJ, 2002

- Master of Science in Structural Engineering,
  Sharif Institute of Technology, Tehran, Iran, 1994

- Bachelor of Science in Civil Engineering,
  Polytechnic University, Tehran, Iran, 1991

Major: Civil Engineering

Presentations and Publications:

Yazdani Motlagh, Alireza, M. Ala Saadeghvaziri, "Nonlinear Seismic Response of Stiffening SDOF Systems," Engineering Structures, The Journal of Earthquake, Wind and Ocean engineering, Vol. 23, No. 10, Oct. 2001

Saadeghvaziri, M. Ala, Alireza Yazdani-Motlagh, and Saeid Rashidi, "Effects of Soil-Structure Interaction on Longitudinal Seismic Response of MSSS Bridges," Soil Dynamics and Earthquake Engineering, Vol. 20, No. 1-4, pp. 231-242, Dec., 2000.

Memari, A. M., A. Yazdani Motlagh, and A. Scanlon, "Seismic Evaluation of an Existing Reinforced Concrete Framed Tube Building based on Inelastic Dynamic Analysis," Engineering Structures Journal, Engineering Structures, Vol. 22, Feb. 1999.

Memari, A. M., A. Yazdani Motlagh, M. Akhtari, A. Scanlon, and M. Ghafory Ashtiany, "Seismic Vulnerability Evaluation of a 32 Story Reinforced Concrete Building," Structural Engineering & Mechanics Journal., Vol. 7, No. 1, pp. 1-18, Jan. 1999.

DEDICATION

To my beloved family

ACKNOWLEDGMENT

I would like to express my most sincere gratitude to Dr. M. Ala Saadeghvaziri, my dissertation advisor, for his guidance, technical advice and supervision. I also appreciate the guidance provided by my committee members; Professors William R. Spillers, C.T. Thomas Hsu, Methi Wecharatana, Ali M. Memari, and Engineer Bala Sivakumar.

I thank the New Jersey Department of Transportation / FHWA and the National Center for Transportation and Industrial Productivity (NCTIP) at NJIT for their financial support provided for this study.

TABLE OF CONTENTS

TABLE OF CONTENTS
(Continued)

TABLE OF CONTENTS
(Continued)

Chapter **Page**

LIST OF TABLES

LIST OF FIGURES

LIST OF FIGURES
(Continued)

Appendix Figures **Page**

LIST OF FIGURES
(Continued)

Appendix Figures **Page**

LIST OF FIGURES
(Continued)

Appendix Figures **Page**

LIST OF FIGURES
(Continued)

Appendix Figures **Page**

CHAPTER 1

INTRODUCTION

This study evaluates inelastic earthquake response of stiffening systems resembling Multi-Span Simply-Supported (MSSS) bridges. In this work, the concepts of simple stiffening system models and MSSS bridges are combined in order to obtain and develop practical seismic analysis procedures for MSSS bridges while revealing general dynamic characteristics of simple stiffening systems.

In general, a stiffening system is a system that its stiffness increases as it goes under large displacements. Unlike the linear and bilinear systems, stiffening systems are not sufficiently studied, and the lack of information about their nonlinear behavior under dynamic loads hinder a practicing engineer to reliably predict the accurate responses using routine and simplified pseudo-static methods [Yazdani and Saadeghvaziri, 2001]. One of the most important structures that behaves in stiffening fashion is the Multi-Span Simply-Supported (MSSS) bridge. A typical MSSS bridge has several simply supported decks that rest on intermediate pier bents and two end abutments. In such bridge, decks are separated from each other and from end abutments by gap sizes in range of 25-77 mm (1"-3"). Stiffening behavior for MSSS bridges, is the result of gap closure (especially the gap closure between abutments and pier bents) causing pier bents to gain more stiffness.

MSSS bridges, especially in eastern part of the United States, have primarily been designed for gravity loads, and now that earthquake loads are main design and retrofitting concerns, determining accurate dynamic responses and behaviors of MSSS bridges have gained particular attention [Mander *et al.*, 1992]. Bridge specifications for seismic design and retrofitting [AASHTO, 1996; CALTRANS, 1989; FHWA, 1995] have simplified

pseudo-static methods applicable to MSSS bridges. These methods acknowledge the possibility of the gap closure among different bridge components that changes the dynamic characteristics of the system. The recently favored and meanwhile more involved method for analyzing MSSS bridges is pushover analysis. In this method, which is also called Capacity-Demand analysis [Chopra and Goal, 1999], the demand and capacity curves are drawn in force-displacement coordinates. The crossing point of these two curves determines the displacement demand. In this regard, the main deficiency in current codes lies in using linear design response spectra for analyzing MSSS bridges when responding in stiffening fashion. This consequently, compromises the accuracy and reliability of the results obtained.

In evaluating current design procedures, one might also use the relatively new concept of performance-based design, which looks beyond displacements and forces as the only design criteria [Krawinkler, 1995]. A performance-based design involves a set of methods by which a structure is designed in a controlled way such that its desirable behavior under earthquake loads is ensured at predefined performance levels. The performance behavior of the structure is controlled by limiting the levels of damage to structural and nonstructural components under increasing loads. In this regard, damage can be associated with various response parameters such as energy and low cycle fatigue rather than just displacements and forces. Therefore besides displacement, several other response parameters useful in the bridge performance-based design [Hose *et al.*, 1999] have to be considered for investigating stiffening systems and comparing them to the simple bilinear systems.

1.1 Background

Previous works in modeling and investigating MSSS bridges under earthquake loads have shown different aspects and characteristics of these bridges. Impact (collision-like) between different components (i.e., pier bents and abutments), soil-structure interaction, and failure and post failure behavior of bearings are among the most important characteristics [Tseng and Penzien, 1973; Chen and Penzien, 1975; Dicleli and Bruneau, 1995].

In determining the dynamic behavior of bridges, time history analysis using a finite element (FE) model has been the main tool to conduct analytical studies [Zimmerman and Brittain, 1979; and Chen and Penzien, 1975]. However, this approach is not practical for use by engineers in day-to-day designs. Furthermore, due to computational limitations only a few number of major actual earthquakes or synthesized records are used in analysis, compromising extend of the general conclusions drawn for a particular type of bridge or a behavior aspect.

Bridge seismic design specifications and seismic retrofitting manuals [AASHTO, 1996; AASHTO-LRFD, 1998; FHWA, 1995] have introduced simplified pseudo-static methods as an alternative to time history analysis for regular bridges with one dominant mode of vibration. In these simplified methods, linear elastic design response spectra are used in the analysis despite of the fact that MSSS bridges may act in stiffening fashion. For bilinear systems, the use of linear RS may underestimate the calculated responses [Chopra and Rakesh, 2001], and therefore current building seismic rehabilitation and retrofitting manuals [FEMA 273 and 274, 1997; ATC-40, 1996] include the nonlinear behavior and dissipated hysteretic energy in their design response spectra. Considering

the fact that using a representative response spectrum (RS) for nonlinear systems is the accurate way of calculating their responses, there is a need to develop suitable design response spectra for MSSS bridges responding in stiffening fashion.

For developing a design RS, simplified models (e.g., mass-spring systems) are used in determining the overal response characteristics of regular structural systems without compromising the accuracy of the results. For this, an MSSS bridge in longitudinal direction can be viewed as several single-degree-of-freedom (SDOF) systems that interact and pound to each other [Pantelides and Ma, 1998; Maragakis *et al*, 1991]. A simple model based on this view, which is referred to as simple stiffening system [Yazdani and Saadeghvaziri, 2001] has several stiffening parameters including base hysteretic curves for pier bents and abutments' back-fill soil, gap sizes between different components, lumped masses, and damping.

Considering the possible range of stiffening parameters for the MSSS bridges, a comprehensive parametric study will lead to development of appropriate design response spectra for the bridges [Kim *et al.*, 2000; Maragakis *et al.*, 1998]. The ranges considered are reflective of different bridge configurations and soil properties. Furthermore inherent in any measurement, determining some of the parameters may involve uncertainties that require range of values to be considered for the parameters. For example, the soil properties and the mobilized soil masses at the abutments are affected by various soil and weather conditions in different times of the year, introducing a range for the parameters.

Besides displacement, there are several different response parameters that measure degree of damage to a particular structural system [Hose *et al.*, 1999; McCabe and Hall, 1989; Zahra and Hall, 1982; Chai *et al.* 1995]. Calibration of these response parameters

to different performance levels is one of the major experimental bridge research areas [Hose *et al.*, 1999]. The following list includes several response parameters that are used in damage assessment of bridges and are useful in evaluation of stiffening systems for this study; dissipated hysteretic energy, low cycle fatigue damage index, curvature ductility factor, residual deformation index, equivalent viscous damping ratio, and normalized effective stiffness.

1.2 Objectives and Scope

In summary, the following steps need to be followed to fulfill the research needs regarding stiffening systems and MSSS bridges.

1) Perform a case study of existing MSSS bridges in order to:

   - Investigate the earthquake response characteristics of MSSS bridges through nonlinear time history analysis and parametric study.

   - Evaluate the current pseudo-static methods introduced for analysis of MSSS bridges.

2) Develop a simple stiffening system that includes important dynamic characteristics of MSSS bridges.

3) Develop an efficient and accurate solution scheme to perform time history analysis suitable and customized for the simple stiffening systems. The analysis will be carried out by a computer program (preferably written in an Object Oriented language like C++), which has to model the impact between different components and use a variable time-step scheme.

4) Select response parameters that are useful in performance-based seismic engineering of MSSS bridges and implement their calculations into the time history analysis program.
5) Perform an extensive parametric study using a large number of major earthquake records, and develop response databases for bilinear and simple stiffening systems in order to investigate and compare their seismic responses.
6) Develop design response spectra for Stiffening Single-Degree-Of-Freedom (S-SDOF) systems that can be used in the pseudo-static analysis of MSSS bridges.

CHAPTER 2

MSSS BRIDGES: CASE STUDY

A commonly used type of bridge in the eastern United States, including New Jersey, is Multi-Span-Simply-Supported (MSSS) system. Figure 2-1 shows the plan and elevation of a typical MSSS bridge. As is seen in the figure, in an MSSS bridge each span is simply supported with separation gaps between the adjacent spans and between the end spans and the abutments. The gap size is normally in the range of 25 to 76 mm (1 – 3 inches). Framing consists of slab-on-girder deck supported on pier bents (normally multi-columns) and seat-type abutments.

Bridge columns in New Jersey are normally circular or square in cross section. The lateral reinforcement is different for circular and square columns. Generally, abutments are seat-type supported on footings, although some are supported on piles. Steel bearings (fixed and expansion) are normally used as a means of load transfer from the superstructure to the substructure. Thus, in addition to well-defined seismic deficiencies in some bridges, such as small seat width, inadequate transverse reinforcement in the columns/piers, and soil liquefaction hazard reported during past earthquakes around the world, there are other important sources of possible damage in the event of an earthquake for MSSS bridges. These are related to steel bearings, impact between adjacent spans and between the end-span and the abutment, soil-structure interaction (especially at the abutments), and frictional characteristics following bearing failure.

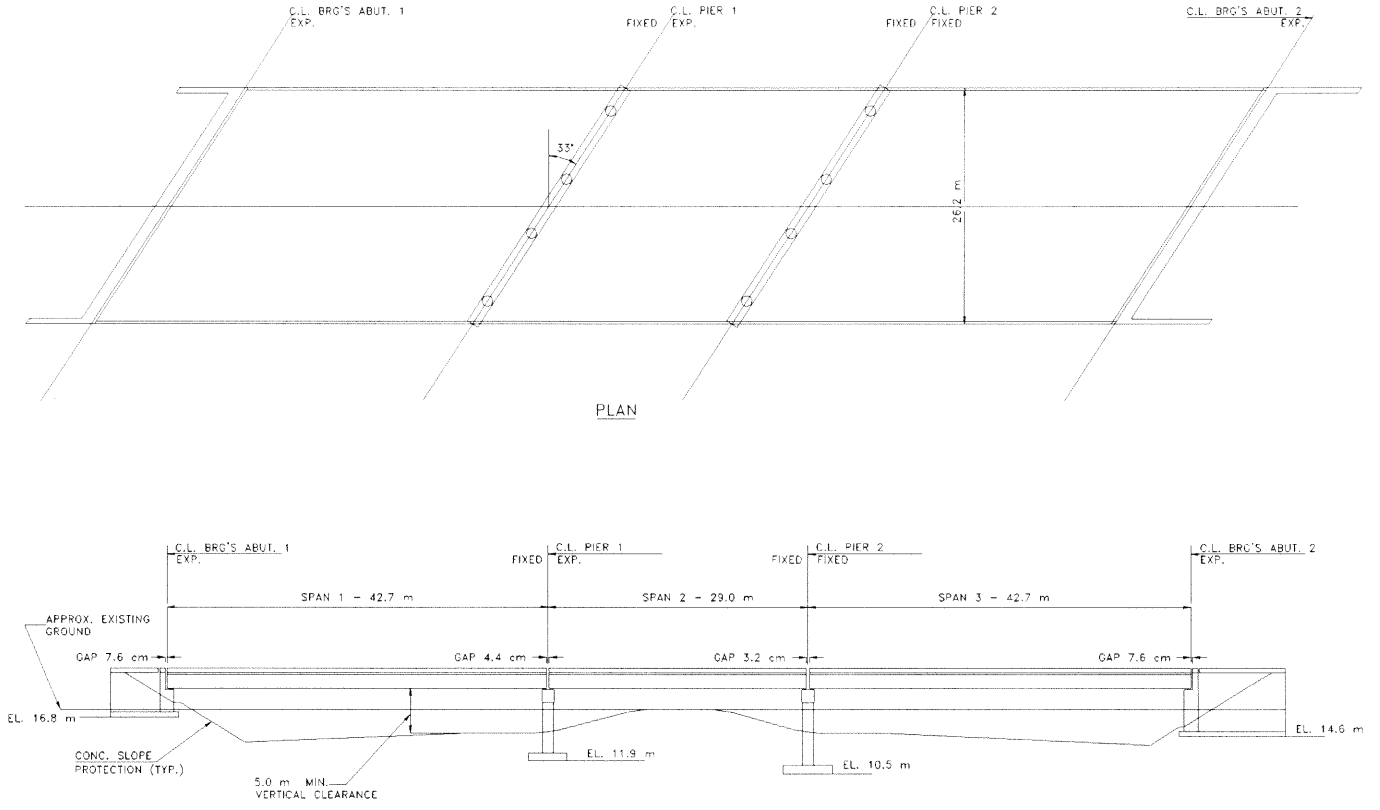

Figure 2-1 Plan and Longitudinal Elevation of a Typical MSSS Bridge (Bridge #1)

The frictional characteristics of failed bearings are important because even under low level of ground motion the impact forces can, at least theoretically, cause failure of the bearings in the form of shear failure at the anchor bolts and/or at the connection bolts between the girder and the bearing top sole plate. Therefore, post-bearing failure response of the bridge system should be considered using models representing Coulomb friction. An equally important factor in the seismic response of MSSS bridges is the possibility of abutment backwall failure due to impact forces.

Due to concerns about the possibility of a damaging earthquake in the central and eastern states, the 1988 NEHRP maps have placed many areas including New Jersey into higher seismic risk categories. Consequently, based on AASHTO (1996) seismic design guidelines, which adopted the NEHRP maps, the acceleration coefficient for northern New Jersey has increased to 0.18, and for the southern coastal areas to 0.1. Thus, the entire state is classified as seismic performance category (SPC) B. In addition to consideration of seismic load in the design of new bridges, the New Jersey Department of Transportation (NJDOT) also adopted the Seismic Retrofitting Manual for Highway Bridges [FHWA, 1995] for seismic assessment and rehabilitation of existing bridges. Furthermore, as part of its seismic retrofit and design efforts, NJDOT sponsored a research program to investigate the seismic response of MSSS bridges considering their unique behavioral characteristics. General issues related to seismic design and retrofit of MSSS bridges along with results of analyses on the effect of steel bearings on seismic performance of MSSS bridges, including detailed finite element analysis of critical components, have been reported by Saadeghvaziri and Rashidi (1997, 1998).

This section presents the results of a comprehensive nonlinear time history analysis of three actual bridges quantified through detailed capacity / demand ratios for key elements, and discusses design and modeling issues as well as the research needs related to MSSS bridges (Details of the work presented in this section can be found in Saadeghvaziri and Yazdani-Motlagh, 1999). It is shown that MSSS bridges respond is stiffening fashion and for implementing an accurate pseudo-static analysis method there is a need to develop design response spectra for stiffening systems.

2.1 Description of the Bridges

Three simple span and simply supported bridges, representative of typical bridges in New Jersey, are evaluated under this study. For these bridges, the number of spans varies and is equal to two, three and four. They are reinforced concrete bridges with concrete slab-on-girder decks. The gap sizes between adjacent decks or end spans and abutments vary from 25 to 76 mm (1 to 3 inches). Pier columns and abutments have spread footings without piles. The pier columns are all circular with spiral or circular lateral reinforcements. The level of concrete confinement varies for each bridge. The lowest confinement belongs to Bridge #1 (3-span bridge) with #3 circular hoops at 305 mm (12") spacing. On the other hand, Bridges # 2 and 3 (2 and 4 span bridges, respectively) both have well confinement details for their pier columns, which consist of spiral reinforcement at small pitch (89 to 57 mm, or in inches 3.5" to 2.25").

Bridge #1 has three spans with lengths of 42.7, 29, and 42.7 m (140', 95', and 140') and with skewness equal to 33°. The width of the bridge is made of two separated symmetric half-decks and has a total width of 26.2 m (86'). Each half-deck has six 1626

mm (64") high girders supporting a 241 mm (9.5″) thick concrete slab. Separate pier bents beneath each half-deck consist of two 1.22 m (4') diameter circular columns and a 1.4 m (4.6') high cap beam.

Bridge # 2 is a straight (only 3° skewness) bridge with two equal spans of 29.7 m (97'-4"). Each deck has 15 girders with 1143 mm (45") in height supporting a 222 mm (8.75″) thick concrete slab. The deck cross section has two unequal parts, namely, part 1A (with 9 girders) and part 1B (with 6 girders), and it has a total width equal to 34.1 m (112 feet). Correspondingly, the pier bent consists of two parts with a total of 10 circular columns with a diameter of 0.91 m (3′).

Bridge # 3 has four spans in lengths of 12.8, 39.6, 36.6, and 26.8 m (42', 130', 120' and 88') with skewness equal to 45°. Each deck has 7 girders 2184 mm (86″) apart, supporting a 203 mm (8″) thick concrete slab. Each column bent consists of five 1.07 m (3.5′) diameter circular columns and a 1.37 m (4.5') height cap beam. Since the details of steel girders were not available, typical and estimated dimensions were assumed considering the similarities with the other two bridges. The girder information is needed here for the determination of the total mass, and in light of its relatively small weight compared to that of the deck, the assumed estimated values are adequate. With regard to stiffness, the deck-girder system is very rigid regardless of the exact values for area and moment of inertia for individual elements. The stiffness of the bridge system is controlled by the weaker elements (i.e., columns and abutments).

All three bridges use steel bearings to connect superstructure to the substructure. Typically four 22 mm (7/8") diameter A325 steel bolts are used to connect the bearing to the girder, and two 38 mm (1.5") diameter A615 steel anchor bolts are used to connect

the bearings to the abutments and cap beams. These elements are the weak links in the load transfer from the superstructure to the substructure through the bearings. The edge distance or seat width is in the range of 178 to 254 mm (7 to 10 inches). The detailed information on the bridge geometry and design parameters are discussed by Saadeghvaziri and Yazdani-Motlagh (1999).

2.2 Analytical Modeling

Analysis of MSSS bridges under gravity loads is simple and straightforward and this is indeed the reason behind using this system. Under transverse seismic load for straight bridges, the system can be easily analyzed as a series of independent simply-supported beams with boundary springs. However, the response of MSSS bridges in the longitudinal direction is more complicated because of the potential impact between adjacent spans and soil-structure interaction. If the displacements due to a design earthquake obtained from linear analysis exceed the expansion joint width then a nonlinear dynamic time history analysis that includes impact will be required.

For straight bridges, the important response quantities with respect to longitudinal motion can be captured with a two dimensional (2-D) model. However, for skewed bridges, there is an interaction between the longitudinal and transverse mode shapes and three-dimensional (3-D) models are required. Therefore, in this study both 2-D and 3-D models were employed to perform in-depth analyses of these three bridges. Note that the use of 2-D models is more efficient than performing unidirectional analysis as a special case of the 3-D models.

Special emphasis was placed on detailed parametric studies under the longitudinal earthquake excitation because some studies of the damage to MSSS bridges have shown that seismic waves in this direction have caused more damage than transverse waves [Zimmerman and Brittain, 1979]. Furthermore, under the most likely mode of damage (i.e., bearing failure) the system possesses high degree of redundancy in the transverse direction; however, in the longitudinal direction this may not be the case. Depending on the available seat length and the soil-structure interaction at the abutments the system can fail as a result of span fall-off.

2.2.1 Two Dimensional (2-D) Analytical Model

All three bridges were analyzed using DRAIN-2DX [Prakash *et al.*, 1992]. The 2-D model for Bridge #1 is shown in Figure 2-2. Beam-column element (Type 02) is used to model decks, columns, and cap beams. For the columns, nonlinear behavior is modeled by concentric plastic hinges at the element ends. Plastic hinges are capable of considering P-M interaction curves for steel and reinforced concrete column sections. Bearings, abutment foundation and back-fill soil (with inelastic unloading) and soil springs at the column footings are modeled using simple connection element (Type 04). To model gap and impact between adjacent spans and between an end-span and the abutment the link element (Type 09) is employed.

2.2.2 Three Dimensional (3-D) Analytical Model

DRAIN-3DX [Powell and Campbell, 1994] is used for 3-D nonlinear time history analysis. Only Bridges #1 and #3 are modeled since Bridge #2 is not skewed and no significant coupling of responses in the horizontal and longitudinal directions is expected.

Figure 2-3 shows the 3-D model for Bridge #1. Similar to the 2-D model, simple connection element (Type 04) and compression/tension link element (Type 09) are used to model the bearings, abutments and foundations, and impact. Elastic beam-column element (Type 17) is used to represent the decks, and cap beams. The columns are modeled using fiber hinge beam-column element (Type 08) with P-M hinge option. For both 2-D and 3-D models, 5% Rayleigh's damping is assumed.

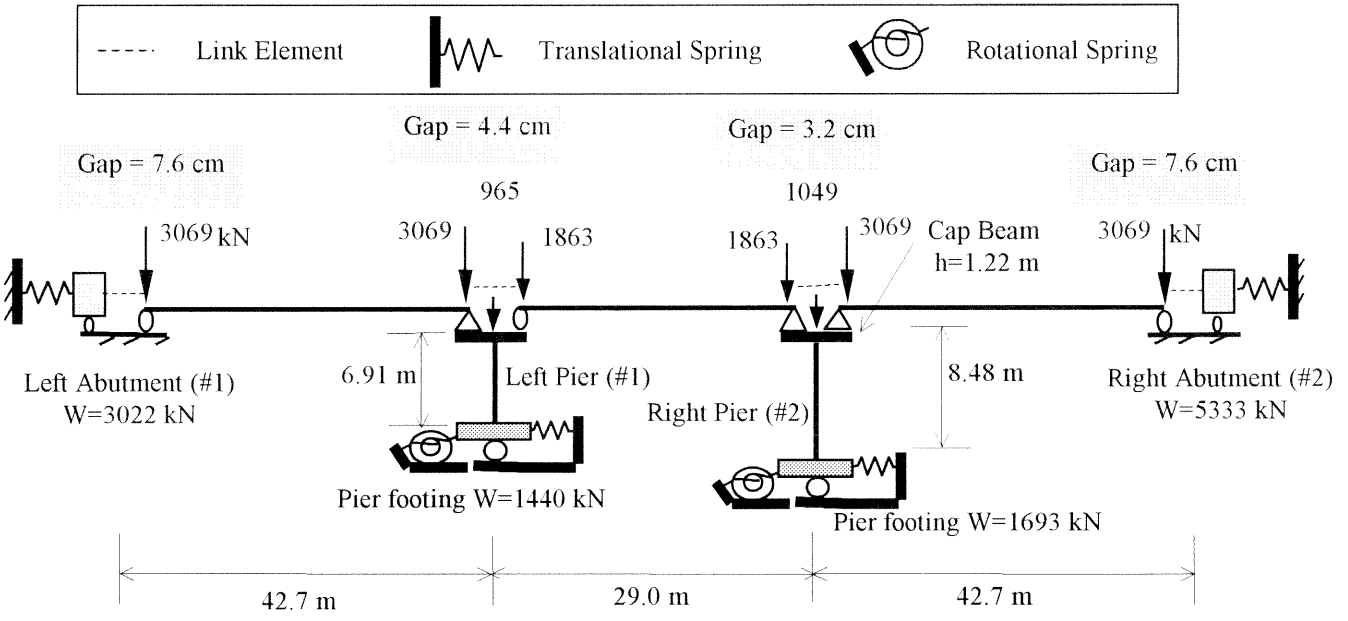

Figure 2-2 A typical 2-D model (Bridge #1 – Concentrated forces are gravity loads)

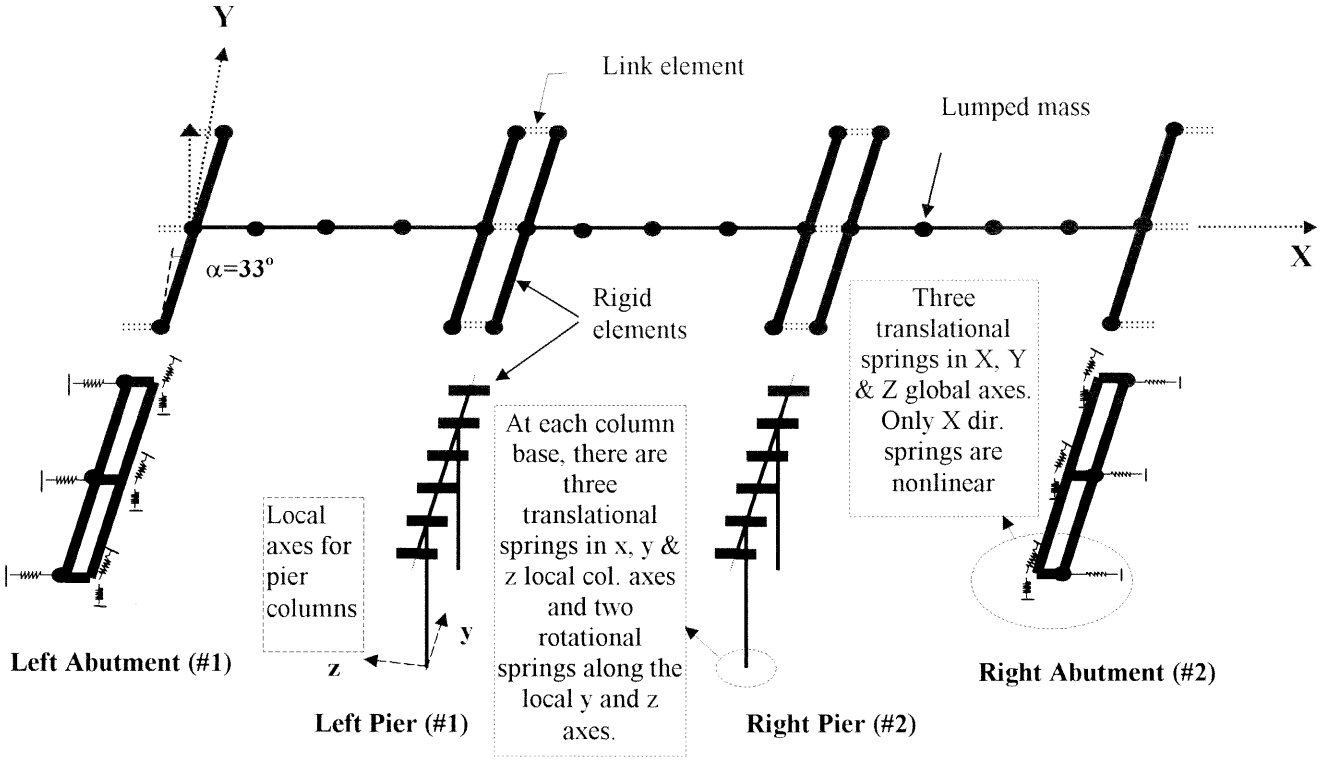

Figure 2-3 A typical 3-D model (Bridge #1)

2.3 Soil-Structure Interaction (SSI) Modeling

The flexibility and strength of supports at piers and abutments are one of the most important parameters on the dynamic response of highway bridges and is well recognized by various organizations like AASHTO and CALTRANS (California Department of Transportation). Many research studies have tried to quantify the stiffness and the strength characteristics of soil-structure interaction in terms of different soil properties. However, the availability of the required properties for a specific site, the preciseness of the measurements involved, and variation of the soil properties even by different seasons are issues that prohibits precise and final quantification of soil-structure interaction. Therefore, it is preferable to select a soil-structure model that includes minimal number of soil properties and to consider a range of values to account for possible property variations [Saadeghvaziri, Yazdani, and Rashidi, 1999].

Here, the procedures given by FHWA's Seismic Design of Highway Bridge Foundations [FHWA, 1986] and Wilson and Tan [Wilson and Tan, 1990] are chosen to define the boundary soil springs at the abutments and at the base of the column piers. These methods are chosen because of their simplicity and having similar parameters in their proposed methods. A brief description of methods for estimating stiffness and strength of soil springs are given below. Detailed documentation is given in a separate report [Saadeghvaziri and Yazdani-Motlagh, 1999].

2.3.1 Footing Soil Spring Stiffness

FHWA's procedures (1986) for rigid footing foundation on a semi-infinite elastic half-space are used to determine translational and rotational stiffnesses for various footings at the abutments and piers foundation. It is reported (FHWA 1986) that for most highway bridges the dynamic effects can be ignored in evaluating the stiffness characteristics of footings. For footings under pier columns and abutments walls, it is assumed that their response is elastic.

The 6 X 6 stiffness matrix, K, for a rigid footing along with the directions of translational degrees of freedom is shown in Figure 2-4. The vertical translation and torsional rotation degrees of freedom are uncoupled from the other degrees of freedom. The two components of translation in the horizontal plane are coupled with the rotational degrees of freedom in this plane resulting in off-diagonal terms. However, the values of these off-diagonal terms are small especially for typical highway bridge where the footings are shallow.

The following general equation is recommended by FHWA (1986) for stiffness matrix, K, of an embedded footing:

$$K = \alpha * \beta * K_0 \tag{1}$$

Where K_0 is the stiffness matrix of an equivalent circular footing bonded to the surface of an elastic half-space, α is the shape correction factor for the foundation, and β is the foundation embedment factor. The stiffness coefficients for various degrees of freedom of matrix K_0 can be determined using the following relationships:

$$\text{Horizontal Translations, } K_{11} \text{ and } K_{22} = 8GR / (2-\nu) \tag{2}$$

$$\text{Vertical Translation, } K_{33} = 4GR / (1-\nu) \tag{3}$$

$$\text{Rocking Rotations, } K_{44} \text{ and } K_{55} = 8GR^3 / 3(1-\nu) \tag{4}$$

$$\text{Torsional Rotation, } K_{66} = 16GR^3 / 3 \tag{5}$$

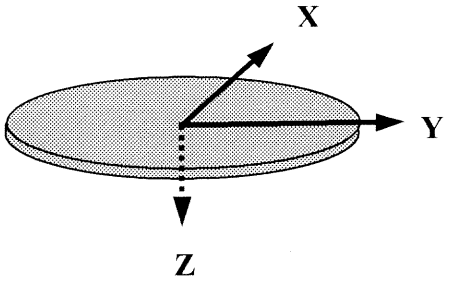

$$\begin{array}{c} \begin{matrix} \delta_X & \delta_Y & \delta_Z & \theta_X & \theta_Y & \theta_Z \end{matrix} \\ \begin{bmatrix} K_{11} & 0 & 0 & 0 & -K_{15} & 0 \\ 0 & K_{22} & 0 & K_{24} & 0 & 0 \\ 0 & 0 & K_{33} & 0 & 0 & 0 \\ 0 & K_{42} & 0 & K_{44} & 0 & 0 \\ -K_{51} & 0 & 0 & 0 & K_{55} & 0 \\ 0 & 0 & 0 & 0 & 0 & K_{66} \end{bmatrix} \end{array}$$

Figure 2-4 Stiffness Matrix of an Equivalent Circular Footing (K_o)

In these equations, G and ν are the shear modulus and Poisson's ratio for the elastic half-space, respectively. R is the radius of circular footings. The application of these equations to rectangular footings involves two steps. First the radius of an equivalent circular footing must be determined as shown in Figure 2-5. The next step requires determination of the shape factor, α, which depends on aspect ratio (Length, L / Width, B) and mode of displacement. FHWA (1986) provides graphical representation for this factor in range of 1.0 to 1.2 for typical L/B values between 1.0 and 4.0. Similarly, the

embedment factor, β, for various modes of displacement is graphically presented by FHWA (1986). This factor depends on the embedment ratio, which for typical situations for highway bridges is equal to the ratio of footing depth (D) to footing radius (R). For D/R ratios in the range of 0.0 to 2.5, the β factor for translational degrees of freedom is between 1.0 and 2.75, and for torsional and rotational modes it varies from 1.0 to as high as 8.

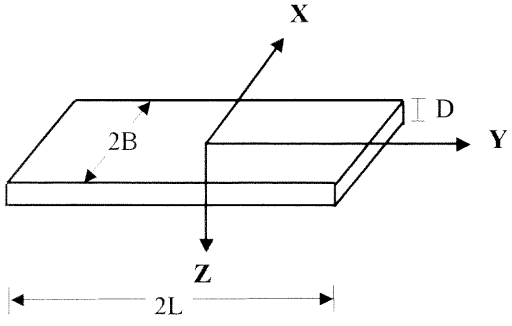

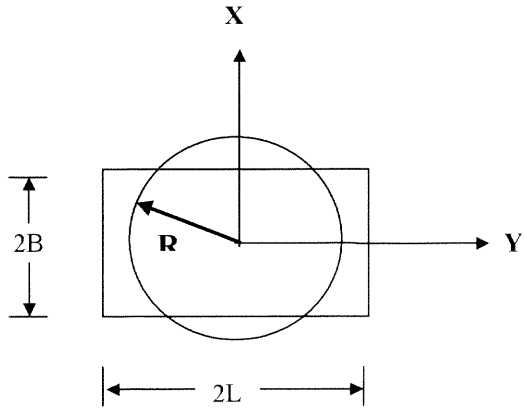

Translation		$R = \sqrt{(4BL)/\pi}$
Rotation:	(X-axis Rocking)	$R = \left[(2B)(2L)^3/(3\pi)\right]^{\frac{1}{4}}$
	(Y-axis Rocking)	$R = \left[(2B)^3(2L)/(3\pi)\right]^{\frac{1}{4}}$
	(Z-axis Torsion)	$R = \left[(4BL)(4B^2 + 4L^2)/(6\pi)\right]^{\frac{1}{4}}$

Figure 2-5 Equivalent Radius for Rectangular Footings

For the bridges considered in this study, the α factor is about 1.1, and the β factor in translational degrees of freedom is about 1.1, and in rotational/torsional degrees of freedom is about 1.4. At the abutments, the footings for the wing walls and the backwall are continuous, forming a single U-shape foundation. Furthermore, due to skewness of the bridge the footings are also skewed. In order to use the FHWA's procedure, the U-shaped skewed footings at the abutments are divided into equivalent rectangular segments and the above procedure is then applied to the individual segment.

2.3.2 Abutment Wall Soil Spring Stiffness

In determining abutment wall-backfill stiffness, the FHWA's procedure (1987) considers the soil pressure and displacement distribution when the wall is displaced (pushed) into the backfill by longitudinal seismic force from the bridge deck. It is assumed that the abutment wall is always in contact with back fill soil and always contributes to overall abutment stiffness. Employing the appropriate pressure diagrams for translational and rotational cases, the resultant stiffnesses for longitudinal translational and rotational (tilting) modes can be obtained using the following equations:

$$\text{Translational stiffness (longitudinal)}, K_w = 0.425 * E_s * B \quad (6)$$

$$\text{Rotational stiffness}, K_{Rw} = 0.072 * E_s * B * H^2 \quad (7)$$

Where E_s is the young's modulus of soil that is equal to $2*(1+\nu_{soil})* G_s$, ν_{soil} is Poisson ratio of soil, which is assumed to be equal to 0.4, G_s is shear modulus of soil, B is width of the abutment wall, and H is height of the wall. These two springs, which their stiffnesses are calculated using Equations (6) and (7), will be located at 0.37 of the height of the wall above the base of the wall.

2.3.3 Abutments in Transverse and Vertical Direction

Elastic and linear transverse and vertical translational springs were calculated based on the methodology presented by John C. Wilson (1990). Note that FHWA does not provide any guidelines in regard to the transverse and vertical directions. Based on Wilson's method, transverse and vertical stiffnesses are dependent on soil embankment dimensions and soil elastic and shear modulus. Following are the equations that were used for this purpose.

Transverse stiffness of the soil embankment for unit length,

$$k_t = \frac{2SG_S}{Ln\left(1+2S\frac{H}{W}\right)} \tag{8}$$

Vertical stiffness of the soil embankment for unit length,

$$k_{vt} = \frac{2SE_S}{Ln\left(1+2S\frac{H}{W}\right)} \tag{9}$$

Where S is the side slope of the embankment soil, W is the top width of the embankment soil, and H is the height of the embankment soil. Figure 2-6 shows the dimensions of a typical embankment used in above equations. Here, the length (L) of the embankment soil was assumed to be equal to the abutment's wing wall length.

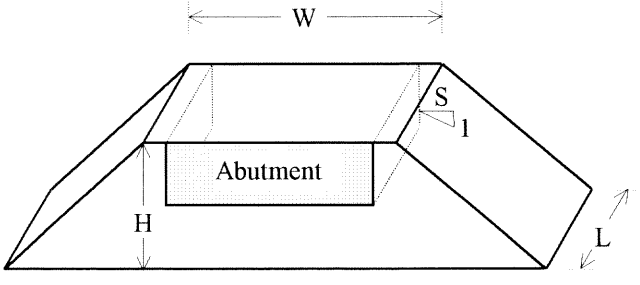

Figure 2-6 Abutment Embankment Dimensions

2.3.4 Abutment Strength

It is assumed that abutment behavior in transverse and vertical directions is elastic. A bilinear load-deformation is assumed for the translational springs in the bridge longitudinal direction. For this spring, the non-linearity includes yielding with unequal strengths under compressive and tensile loads. Under compressive load, the established Mononobe-Okabe pseudo-static approach for passive force is employed to determine the yield strength in compression. Under the assumptions of full mobilization of soil strength, cohesionless back-fill soil, and lack of liquefaction, the suggested formula for compressive yield force, C_y, is [FHWA, 1986]:

$$C_y = (\tfrac{1}{2}) * \gamma * H^2 * (1 - K_v) * K_{PE} * B$$

$$K_{PE} = \frac{\cos^2(\phi - \theta + \beta)}{\cos\theta * \cos^2\beta * \cos(\delta - \beta + \theta) * \left[1 - \sqrt{\frac{\sin(\phi - \delta) * \sin(\phi - \theta + i)}{\cos(\delta - \beta + \theta) * \cos(i - \beta)}}\right]^2} \quad (10)$$

where,

H = height of backfill soil (here, from bottom of back wall footing)

B = Abutment width

γ = Unit weight of soil, here 19.6 kN/m^3 (0.125 kip/ft^3)

ϕ = Angle of friction of soil, here 20° for Gs= 2.76 Mpa and 27.6 Mpa (i.e., 0.4 and 4 ksi), and 45° for Gs=276 Mpa (i.e., 40 ksi)

θ = Arc tan [k_h / (1 - k_v)]

δ = Angle of friction between soil and abutment, assumed equal to (ϕ / 2)

k_h = Horizontal acceleration coefficient; for New Jersey this is 0.18

k_v = Vertical acceleration coefficient, here this is ignored.

i = Backfill slope angle, here zero.

β = Slop of soil face, here zero.

Tensile yield strength at the abutment, T_y, is assumed to be equal to frictional sliding capacity. That is:

$$T_y = N * \tan \delta \tag{11}$$

where, δ is the frictional angle between abutment footing and foundation soil and is assumed to be equal to $\phi/2$. N is the total normal force at the interface, which is equal to the sum of dead load plus the entire abutment system (wing walls, back wall, footings) including fill soil over footings.

2.3.5 Damaged Abutment

The actual geometry of abutment backwall consists of two segments. One portion that is narrower is the back of the seat, which is slightly longer than the depth of the superstructure and is referred to as the backwall. The second segment, which extends from the seat to the top of the footing, is called the breast wall.

It is quite possible for inertia forces in the longitudinal direction to cause shear failure of the abutment at the juncture of these two segments, normally called backwall failure. It is even recommended (FHWA 1995) in seismic design to use such a mode of damage as a "fuse" since it is much easier to fix the upper portion of the abutment. As a parametric study in this investigation, special attention is devoted to such a highly possible mode of failure. For this purpose, the stiffness of the abutment in the longitudinal direction is determined based on mobilizing only the soil equal to the depth of the superstructure.

Two different load transfer mechanisms control the capacity of a section at the juncture of the backwall and breast wall, namely: i) shear resistance provided by the concrete, and ii) shear friction, which is a post failure behavior and follows the first mode. The strength of the latter mode is actually larger and that is used. In accordance with AASHTO LRFD (1998), the following equation can be used to determine the nominal shear capacity, V_n:

$$V_n = \mu * A_{vf} * F_y \tag{12}$$

Where, μ is frictional coefficient between two sliding surfaces which here assumed to be equal to one for concrete placed against hardened concrete, A_{vf} is the sum of areas of vertical rebars at the juncture, and F_y is yield strength of the rebars.

If time history analysis indicates that this shear capacity is exceeded, the model is modified such that the backwall stiffness and compressive strength corresponds to only the height of the back wall (i.e. total abutment height less breast wall height). The strength of the abutment in tension is also reduced since in tension, the frictional resistance at the juncture of back wall and breast wall is the only resisting force.

2.3.6 Simplified Abutment Soil-Spring Model

The abutment model can be further simplified to an equivalent mass-spring by lumping all the abutment mass to the point of impact between abutment and deck and substituting all springs by an equivalent translational spring at the same impact point. The equivalent spring is calculated by assuming the rigid body movement for the abutment structure. In agreement to this assumption, it is shown by experimental investigation that the abutment

movement is indeed rigid body movement [Maroney, 1994]. Figure 2-7 presents the brief description and steps taken to arrive at the final simplified mass-spring model.

As shown in Figure 2-7 (a) and (b), the rotational and translational stiffness springs from various footings and back wall are moved to the center of stiffness located at height **x** above the base of the footing. The resultant translational stiffness is simply equal to the algebraic sum of all translational stiffnesses, that is:

$$K_T = K_{f1} + K_{f2} + K_w \tag{13}$$

Where, K_{f1} is the stiffness of the backwall footing, K_{f2} is the stiffness of wing wall footings (sum of the two), and K_w is the stiffness of the backwall. The resultant rotational stiffness is equal to:

$$K_R = K_{RW} + K_{R1} + K_{R2} + K_W*(0.37H_w + t_f - x)^2 + (K_{f1} + K_{f2})*x^2 \tag{14}$$

Where K_{RW} is rotational stiffness for the backwall, K_{R1} rotational stiffness for the backwall footing, K_{R2} rotational stiffness for the wing wall footings (sum of the two), H_w is height of the backwall, and t_f is the depth of the footing. x is center of stiffness from the base of the footing and is equal to:

$$x = (K_W / K_T) * (0.37H_w + t_f) \tag{15}$$

Continuing on the assumption of rigid body movement of the abutment, the model of Figure 2-7 (b) is further simplified into an equivalent translational stiffness, K_h, as presented in Figure 2-7 (c) and Equation (16). The mobilized abutment mass is lumped at the point of impact between the deck and abutment forming a simple spring-mass system as shown in Figure 2-7 (c). Note that the point of impact is assumed to be at the centroid of the deck.

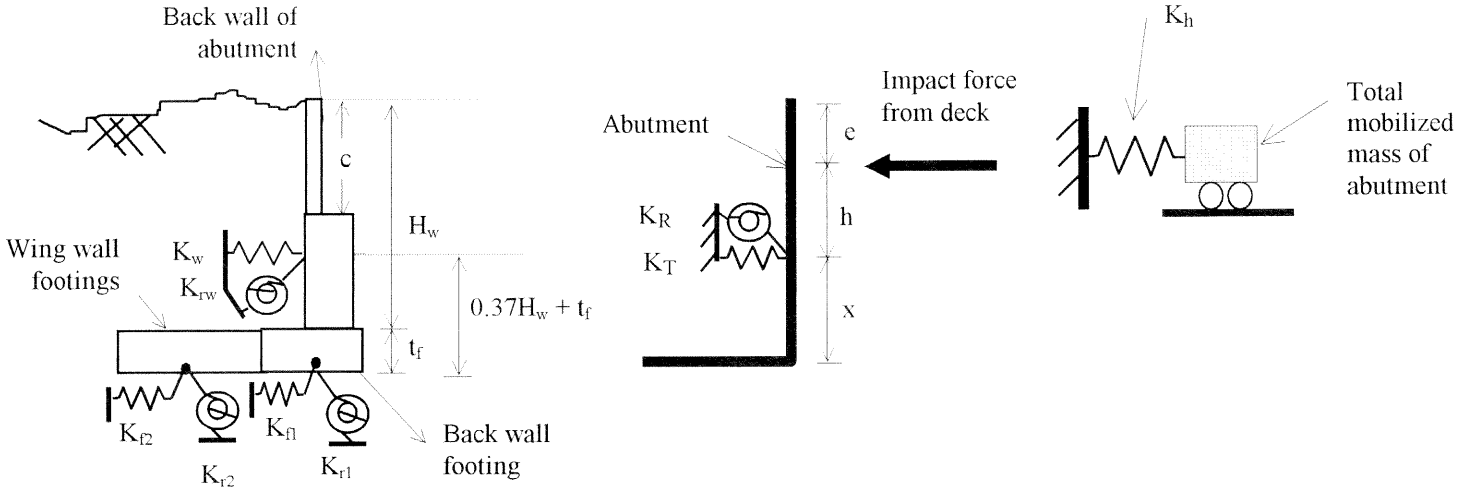

Figure 2-7 Abutment Simplified Modeling in Bridge Longitudinal Direction

$$K_h = (K_R * K_T) / (K_T * h^2 + K_R) \quad (16)$$

As an example, using the above procedure and Equation (16) the final value of translational springs at the abutments for Clements Bridge (Bridge #1) are 47.6G kN/mm (1875G k/in) and 1930G k/in, where G, the shear modulus of soil, is in Mpa (ksi for us units). For a typical value of G = 27.6 Mpa (4 ksi), the abutment longitudinal stiffness is 1330 kN/mm (7,600 k/in). For the same bridge, CALTRANS' simplified procedure (CALTRANS, 1989), which only depends on the width of the bridge, will result in a value of 3009 kN/mm (17,200 k/in). The difference factor of two is consistent with the results reported by Goel and Chopra (1997).

2.4 Property and Capacity Calculations for Various Bridge Components

The values of various parameters for analytical models and for use in capacity/demand evaluation were determined using detailed analyses based on AASHTO LRFD (1998), FHWA Seismic Retrofitting Manual for Highway Bridges (1995), and established principles. For the sake of brevity, only a short description of the procedures employed for critical components is presented here. More detailed information can be found in the original report [Saadeghvaziri and Yazdani-Motlagh, 1999].

2.4.1 Pier Columns

All three bridges analyzed in this study have round columns. The exact moment-curvature relationship and moment-axial load interaction for column cross-sections are determined. This is achieved by dividing the cross-section into a number of fibers and satisfying compatibility and equilibrium using commonly used stress-strain relationships

for concrete and steel. Per FHWA's seismic retrofit guidelines (1995) the ultimate compressive strain of 0.005 is assumed for unconfined concrete, and the equation given based on energy-balance is used to determine the ultimate compressive strain for confined concrete. For this purpose, the ultimate compressive stress for confined concrete is calculated based on the approach proposed by Mander, et al. (1988). The ultimate curvature is reached when concrete strain reaches the ultimate compressive strain or when the moment decreases to 85% of the maximum moment reached on the moment-curvature diagram, whichever happens first.

The effect of column curvature ductility on shear capacity through lateral reinforcement is also considered by using the equation given by the FHWA guidelines (1995). However, the contribution of axial load to shear capacity is ignored to implicitly account for variation in axial load due to frame action in mutli-column bents and for the adverse effect of vertical component of ground motion, which is not considered directly.

The actual moment-curvature relationships along with the equations given by FHWA (1995) for plastic hinge rotation and plastic hinge length are used to determine the plastic rotation capacity. Summary of the calculations is shown in Table 2-1. The column is then modeled using elasto-plastic beam elements with an initial stiffness based on the effective moment of inertia determined using FHWA's seismic retrofit guidelines (1995). The plastic moment capacity is determined by fitting the bilinear model to the actual moment-curvature relationship.

Table 2-1 Basic design parameters along with shear, and flexural capacities for pier columns

Bridge	f'_c (Mpa)	f_y (Mpa)	D (m)	Longitudinal Rebar	Transverse Steel	V_c (kN)	V_s (kN)	M_n (kN-m)	ε_{cu}	ϕ_u (rad/m)	θ_p (rad)
1	20.7	413.7	1.22	#9 (20)	#3 @ 305 mm Circular hoop	422 to 1235	169	3516	0.005	0.022	0.015 to 0.017
2	27.6	413.7	0.91	#10 (16)	#5 @ 89 mm Spiral	276 to 800	1164	2120	0.024	0.177	0.126
3	20.7	275.8	1.07	#11 (9-20)	#4 @ 57 mm Spiral	324 to 942	929	1556 to 2610	0.024	0.157	0.098 to 0.124

Notes:

- Since there are more than one column types for each bridge, some values are shown as a range accounting for such variation. However, for concrete shear contribution the range corresponds to curvature ductility factors of 2 and 4 per FHWA (1995).
- D = Diameter of pier column (m), f'_C=Design compressive strength of concrete (Mpa), f_y=Yield stress limit for steel (Mpa) , M_n=Nominal flexural strength of pier column under gravity load (kN-m), V_C= Shear strength contribution from concrete (kN) , V_S=Shear strength contribution from lateral reinforcement (kN), ε_{CU}=Ultimate compressive strain for confined concrete in pier column, ϕ_U=Ultimate curvature ductility capacity of pier column section (rad/m), θ_P=Plastic rotation capacity of pier column (rad)

2.4.2 Bearings

Typical fixed bearing commonly used in the State of New Jersey is shown in Figure 2-8. It typically consists of a parted metal casing with each part welded to top and bottom steel plates. The top steel plate is connected to the deck steel girder by 4 ϕ 22 mm (7/8") connection bolts and the bottom steel plate is connected to the concrete seat by 2 ϕ 38 mm (1.5") anchor bolts.

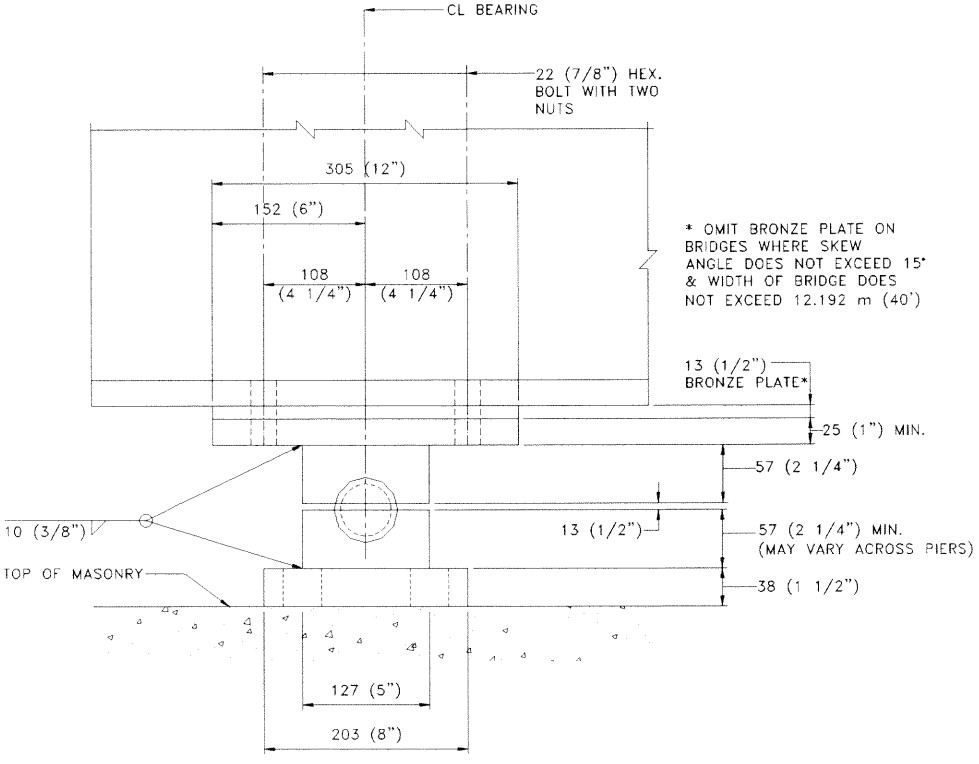

Figure 2-8 A typical fixed bearing

Evaluation of the shear strength of the weld and the shear strength of the connecting bolts indicates that the latter is the weak link in the load transfer from the superstructure to the substructures through the bearing. Based on AASHTO-LRFD (1998), these connection bolts can provide about 444 kN (100 kips) shear capacity for each fixed bearings. Impact forces, under even low level of ground motion, can easily exceed this capacity. This by itself does not constitute bridge failure and the system can function depending on post-failure response. Therefore, post-failure behavior of the bearings is an important factor in proper evaluation of seismic response of MSSS bridges.

Assuming Coulomb friction behavior upon shear failure of the bolts a bilinear force-deformation relationship is used to model the post-failure response. The yield strength is equal to the coefficient of friction times the normal gravity force per bearing. The coefficient of friction is taken to be in the range of 0.2 to 0.6 as a parameter. Relatively large values are assumed for the stiffness of the force-deformation relationship representing Coulomb friction. For roller or expansion bearings, except for the nature of the casings, which have a special configuration to allow free movement of the deck in the longitudinal direction, the details are similar to the fixed bearings. Thus, the modeling allows for free translation in the longitudinal direction and no movement in the transverse direction.

2.4.3 Edge Distance (e)

In case of the shear failure at fixed bearings or excessive movement over roller bearings, one of the important parameters in preventing the deck from falling off of its support is the edge distance "e". Edge distances are measured from the corner of bearing casings to the edge of the support in the bridge longitudinal direction and for considered bridges

ranges from 178 to 2540 mm (7 to 10 inches). This distance can be compared to the deck relative movement to its support and if this relative movement is greater than the edge distance then there is a possibility of falling off the deck.

2.5 Time History Analysis

Using the models described in the previous sections, a large number of time history analyses were performed to evaluate the seismic response through capacity / demand ratios for critical components. The parametric study included three types of soils (reflected in shear modulus of 2.76, 27.6, 276 Mpa), two abutment backwall conditions (intact and damaged), and three bearing conditions (intact, failed with low coefficient of friction of 0.2, and failed with high coefficient of friction of 0.6). Furthermore, the effect of modeling approach (2-D vs. 3-D) on seismic response was also evaluated.

Three different earthquake ground motion records representative of interplate and intraplate earthquakes were used. These records are as follows:

1) Parkfield, California earthquake, Cholame, Shandon, June 27, 1966 (component-1, N65Earray N0. 2, and component-2, N05W array N0. 5)
2) El Centro site Imperial Valley irrigation district, May 18, 1940 (component-1, S00E, and component-2, S90W)
3) Nahanni aftershock, Dec 23, 1985, Canada (one component for 2-D models only; Site-2, Slide Mountain, Component 240).

The records were scaled by peak ground acceleration (PGA) and two different PGAs of 0.18g and 0.4g were employed for the time history analyses. The former is the maximum acceleration coefficient in New Jersey, while the latter is for higher seismicity

regions such as California and can be considered as an event with a longer return period for the state of New Jersey. For the 2-D analyses, the primary horizontal record (strongest based on the original PGA) for each site was used as input. However, for the 3-D analyses two possible alternatives were considered: namely, primary record as longitudinal input and the second horizontal record as transverse input, and the reverse of this. The same PGA is used in orthogonal directions.

2.5.1 Results of 2-D Analysis

Among the three earthquake records used, almost always the Nahanni record (representative of intraplate earthquakes) caused the lowest response in all three bridges, regardless of the level of PGA, soil-structure interaction, and bearing condition. Although a similar observation cannot be made about the other two records (both from California Earthquakes), responses were higher more often for the Parkfield record. For an input motion with PGA of 0.18g, the overall seismic response in the longitudinal direction, using a 2-D model, is marginal with the lowest capacity / demand ratio of 1.04 for the seat length. This is aside from bearing performance, which as it will be discussed can potentially fail under impact forces.

The minimum capacity / demand (C/D) ratios in Bridge #1, which has the poorest performance, subjected to peak ground acceleration of 0.18g in the longitudinal direction are in the range of 1.04 to 7.9. Critical response parameters considered are deck relative displacement (deck sliding), column shear, curvature ductility, and plastic rotation demand. Thus, aside from shear failure in the bearing bolts; the bridge is marginally safe under this level of ground acceleration. Note that the lowest C/D ratio of 1.04 corresponds to the seat length over abutment #2. A C/D of less than unity for the deck

relative displacements will imply fall-off of the span. However, it is for a very soft soil condition that may not represent actual cases and it is taken as an extreme condition.

Longitudinal response of MSSS bridges is complicated by the impact between adjacent spans. In general, impact reduces displacements, but significantly increases the level of the forces in the bearings. Consequently, even under low levels of peak ground acceleration bearing failure and possibly backwall damage are likely.

The level of impact force depends on the soil-type and abutment condition (intact vs. damaged back wall). When the abutment is assumed intact, the impact forces are increasing as the soil stiffness decreases. In the case of damaged backwall, the trend is reversed. For the same soil type, there is less impact force in a damaged backwall case compared to an intact abutment. These variations have to do with the relative value of the abutment stiffness with respect to its mobilized mass. Depending on the values of these two parameters, the amplitude of abutment response will change resulting in different dynamic interaction and impact forces within the bridge-abutment system. This should not be taken as a general trend, but it rather highlights the importance of soil-structure interaction that should be considered in seismic analysis of MSSS bridges. For example, the C/D ratios for the deck relative displacement (deck sliding) at abutment #2 in Bridge #1, ranges from 1.04 to more than 2. The C/D is lower for softer soil and for smaller coefficient of friction at bearings.

Impact forces between two adjacent spans or between an end-span and the abutment are large enough to cause damage to the bridge in the form of bearing bolts shear failure. Results show that failure of the bolts will not necessarily cause large displacement in the deck, which can otherwise cause span fall off. For example, in Bridge

#1 subjected to the Parkfield record with PGA of 0.18g, and with medium soil condition (i.e., shear modulus of 27.6 Mpa) the C/D ratios for the deck relative displacement at abutment #2 are 1.9, 1.8, and 1.6 for intact, bearing with $\mu = 0.6$, and bearing with $\mu = 0.2$, respectively. For the shear force in the pier columns, the trend is even reversed and the C/Ds are higher for bearings with lower coefficient of friction, as discussed under the 3-D results.

It appears that upon failure of the bearings there is a reduction in seismic demands because of period elongation and higher energy dissipation. Thus, failure of the bearing followed by stable Coulomb friction behavior can act like a fuse and limit the seismic response of the bridge system even for higher PGAs. In light of the importance of this phenomenon, further experimental and analytical studies should be conducted to validate such a behavioral characteristic, especially for high bearing where stability is also an issue. Responses of the bridges under a PGA of 0.4g, which could be construed as an earthquake event with much longer return period in New Jersey, are more critical with the possibilities of span fall-off (in the case of weak abutments) and column shear failure. This is further discussed under the 3-D results.

2.5.2 Results of 3-D Analysis

Only Bridges #1 and #3, which are skewed, were also analyzed using 3-D models. As expected, skewness has significant effect on dynamic characteristics and seismic response by causing coupling of responses in two orthogonal horizontal directions. Table 2-2 shows the periods for fundamental modes of Bridge #1 comparing 2-D and 3-D models for medium soil (i.e., G_S equal to 27.6 MPa). Note that for the 3-D model the mode shapes are coupled and the values shown are for the dominant mode shapes in each

direction. As it can be seen from this table, the periods for longitudinal mode shapes are lower when a 3-D model is employed. This is due to stiffening effect of transverse elements on the longitudinal motion. For example, both fixed and roller support act as fixed in the transverse direction. Consequently, due to skewness there is a restraining effect on the longitudinal movement due to fixity in the transverse direction.

Table 2-2 Comparison of fundamental periods (Bridge #1, G_S=27.6 Mpa)

Model	Longitudinal (sec)		Transverse (sec)
	Pier #1	Pier #2	
3-D	1.10	1.67	0.52
2-D (Longitudinal)	1.40	2.26	N/A

Similarly, due to framing action the column bents are much stiffer in the transverse direction, which has an effect on longitudinal response. For the same reason, a 3-D model provides a better representation of the axial forces in the columns, which vary due to frame action even under longitudinal motion. Variation in the axial load affects the plastic hinge behavior of the columns.

The effect of abutment backwall failure on the displacements in the longitudinal direction is less significant in the case of 3-D model because of higher contribution of the column bents to longitudinal stiffness. Finally, due to a more distributed representation of the mass and stiffness of various components, the impact is smoother and the levels of impact forces appear to be more realistic. For example, using the 2-D model for Bridge #1 (for a typical case) the impact forces are equal to zero and 103,545 kN (23,300 kips) at abutments 1 and 2, respectively. However, based on the 3-D model for the same case, the

impact forces in the longitudinal direction are equal to 15,994, and 33,374 kN (3,599, and 7,510 kips) at abutments 1 and 2, respectively. Similar pattern is observed for other cases (i.e., different earthquake record, soil-type, etc.) and for Bridge #3.

Skewness and low concrete lateral confinement of the pier columns are among the seismically undesirable characteristics of Bridge #1. However, under the PGA of 0.18g, it has C/D ratios larger than 1.0 for most cases. As shown in Table 2-3, the only condition that leads to pier column shear failure is a model with elastic bearings (i.e., intact bearings). In an actual situation, as discussed, most likely the fixed bearings will fail under impact forces, even at a PGA as low as 0.18g. This will cause isolation of the superstructure and provide dissipation of energy through Coulomb friction, which in turn limits the bridge response and the shear demands in the columns. Figure 2-9 shows the time histories of the resultant shear force demand in right pier columns of Bridge #1 considering both cases of elastic bearings and failed bearings where post-failure behavior is defined by Coulomb friction with μ =0.6. It can be seen that the maximum shear force demand for pier columns is higher in the case of elastic (intact) bearings than the case of failed bearing. Thus, considering the C/D ratios for shear (Table 2-3), for medium soil (i.e., G_S = 27.6 MPa) the directional C/D ratios have increased from 0.4 to 1.3 in the transverse direction (i.e., y-y axis for shear) and from 1.3 to 2.5 in the longitudinal direction (i.e., z-z axis for shear).

Similarly, the plastic rotation demands decrease significantly for failed bearings. This can be seen in Table 2-3 where plastic rotation demands have reduced to almost zero when Coulomb friction was considered at the bearings. Thus, assuming stable post-failure behavior at the bearings over the pier bents, their failure can act like a fuse

limiting the seismic response of the bridge and preventing brittle failure. However, this is an important assumption and should be verified through further studies.

To investigate the effect of higher ground motion acceleration many cases were analyzed with PGA of 0.4g. The summary of the minimum C/D ratios for both Bridge #1 and 3 are shown in Table 2-4 and Table 2-5, where it can be seen that the columns' shear demands for various conditions greatly exceed the shear capacities (i.e., C/D lower than unity). Unlike, the case of 0.18g, here column shear failure occurs regardless of the bearing condition (i.e., intact or failed).

It should be noted that Bridge #1 has the poorest response under both levels of peak ground acceleration because of low confinement of the columns. Bridge #3 performs well under the PGA of 0.18g because of better column confinement. However, under 0.4g PGA shear failure of pier columns are possible if the shear capacities are reduced for curvature ductility demand larger than 2 (FHWA, 1995).

Most column shear failures occur for medium soil since for very stiff soil restraining effect of the abutments is enhanced resulting in lower displacement and, therefore, lower force demands on pier bents. For very soft soils, the rotational restraining at the base of the pier columns is decreased resulting in more flexible pier bents, which in turn causes larger displacements but less curvature ductility and shear demands in the columns. Thus, it is a balance between these factors that determines the worst situation, which reflects the importance of consideration to the soil-structure interaction.

Table 2-3 The minimum C/D ratios for Bridge #1 under PGA of 0.18g (3-D Model)

G_S (Mpa)	Directional C/D ratios		
	Pier column shear C/D ratios in column local axes (y-y, z-z)	Column plastic rotation C/D ratios about column local axes (y-y, z-z)	Deck sliding C/D ratios in bridge longitudinal direction
2.76	(0.8,1.3) Failure Case: EL, Elastic bearing (2.0,3.3) for μ =0.6 No shear failure when bearing failure is followed by Coulomb-friction behavior	(1.3,1.3) Case: EL, Elastic bearing Almost zero demand when bearing failure is followed by Coulomb-friction behavior	1.1 Case: PF, Elastic bearing
27.6	(0.4,1.3) Failure Case: PF, Elastic bearing (1.3,2.5) for μ =0.6 No shear failure when bearing failure is followed by Coulomb-friction behavior	(2.5,1.3) Case: PF, Elastic bearing Almost zero demand when bearing failure is followed by Coulomb-friction behavior	1.6 Case: PF, μ = 0.6
276	(0.4,1.7) Failure Case: EL, Elastic bearing (1.3,2.5) for μ =0.6 No shear failure when bearing failure is followed by Coulomb-friction behavior	(1.4,1.4) Case: EL, Elastic bearing Almost zero demand when bearing failure is followed by Coulomb-friction behavior	1.8 Case: PF, μ = 0.2

Notes:

- In the above table, failure is determined by C/D ratios less than one for either one direction or the resultant of two directions.
- PF=Parkfield earthquake record, EL=El Centro earthquake record
- μ=Coulomb frictional coefficient at failed bearing, G_S=Soil shear modulus (Mpa)

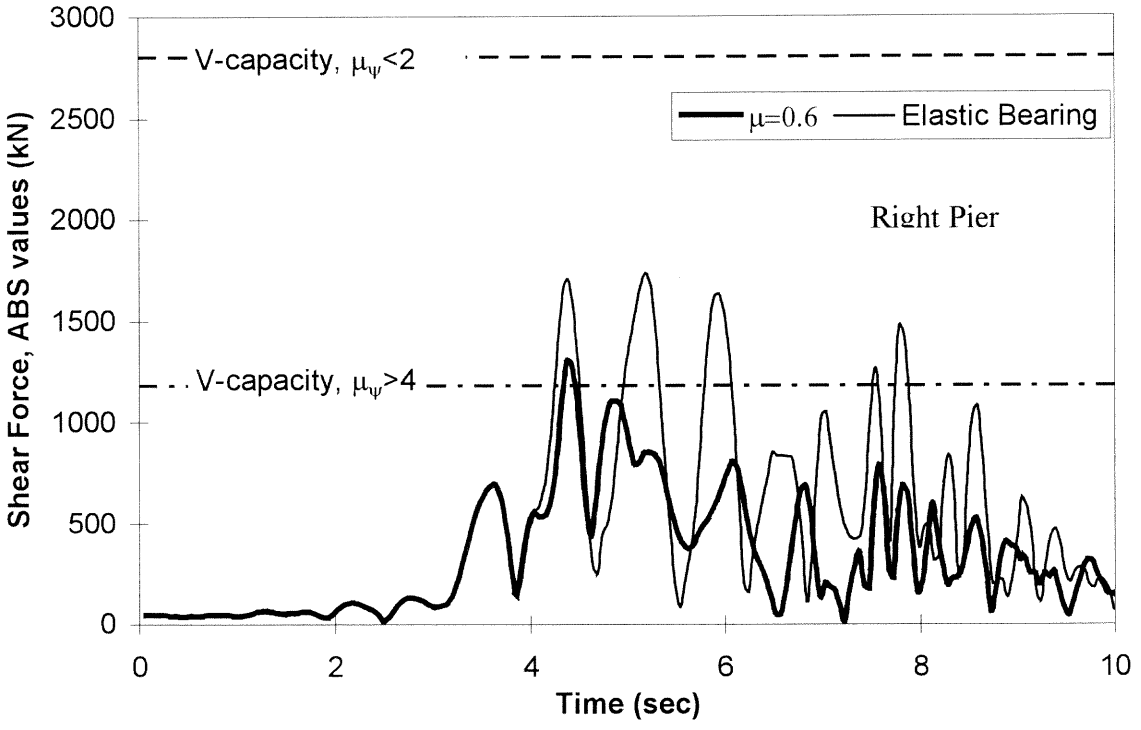

Figure 2-9 Time Histories of Resultant Shear Force at the Right Pier in Bridge #1 (3-D model, PGA=0.18g, Parkfield record, and G_S = 27.6 MPa)

For Bridge #3 under the PGA of 0.4g, unlike Bridge #1, for most cases the maximum response occurs for the case of bearings with smaller Coulomb frictional coefficient, as it can be seen by comparing Table 2-4 and Table 2-5. This is due to the fact that bridge #3 has fixed bearings over the right abutment, which results in higher contribution of the abutment in limiting the response of the pier columns. Thus, bearing failure decreases the restraining effect of the right abutment on the rest of the bridge causing more displacements and forces in the pier bents. Furthermore, the lower the coefficient of friction the higher will be pier columns responses for bridges with fixed bearing over the abutment. Therefore, the general statement about failed bearing acting like a fuse should be recast as: bearing failure "over pier bents" acts like a fuse in reducing the pier bents shear forces and plastic rotation demands.

Table 2-4 The minimum C/D ratios for Bridge #1 under PGA of 0.4g (3-D Model)

G_S (Mpa)	Directional C/D ratios		
	Pier column shear C/D ratios in column local axes (y-y, z-z)	Column plastic rotation C/D ratios about column local axes (y-y, z-z)	Deck sliding C/D ratios in bridge longitudinal direction
2.76	(0.4,1.0) Failure Case: EL, Elastic bearing (0.4,0.9) Failure Case: EL, $\mu = 0.6$ (0.6,1.3) Failure Case: EL, $\mu = 0.2$	(3.3,0.9) Failure Case: EL, Elastic bearing No plastic rotation failure when bearing failure is followed by Coulomb-friction behavior	1.0 Case: EL, $\mu = 0.2$
27.6	(0.2,0.8) Failure Case: PF, Elastic bearing (0.3,1.1) Failure Case: EL, $\mu = 0.6$ (0.5,0.8) Failure Case: EL, $\mu = 0.2$	(3.3,0.9) Failure Case: PF, Elastic bearing No plastic rotation failure when bearing failure is followed by Coulomb-friction behavior	1.2 Case: EL, $\mu = 0.2$
276	(0.3,1.3) Failure Case: EL, Elastic bearing (0.4,0.8) Failure Case: EL, $\mu = 0.6$ (0.5,1.0) Failure Case: EL, $\mu = 0.2$	(5.0,0.8) Failure Case: EL, Elastic bearing No plastic rotation failure when bearing failure is followed by Coulomb-friction behavior	1.3 Case: EL, $\mu = 0.2$ & 0.6

Notes:

- In the above table, failure is determined by C/D ratios less than one for either one direction or the resultant of two directions.
- PF=Parkfield earthquake record, EL=El Centro earthquake record
- μ=Coulomb frictional coefficient at failed bearing, G_S=Soil shear modulus (Mpa)

Table 2-5 The minimum C/D ratios for Bridge #3 under PGA of 0.4g (3-D Model)

G_S (Mpa)	Directional C/D ratios		
	Pier column shear C/D ratios in column local axes (y-y, z-z)	Column plastic rotation C/D ratios about column local axes (y-y, z-z)	Deck sliding C/D ratios in bridge longitudinal direction
2.76	(1.7,2.0) Case: EL, Elastic bearing (1.1,1.4) Failure Case: EL, μ = 0.6 (0.83,1.0) Failure Case: EL, μ = 0.2	(5,5) Case: EL, μ=0.2 ~(10,10) for most cases	1.3 Case: EL, μ = 0.2
27.6	(0.9,1.0) Failure Case: EL, Elastic bearing (1.0,1.1) Failure Case: EL, μ = 0.6 (0.9,0.9) Failure Case: EL, μ = 0.2	(5,10) Case: EL, Elastic bearing ~(10,10) for most cases	1.6 Case: PF, Elastic bearing
276	(1.4,1.7) Case: PF, Elastic bearing (2.0,1.7) Case: EL, μ = 0.6 (1.4,1.3) Failure Case: PF, μ = 0.2	(24.7,10) Case: PF, μ = 0.2 Demand is very small at all cases	2.9 Case: EL, μ = 0.2

Notes:

- In the above table, failure is determined by C/D ratios less than one for either one direction or the resultant of two directions.
- PF=Parkfield earthquake record, EL=El Centro earthquake record
- μ=Coulomb frictional coefficient at failed bearing, G_S=Soil shear modulus (Mpa)

2.6 Pushover Analysis

Based on current seismic design guidelines, two approaches are common in determining the seismic demand in MSSS bridges or continuous bridges with expansion joints in the longitudinal direction. The first approach is to find the range of demands by using elastic tension and compression models. The former assumes that the gaps are all open and each segment of the bridge system is analyzed separately. The latter (compression model) assumes that the gaps are all closed and will remain closed, thus, the entire bridge-abutment system is used to determine the seismic demands. Generally, the tension model gives the upper bound to displacements and the compression model provides the lower bound. For example, for Bridge #1 subject to El Centro record with PGA of 0.4g at the top of Pier-2, the displacement is equal to 279 mm (11") using the tension model and it is equal to 24 mm (0.94") using the compression model.

The second approach is to use an iterative procedure using the effective stiffness of the bridge-abutment system. This procedure will result in more accurate results, however it is more involved. A more recent and efficient method is to use pushover analysis. This is a graphically useful method to compare the demand and capacity. Figure 2-10 shows the results of such an analysis for Bridge #1 based on AASHTO's response spectrum. AASHTO's response spectra for 0.18 and 0.4 g are also plotted for comparison. It is assumed that the stiffness coefficient is equal to load divided by displacement and then, using the weight of the bridge, the response spectrum is transferred from acceleration vs. period space to load vs. displacement. Thus, on this diagram lines radiating from the origin will show systems with different periods (e.g. x-axis is a system with infinite period and y-axis a system with zero period).

The load-deformation for the bridge is obtained by applying an increasing force at the level of the deck in the longitudinal direction. Note that in Figure 2-10 the load-deformation is obtained by pushing span-3 (between right pier and right abutment) to the left. The load-deformation relationship, in general, is highly nonlinear and originally of stiffening nature as the gaps close and other elements of the bridge system get involved. Note that pushover analysis is direction dependent if the gap sizes are not identical at the abutments and at the top of the piers. It also depends on how the two types of connections (fixed or roller) are combined at various locations.

The maximum displacement, in this example, is limited by the sum of the gap openings at the left pier and at the left abutment plus the elastic deformation in the left abutment (i.e., 121 mm plus the elastic deformation in the left abutment). Thus, as it can be seen, the stiffness and strength of the abutments significantly influence the load-deformation behavior of the system.

Comparison of the load-deformation curves indicates that abutment strength would have more effect on the seismic response of the bridge system than abutment stiffness. This point is also supported by the time history analysis results as discussed. Using compression method under PGA of 0.4g, the bridge displacement is about 25 mm (1") and for the tension models of pier-1 and pier-2 the displacements are 185 and 356 mm (7.3" and 14"), respectively.

Shown in Figure 2-10 is also the bridge response using CALTRANS approximate approach, where the maximum strength is based on the maximum soil-strength of 369 kPa (7.7 ksf) and the stiffness is equal to 114.8 kN/mm per unit width of the deck in meter (200 kips/inch per unit width of the deck in foot). Based on CALTRANS approach,

the displacement of the bridge in the longitudinal direction is limited due to high stiffness and strength at the abutment. Actually, using this method there is not much difference in longitudinal deck displacement between the two seismic coefficients (0.18 and 0.4). The abutment deformation is small due to high stiffness and this is the reason for only a very small difference between seismic coefficients of 0.18 and 0.4.

Note that in obtaining the load-deformation curve in Figure 2-10 the pier columns are assumed elastic, thus, the demand and supply are compatible as both are for an elastic system. To advance this approach demand curves that are based on nonlinear behavior of the system needs to be developed. Thus, work on stiffening single degree of freedom systems (S-SDOF) needs to be expanded in order to develop nonlinear response spectrum that can be used along with pushover analysis [Yazdani-Motlagh and Saadeghvaziri, 2001]. A stiffening system consists of an elastic-plastic base system (such as Pier-2 of Bridge #1 and the weight it supports) and the interacting environment (such as the abutments). Such study must consider the effect of various parameters, such as ductility of the base system; size of the gaps; stiffness, strength, and mass of the interacting environment; period of the base system; and ground motion characteristics.

In the next chapter, a simple stiffening model representative of MSSS bridges is developed and based on that an extensive parametric study is performed. The results of the parametric study are helpful to understand the seismic response of S-SDOF systems and to develop an appropriate pseudo-static method for analyzing these types of systems.

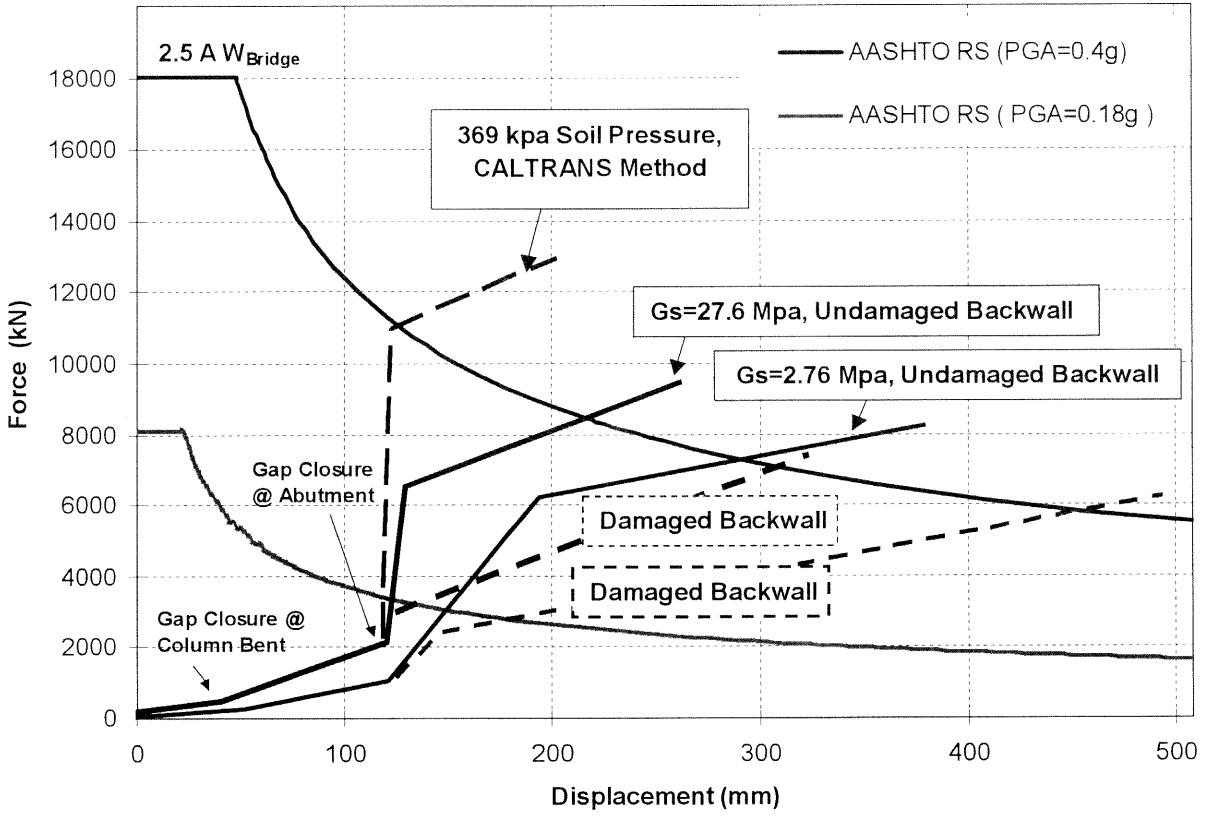

Figure 2-10 Pushover Analysis of Bridge #1 Considering Different SSI Conditions (2-D model)

2.7 Conclusions and Research Needs

Based on the results of this comprehensive analytical study, which included many computer simulations, the following specific conclusions can be made about the seismic response of these three bridges, which are representative of typical east coast MSSS bridges:

- Seismic response of this type of bridge is complicated by the potential impact between adjacent spans. Generally, impact reduces displacements, however it significantly increases the level of forces in the bearings. Due to impact forces bearing failure is quite possible even under low level of peak ground acceleration.

- Seismic response of MSSS bridges is sensitive to soil-structure interaction and it should be considered in dynamic analysis of this class of bridges. Among important parameters (mobilized mass, strength, and stiffness) abutment strength has the most significant effect on the overall response of the bridge.

- Assuming a post-failure behavior at the bearings characterized by stable Coulomb friction, bearing failure over pier bents will act like a fuse and reduces the demand on the pier bents. Should the bearing remain elastic (not fail), shear failure of pier columns with low lateral reinforcement is likely, even under low levels of PGAs.

- For the bridges considered, the seat lengths are only marginally adequate. Therefore, it is important to ensure their integrity through regular inspections.

Furthermore, for more critical bridges or for those with high steel bearings consideration should be given to increasing the seat length.

- Three-dimensional models must be used in nonlinear time history analyses of skewed MSSS bridges to better represent distributed impact and coupling in orthogonal directions and to model the effect of varying axial load on the response of pier columns.

- Under earthquakes with 0.4g PGA, all three MSSS bridges considered would sustain column shear failure that can possibly lead to collapse of the bridge. However, this level of ground acceleration is higher (in many locations much higher) than AASHTO's seismic coefficient for New Jersey. Therefore, earthquakes with this level of accelerations may be considered as an event with significantly higher return period for New Jersey.

One immediate observation by pushover analysis according to AASHTO and FHWA guidelines, as shown schematically in Figure 2-11, is that MSSS bridges (as a stiffening system) always have smaller displacement demands than the corresponding base systems alone. Despite the fact that stiffening systems will undergo smaller displacements, there is no guarantee that they have limited responses under other damage criteria such as dissipated energy and low cycle fatigue.

As bridge engineering move further toward performance based seismic design, it is important to develop realistic response spectra that reflect the actual level of nonlinear behavior. To this end, in order to be able to quantify the effects of soil-structure interaction and impact in a "design" format, consideration should be given to detailed

study of nonlinear systems with stiffening load-deformation characteristics. Thus, there is a need for parametric study of the nonlinear seismic response of stiffening single degree of freedom (S-SDOF) systems in order to develop demand diagrams that can be used in the design of MSSS bridges.

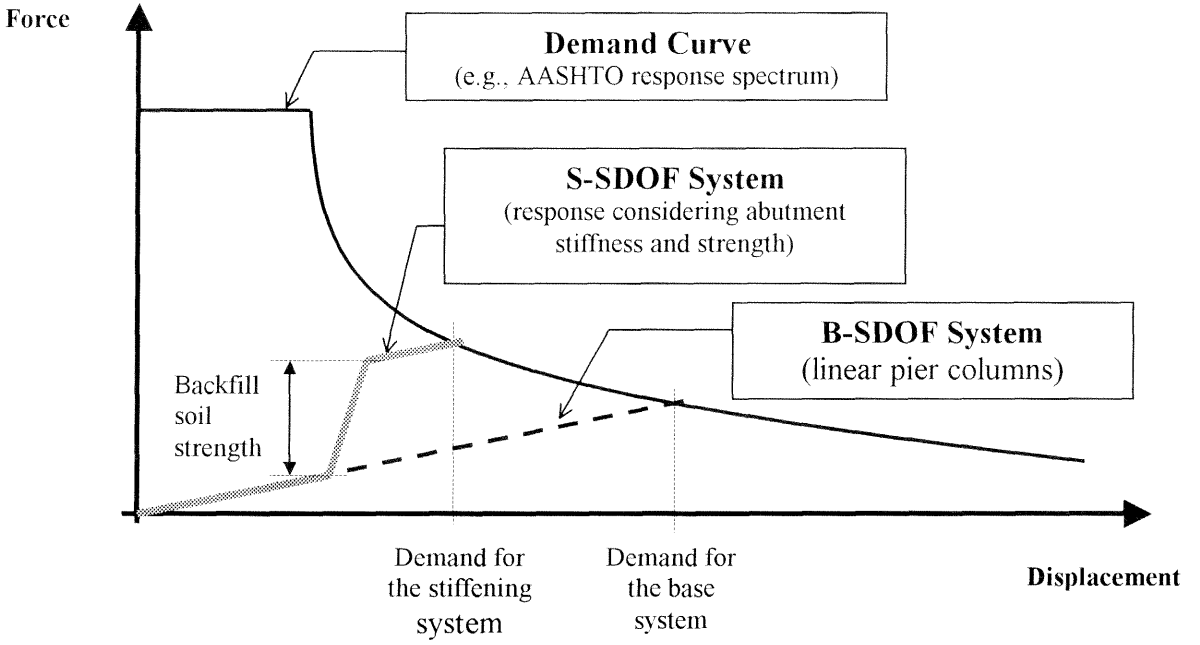

Figure 2-11 Comparison of the Pseudo-Static Analysis Results for B-SDOF and S-SDOF Systems

CHAPTER 3

DEFINITION AND FORMULATION OF SIMPLE STIFFENING SYSTEMS

In general, a stiffening system is a system that its stiffness increases as it goes under large displacements. This can happen as a result of interaction between the structure (base system) and its surrounding environment (e.g., substructure or an adjacent structure). For a typical MSSS bridge, the stiffening behavior is mainly the result of the gap closure between different components especially between end span and the abutment. This can be seen in chapter 2 from Figure 2-1and Figure 2-10 that show the plan and elevation of a 3-span MSSS bridge and its pushover analysis using AASHTO and FHWA guidelines.

As is seen in Figure 2-10, when the right end deck is pushed to the left, toward the left abutment, initially the only elements providing resistance are Pier #2 columns. As the gaps close, the system stiffness and strength increase. This increase is significant after gaps are closed and the left abutment involves in the bridge response. As the abutment is further pushed, the backfill soil yields and in turn the initial gap size between the abutment and the end-span grows. In this analysis, the demand is the crossing point between the load-displacement curve and the demand curve. In Figure 2-10, two demand-curves corresponding to PGA 0.18g and 0.4g, and also several different abutment models (i.e., CALTRANS model, and FHWA models considering Mononobe-Okabe passive yield, damaged and undamaged backwall) and two soil types are considered.

Nonlinear analysis plays a significant role in determining different nonlinear response parameters that are useful in the performance-based seismic engineering [Krawinkler, 1995; Hose *et al.*, 1999]. The exact method of calculating the nonlinear response parameters through a nonlinear dynamic time history analysis is not simple and

suitable for practical purposes, therefore simplified methods, like pushover analysis are more desirable for an engineering office. The pseudo-static methods introduced so far [ATC-40, 1996; FEMA 273, 1997; Chopra and Goel, 1999; Veletsos and Newmark, 1960; AASHTO, 1996; FHWA, 1995 and 1996; CALTRANS, 1989], analyze elastic or bilinear single-degree-of-freedom (SDOF) systems to determine displacement responses. The pseudo-static methods are based on a single response parameter (e.g., displacement ductility) and lack to consider every important aspect of a nonlinear response (e.g., dissipated hysteretic energy and low cycle fatigue), and consequently might lead to an unsafe design [Chai *et al.* 1995; Zahra and Hall, 1982; McCabe *et al.*, 1989]. Furthermore, for multi-span simply-supported (MSSS) bridges behaving in stiffening fashion, only the AASHTO and FHWA specifications provide pseudo-static methods which are based on the design response spectra for elastic linear systems and there is no guidelines which requires specific demand curve for the stiffening behavior.

In this chapter, simple stiffening systems resembling MSSS bridges are defined so they can be used to develop proper stiffening response spectra and to investigate their different response parameters used in performance based seismic engineering. This is done through an extensive parametric study, which considers different yield limits, stiffnesses, gap sizes, strengths, and masses for different components of stiffening systems. For calculating valid and reliable statistical responses (i.e., mean and mean plus one standard deviation), several earthquake records (i.e., 41 records) representative of different soil types were employed in analyzing each stiffening system. In the following sections, the details of the analysis and modeling methods used in the parametric study are described.

3.1 A Simple Model for Stiffening Systems

The seismic response of the various components of a complex MSSS bridge is dominated by the 1st mode response. Therefore, each component can be modeled as a Single-Degree-Of-Freedom (SDOF) system. In the simplest case, there is one base SDOF system (as a pier bent) and two symmetric surrounding interacting components (as two abutments). When the base component is considered alone, separated from the interacting environments (IE), it is referred to as the base SDOF (B-SDOF) system, and when it is considered within the surrounding environment, it is referred to as Stiffening SDOF (S-SDOF) system.

Figure 3-1 presents a simple stiffening system and its components and base bilinear hysteretic curves. The hysteretic curves for different components are bilinear load-displacement curves with typical 1% kinematic strain-hardening. A unit mass is considered for the base system and a 5% mass-proportional viscous damping ratio is assigned for all components.

As is seen in the Figure 3-1, there are several parameters involved in defining a simple stiffening system. These parameters are; initial period (T_0) of both S-SDOF and B-SDOF systems, yield force limit (F_y) of both S-SDOF and B-SDOF components, gap size between S-SDOF and IE components, the yield force limit of the IE components (βF_y), the stiffness of the IE components (αK_0), and the mass ratio of the IE component to the S-SDOF component (**m**). Since unit mass is used for both the B-SDOF and S-SDOF systems, the latter factor (**m**) is also referred to as the mass of the IE components.

Table 3-1 presents the list of parameters and their definitions as well as corresponding values considered in the parametric study. The values selected for all of

these parameters, except for a few cases that are for comparison and interpolation, are within the range of values that can be found in MSSS bridges [Saadeghvaziri and Yazdani Motlagh, 1999].

Seven periods (T_0) and five yield force limits (F_y) are associated with the bilinear base components. The periods selected are between 0.3 and 3.0 seconds, which includes the range for the pier bents in the longitudinal direction of the typical MSSS bridges. In this study, the yield force limit for the B-SDOF component is presented by the R_y factor, which is ratio of the elastic force response obtained from the AASHTO response spectrum to the yield force limit (F_y) of the base component. This factor is similar to the response modification factor (R) that accounts for the nonlinear response of the systems. Referring to the Table 3-1, three selected values of 2, 3 and 5 are equal to the R-factors for pier bent design in the AASHTO specifications. When the R_y is equal to 0.1, the S-SDOF system is an elastic system vis-à-vis load-deformation behavior. However, the response can become nonlinear due to the impact between the base and IE components. The last value for the R_y factor (i.e., 10) is considered for interpolation purposes when systems with very small yield force limits are investigated.

Gap size factor (R_g) is ratio of the elastic displacement response of the base system (using the AASHTO RS) to the gap size. By this definition, larger values indicate smaller gap sizes. Referring to the Table 3-1, four gap size factors are selected in the parametric study. Gap factors equal to 2, 3, and 5 set the gap size equal to the base component's yield displacement when R_y factor is equal to 2, 3, and 5, respectively, and the gap factor of 20 represents almost a closed gap. By knowing the R_g and R_y factors for a particular

stiffening system, it is easy to find out the relative magnitude of the yield displacement and the gap size and the elastic response of the base system from each other.

The strength ratio (β) is equal to the strength of the IE component divided by the B-SDOF or S-SDOF yield force limit (F_y). Considering abutments as IE components with larger yield limits than pier bents, β factor will be grater than one and in some cases depending on the soil condition and geometry of the bridge could be as big as 20. Here four parameter values of 0.5, 3, 5, and 20 were selected for the parametric analysis, in which the value of 0.5 is used for interpolation and comparison purposes.

The stiffness ratio (α) is equal to the initial stiffness of the IE component divided by the initial stiffness of the base component. Very large values (even larger than 100) are expected for this parameter when stiffening analogy is made to the MSSS bridges. From analytical point of view, there is a limit where beyond that, increasing α will not affect the S-SDOF responses. In this study, the values considered are 0.5 (for interpolation purpose and comparison) 10, 20, and 50. It is determined that larger values for this parameter would not considerablly affect the response of the S-SDOF systems considered.

A unique designation for an S-SDOF system, considering different parameters, can be written as "T_0, R_y, R_g, α, β, **m**". Considering the fact that the designation name includes 7 periods, 5 yield factors, and 4 different values for other parameters, the number of S-SDOF cases has reached to 8960 cases (i.e., 1280 S-SDOF cases for each period). Furthermore, a total of 41 different earthquake records, as will be explained in the following section, were employed. Thus, the total number of S-SDOF cases analyzed reach 367,360 cases.

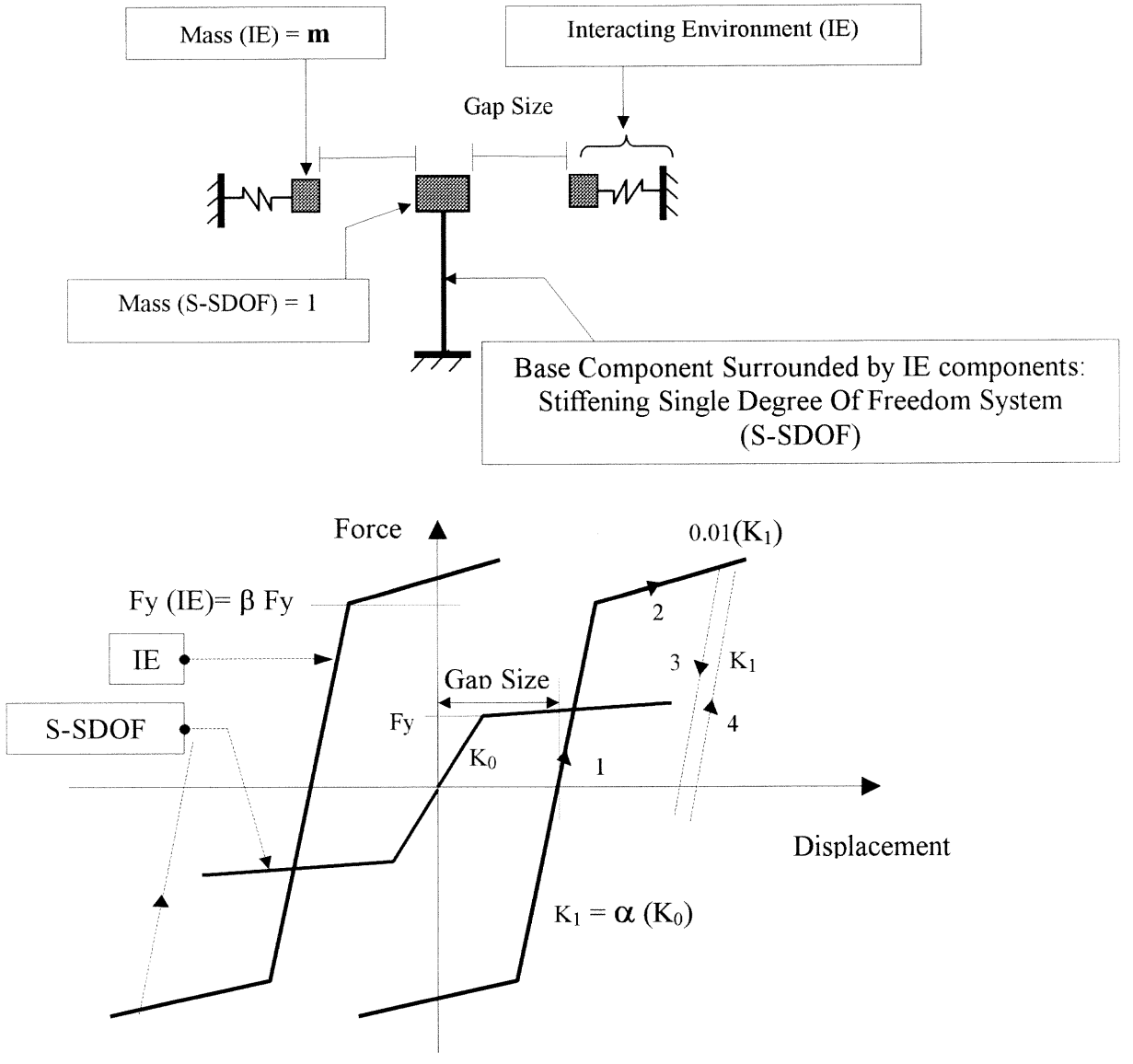

Figure 3-1 The Stiffening-Single-Degree-Of-Freedom (S-SDOF) Component and the Interacting Environments (IE), Defining the Stiffening System

Table 3-1 Definition of the Parameters Associated with Stiffening Systems and Values Considered in the Parametric Study

Parameter	Values	Definition
T_0	0.3, 0.7, 1.0, 1.5, 2.0, 2.5, 3.0	Base System's Period (sec)
Ry	*(0.1)*, 2, 3, 5, *(10)*	Base System Yield Force Factor: F_AASHTO / Fy
Rg	2, 3, 5, 20	Gap Size Factor: d_AASHTO (B-SDOF) / Gap_Size
β	*(0.5)*, 5, 10, 20	Strength Ratio: (IE / B-SDOF)
α	*(0.5)*, 10, 20, 50	Stiffness Ratio: (IE / B-SDOF)
m	0.01, 0.5, 1, 2	Mass Ratio: (IE / B-SDOF)

Note: The value of 0.5 for α and β and the values of 0.1 and 10 for R_y are used for interpolation reasons and are not included in MPOSD calculations.

3.2 Input Ground Motions

Dynamic nonlinear time history analysis (DNTHA) is the most sophisticated and powerful technique for analyzing structural systems that are subjected to the earthquake ground motions. Unlike pseudo-static analysis, DNTHA is a quite versatile procedure and can represent the dynamic characteristics of the system in details and determine any required response parameter. However, based on this method, precise structural modeling and several site-representative ground motions are needed to determine the demand values useful for design purposes. Therefore, as intended in this study, for developing design response spectra and general conclusions for S-SDOF systems, several strong

motion earthquake records representative of different sites and soil conditions are employed.

Four major selected sites and soil categories are; bed rock and hard rock (S1), sedimentary and conglomerated rock (S2), Soil and Glacial Till (S3), and alluvium and unconsolidated deposits (S4). The selected earthquake records on each soil type are presented in Table 3-2 to Table 3-5. In this study, soil types S1 and S2 are combined and referred to as Rock type and types S3 and S4 are combined and referred to as Soil type.

Earthquake records in these tables are sorted by their magnitude, which varies from 8.1 to 5.3 Richter. Magnitude is a measure of the strength of an earthquake determined by seismographic recordings, often expressed by the Richter scale. Each step on the scale, which is logarithmic, indicates a seismic disturbance with ground motion ten times as large as the previous step. A quake of magnitude 2 is the smallest magnitude normally felt by humans; magnitude 6 or greater events are commonly considered major. Magnitude recordings are independent of the place of observation, and are not typically used to express damage.

For reducing the dispersion of the calculated responses, and reaching to the narrowest possible confidence band, and using lower number of earthquake records, a scaling method in conjunction with the time history analysis is used. Among the proposed scaling procedures, scaling to the peak ground acceleration level, scaling to the average spectral acceleration over a frequency range, and scaling to the spectral acceleration at any given period can be mentioned [Shome *et al*, 1998; Martinez-Rueda, 1998]. It is observed [Shome *et al*, 1998] that the scaling to the spectral acceleration at the fundamental frequency of the system is the most efficient among the alternatives and

does not bias the nonlinear estimates. Consequently in this study, AASHTO design response spectrum (5% damping, PGA of 1g and soil type-I) is used as scaling target at any given period. Figure 3-2 shows the scaled El Centro (S00E) response spectrum, which is scaled to AASHTO spectrum at 1-second period. In this method, unlike scaling to a particular PGA level, the scaling factor is not constant. For example, for the El Centro record, scaling factor ranges from 1.9 to 26.7 for the periods between 0.2 and 10 seconds.

3.3 Solution Procedure and Equation of Motion

For implementing nonlinear time history analysis, an object oriented (OO) computer program in C++ language was developed specifically for the simple stiffening systems. The advantage of an OO program is to separate different properties and behaviors into different class objects and let them to handle their specific behavior. By this, not only the program would be more readable and understandable, but also would be more manageable in monitoring and debugging.

In a simple stiffening system, different classes per different behavior and element category are defined. For components with bilinear hysteretic load deformation behavior, a class namely BilinearHysteresis is developed. This class mainly has an initial stiffness value, a yield force limit, a post-yield strain hardening, and a concentrated mass. A link element that extends between two nodes and model the impact between the adjacent components is defined in LinkHysteresis class. This class has mainly a gap size and a stiffness value. The stiffness is zero when the gap is open and has a large value when the gap is closed (here, 100 times bigger than the highest stiffness of the connected

components). Assembling different interacting components into a single stiffening system has accomplished by defining a class, namely StiffeningSystem. This class includes two symmetric bilinear IE components (BilinearHysteresis), one base component (BilinearHysteresis) and two link elements (LinkHysteresis) modeling the impact between the base and the surrounding IE elements.

Time history analysis is formulated in a function that has a stiffening system and an input ground motion matrix as its arguments. This function calculates different response parameters and wraps them into an object defined by a class named Response. The Response class, with the help of a member function, prints out the results in a formatted pattern in an output file.

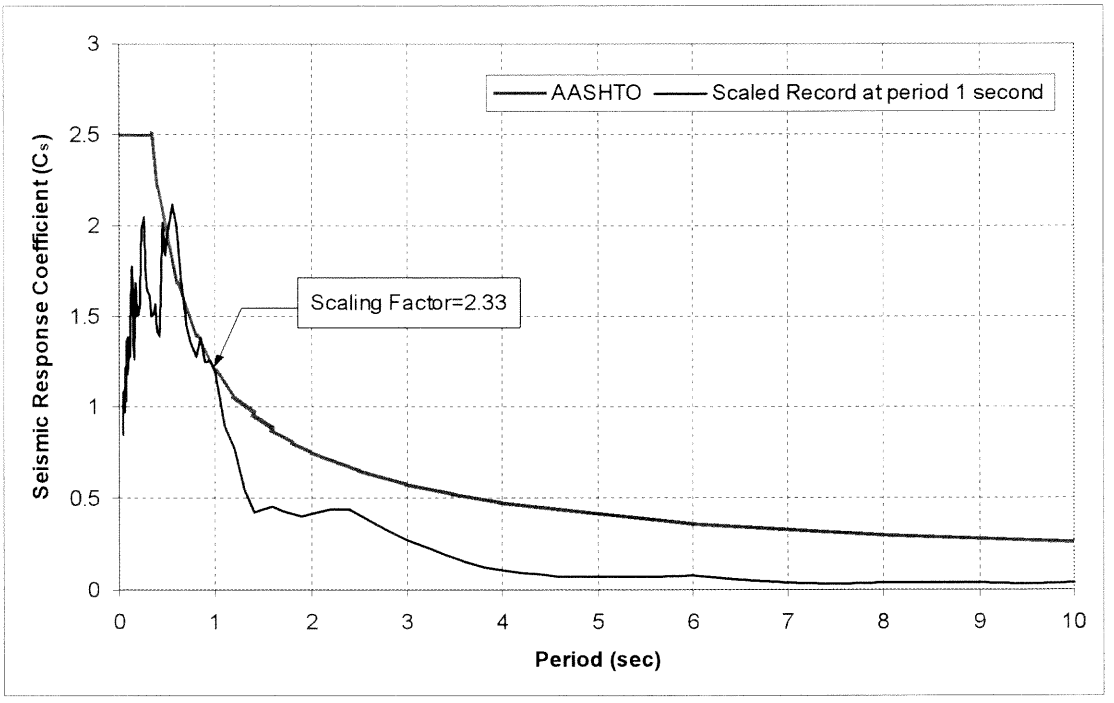

Figure 3-2 El Centro Response Spectrum Scaled at 1-Second Period to the AASHTO Response Spectrum (PGA=1g, Soil Type I)

An implicit time integration scheme, considering the dynamic equilibrium at the time (t+Δt), with Newton-Raphson iteration method is used to determine the responses within the acceptable accuracy. According to these methods, for nonlinear systems, Equation (17) presents the dynamic equilibrium equation in the iterative and incremental format (iteration k at time t+Δt).

$$M\ {}^{(t+\Delta t)}\ddot{U}^{(k)} + C\ {}^{(t+\Delta t)}\dot{U}^{(k)} + {}^{(t+\Delta t)}K^{(k-1)}\ \Delta U^{(k)} = {}^{(t+\Delta t)}R - {}^{(t+\Delta t)}F_s^{(k-1)} \qquad (17)$$

Where U, ΔU, $\dot{U}$, and $\ddot{U}$ are displacement, displacement increment, velocity, and acceleration, respectively. C is the damping coefficient which is equal to $2*\omega*\zeta$ (ω is the natural circular frequency of the system and ζ is the damping coefficient), M is the mass, K is the stiffness, R is the external dynamic force which for an earthquake acceleration record, $g(t)$, is equal to $-M*g(t)$, F_s is the restoring spring resistance force, and the superscript "k" is the iteration number. As is seen in Equation (17), iteration is also done over the stiffness value, $K^{(k-1)}$, which is important for solution convergence in stiffening systems. It should be noted that the elements of the Equation (17) are all matrices referring to the Multi-Degree-Of-Freedom (MDOF) systems.

Step-by-step (or incremental) solution of simultaneous differential equations, as in Equation (17) for MDOF systems, is done by converting the differential system to a set of algebraic equations. This is done by assuming a variation pattern for the acceleration within a short increment of time (Δt) in order to obtain simple relationships between displacement, velocity, and acceleration increments. For the implicit time integration solution, two acceleration variations, namely; constant average acceleration, and linear acceleration, are commonly employed. The linear acceleration method gives better

numerical results using any specified time step length in comparison to the constant average method. Furthermore, in the stiffening systems because of the impact between different components, the change in acceleration is very sharp and sudden and in small increments of time the linear variation is a better representation for the real acceleration response. Therefore, for stiffening systems, linear acceleration method was used for the step-by-step time integration.

With using the linear acceleration method in an iterative solution scheme, velocity and acceleration at time (t+Δt) can be expressed in terms of displacement according to Equations (18) and (19):

$$ {}^{(t+\Delta t)}\dot{U}^{(k)} = (3/\Delta t)\left({}^{(t+\Delta t)}U^{(k-1)} + \Delta U^{(k)} - {}^{(t)}U\right) - 2\ {}^{(t)}\dot{U} - (\Delta t/2)\ {}^{(t)}\ddot{U} \tag{18} $$

$$ {}^{(t+\Delta t)}\ddot{U}^{(k)} = \left(6/\Delta t^{2}\right)\left({}^{(t+\Delta t)}U^{(k-1)} + \Delta U^{(k)} - {}^{(t)}U\right) - (6/\Delta t)\ {}^{(t)}\dot{U} - 2\ {}^{(t)}\ddot{U} \tag{19} $$

Substituting (18) and (19) into (17) and rearranging the equation components, a linear and iterative algebraic equation for obtaining the displacement increment, $\Delta U^{(k)}$, is developed:

$$ {}^{(t+\Delta t)}\left(K_{eff}\right)^{(k-1)}\ \Delta U^{(k)} = {}^{(t+\Delta t)}R - {}^{(t+\Delta t)}F_s^{\ (k-1)} - {}^{(t+\Delta t)}F_m^{\ (k-1)} - {}^{(t+\Delta t)}F_c^{\ (k-1)} \tag{20} $$

Where in Equation (20), followings are the expressions for the different terms:

$$ {}^{(t+\Delta t)}U^{(k)} = {}^{(t+\Delta t)}U^{(k-1)} + \Delta U^{(k)} \tag{21} $$

$$ {}^{(t+\Delta t)}\left(K_{eff}\right)^{(k-1)} = M\left(4/\Delta t^{2}\right) + C\left(2/\Delta t\right) + {}^{(t+\Delta t)}K^{(k-1)} \tag{22} $$

$$ {}^{(t+\Delta t)}R = -M\ g(t+\Delta t) \tag{23} $$

$$ {}^{(t+\Delta t)}F_m^{(k-1)} = M\left\{\left(4/\Delta t^2\right)\left({}^{(t+\Delta t)}U^{(k-1)} - {}^{(t)}U\right) - \left(4/\Delta t\right){}^{(t)}\dot{U} - {}^{(t)}\ddot{U}\right\} \tag{24} $$

$$ {}^{(t+\Delta t)}F_c^{(k-1)} = C\left\{\left(2/\Delta t\right)\left({}^{(t+\Delta t)}U^{(k-1)} - {}^{(t)}U\right) - {}^{(t)}\dot{U}\right\} \tag{25} $$

As it was mentioned before, in stiffening systems impact causes sharp variations in the acceleration response. In the time intervals that these acceleration spikes occur, it is crucial for accuracy of the solution, in order to capture the impact, that smaller time steps are used. A constant time step integration scheme might be a solution for these types of problems, if the time step is very small, but consequently will increase the analysis time and reduces the efficiency of the solution. The variable time step is the best way of solving problems involving impact and is also recommended by well-known finite element software packages [Powell and Campbell, 1994]. Time step variation in this study is set between two extreme cases; one percent (0.01) of the smallest period when gaps are open, and 0.005 of the smallest period when gaps are closed. The criteria for determining the variable time step at any instant depend on the gap state (i.e., close or open) and the intensity of the impact force and the rate of change in the acceleration response.

For accuracy of the solution, it is crucial to have adequate convergence criteria that control the number of iterations (k). These criteria can be associated with displacement, force and energy where with appropriate tolerance values they will assure an accurate step-by-step solution. In this study, three criteria described in Equations (26), (27), and (28), are used concurrently to solve equation (20) at each time step.

$$ \text{Displacement Criterion, } \left| \left(\Delta U^{(k)}\right) \Big/ \left(\Delta U^{(1)}\right) \right| < 10^{-4} \tag{26} $$

$$\text{Force Criterion, } \left| \left(R_{eff}^{(k)}\right) \Big/ \left(R_{eff}^{(1)}\right) \right| < 10^{-4} \tag{27}$$

$$\text{Energy Criterion, } \left| \left[\left(\Delta U^{(k)}\right)\left(R_{eff}^{(k)}\right)\right] \Big/ \left[\left(\Delta U^{(1)}\right)\left(R_{eff}^{(1)}\right)\right] \right| < 10^{-6} \tag{28}$$

In Equations (27) and (28), $R_{eff}^{(k)}$ is determined using Equation (29).

$$R_{eff}^{(k)} = {}^{(t+\Delta t)}R - {}^{(t+\Delta t)}F_s^{(k)} - {}^{(t+\Delta t)}F_m^{(k)} - {}^{(t+\Delta t)}F_c^{(k)} \tag{29}$$

The convergence is numerically achieved in a few number of iterations (usually less than three) and smaller tolerance values would not seem to result in any significant improvements in the accuracy of the results. The results of the program implemented have good agreement to the results obtained from a well-known analytical program, DRAIN-3DX [Powell and Campbell, 1994].

The solution scheme also includes calculations of envelope responses parameters that are useful in determining different damage indices considered in the performance-based design engineering. The definition of these response parameters is the subject of the next section.

Table 3-2 Selected Earthquake Records on Bed Rock and Hard Rock (S1)

No	Event Name	Station	Magnitude	Component
1	Michoacan, Mexico City	Caleta De Campo	8.1	N00E
2	Michoacan, Mexico City	Caleta De Campo	8.1	N90E
3	Southeastern Alaska	Munday Creek	7.3	N000E
4	Nahanni Aftershock	Battlement Creek	6.9	270
5	Nahanni Aftershock	Northwest Territories	6.9	360
6	Northridge, California	Los Angeles, Griffith Observatory	6.8	270
7	Northridge, California	Los Angeles, Griffith Observatory	6.8	360
8	San Fernando	Lake Hughes, Array 4	6.5	S69E
9	San Fernando	Pacoima Dam	6.5	S16E
10	San Francisco Aftershock	Golden Gate Park, San Francisco	5.3	S80E

Table 3-3 Selected Earthquake Records on Sedimentary and Conglomerated Rock (S2)

No	Event Name	Station	Magnitude	Component
1	Sitka	Sitka Magnetic Observatory	7.6	WEST
2	Sitka	Sitka Magnetic Observatory	7.6	NORTH
3	Loma Prieta	Calaveras Array	7.1	360
4	Loma Prieta	Apeel Array	7.1	137
5	Alaska Subduction	Sand Point, Seismic Vault	6.5	N107E
6	Morgan Hill	Gilroy Array #6, San Ysidro	6.2	90
7	Coyote Lake	Gilroy Array #6, San Ysidro	5.8	230
8	Park Field	Cholame Shandon, Temblor No. 2	5.5	S25W
9	Park Field	Cholame Shandon, Temblor No. 2	5.5	N65W
10	Hollister	Gilroy Array #1, Gavilan College, Tower	5.2	S67W

Table 3-4 Selected Earthquake Records on Soil and Glacial Till (S3)

No	Event Name	Station	Magnitude	Component
1	Loma Prieta	Emeryville, 6363 Christie Ave., S Ground Site	7.1	260
2	Loma Prieta	Emeryville, 6363 Christie Ave., S Ground Site	7.1	350
3	Loma Prieta	Apeel Array #2, Redwood City	7.1	43
4	Loma Prieta	Apeel Array #2, Redwood City	7.1	133
5	Alaska Subduction	Simeonof Island	6.3	N340E
6	Alaska Subduction	Simeonof Island	6.3	N070E

Table 3-5 Selected Earthquake Records on Alluvium and Unconsolidated Deposits (S4)

No	Event Name	Station	Magnitude	Component
1	Kern County	Lincoln School, Taft Tunnel	7.7	S69E
2	Kern County	Lincoln School, Taft Tunnel	7.7	N21E
3	Kern County	Hollywood Storage Build. P.E. Lot, L.A.	7.7	S00W
4	Imperial Valley	Irrigation District, El Centro	7.1	S00E
5	Loma Prieta	Hollister Airport, Differential Array	7.1	255
6	Loma Prieta	Hollister Airport, Differential Array	7.1	165
7	Loma Prieta	Anderson Dam	7.1	243
8	Northridge	Littlerock	6.8	210
9	Northridge	Norwalk	6.8	90
10	Imperial Valley	El Centro, Array #4	6.6	140
11	Imperial Valley	El Centro, Array #5	6.6	140
12	San Fernando	Hollywood Storage Bldg, L.A.	6.5	N90E
13	San Fernando	Hollywood Storage Bldg, L.A.	6.5	S00W
14	Park Field	Cholame Shandon, Array #5	5.5	N85E
15	Park Field	Cholame Shandon, Array #5	5.5	N05W

CHAPTER 4

DAMAGE CRITERIA USED IN EVALUATION OF STIFFENING SYSTEMS

In order to have economical designs, design codes allow structures to undergo nonlinear deformations under major earthquakes. A performance-based design procedure first qualitatively defines different levels of desired behaviors as objectives and later tries to quantify these levels in terms of different response parameters (i.e., displacement, dissipated energy, low-cycle fatigue damage index, equivalent viscous damping, etc.). Therefore, by such a procedure the structure behavior can be ensured at predefined performance levels. Recent seismic codes contain performance objectives that are descriptive and have not been quantified by any kind of seismic response parameter [Krawinkler, 1995]. There are new trends in defining and quantifying different limit states and associated performance goals in order to establish a consistent performance-based analysis and design methodology [SEAOC, 1996].

In this section, several response parameters that are useful in evaluating bridge structural components in a performance-based seismic engineering are presented [Hose *et al.*, 1999; McCabe and Hall, 1989]. In the next section, these parameters are used to evaluate the earthquake response characteristics of stiffening systems in comparison to simple bilinear systems. The calibrations of response parameters to different performance levels is a separate task which requires experimental work such as the one conducted at UCSD [1999]. Therefore, the analytical results presented view the relative response characteristics of stiffening systems, which is useful in better understanding of their seismic behavior. Beside displacement, the parameters/criteria considered are dissipated hysteretic energy, low-cycle fatigue damage index, equivalent viscous damping,

normalized effective stiffness ratio, and residual deformation index, which are explained in details in the following sections.

4.1 Dissipated Hysteretic Energy Demand

The maximum displacement ductility response is the most commonly used parameter in damage assessment of different systems but it does not provide any information about the amount of hysteretic energy dissipated. It is well recognized that the severity of the nonlinear response and therefore the extent of the possible damage is better represented by the amount of dissipated hysteretic energy [Chai *et al.*, 1995]. Higher dissipated energy for a specific system is an indication of the larger nonlinear displacements and/or the larger number of hysteretic yield cycles. This energy-based damage concept can be better represented by a dimensionless ratio, N_e, which comparatively presents the severity of the nonlinear response of the system. This parameter is defined as the ratio of the dissipated hysteretic energy in a structure when subjected to ground motion to the area under the resistance-displacement curve for the structure when it is loaded monotonically until it reaches the failure displacement.

Here, the failure displacement ductility is assumed to be equal to the design displacement ductility for the base system. It should be noted that this response parameter has similar definition as the equivalent number of reversals, in which the monotonic load-displacement ends at the maximum displacement response of the system. The first one is a good comparative index for the hysteretic energy dissipated and therefore, for the extent of the possible damages, and the second one is a useful comparative index for the severity of the ground motion [Zahra and Hall, 1982].

In order to apply this parameter in a precise structural damage assessment, an exact correlation between the N_e values and the occurred damages per different systems and material types has to be experimentally established. However, the generic and non-calibrated values of this number can be used to evaluate the relative effect of any variable parameter on the expected seismic damages.

4.2 Low-Cycle Fatigue Damage Index (DI)

The earthquake response of structures has low number of reversals (below a thousand), therefore from fatigue-based point of view the damage can be caused by what is known as low-cycle fatigue behavior. However, the earthquake reversals have random displacement amplitudes and cannot be formulated directly into fatigue theorems that deal with the constant amplitude reversals. In this study, to resolve this problem, the McCabe and Hall [1989] methodology for earthquake reversals is used to investigate the effect of low-cycle fatigue on B-SDOF and S-SDOF systems.

Based on this method [McCabe and Hall, 1989], rather than strain the general context of ductility is selected as the basic parameter to define the low-cycle fatigue model. The ductility consists of elastic and plastic components and the plastic ductility is either monotonic (μ_p) or hysteretic (μ^*) in order to differentiate between monotonic or cyclic plasticity. Under the constant amplitude hysteretic cycles and for the steel material type, the monotonic plastic ductility is related to the hysteretic plastic ductility by Equation (30).

$$\mu^* = \mu_p (2N_f)^{(-0.6)} \tag{30}$$

In this equation, N_f is the number of load cycles (each full cycle contains two load reversals) and the power of $(2N_f)$ component depends on the material under consideration (i.e., -0.6 for steel).

The dissipated hysteretic energy corresponding to the cyclic fatigue failure is the key factor to connect the above formula to the earthquake response with random cyclic displacement amplitude. Dissipated hysteretic energy for N_f equal-shaped cycles with hysteretic plastic ductility of μ^* and negligible strain hardening is determined by the following formula:

$$H_t = \mu^* U_y R_y (2N_f) \tag{31}$$

where, U_y is the yield displacement and R_y is the yield strength of the bilinear system. This amount of energy (H_t) would be the maximum dissipated hysteretic energy before the system fails as a result of reversal fatigue. Comparing this to the amount of hysteretic energy dissipated in an earthquake response, a damage index (DI) is calculated as following:

$$DI = \left[\frac{H_p + H_n}{H_t}\right]^2 + \left[\frac{H_p - H_n}{H_t}\right]^2 \tag{32}$$

where, H_p and H_n are the total amounts of the dissipated energy in positive and negative resistance sides of the hysteretic loops, respectively. The difference between H_p and H_n results in the residual displacements, which is another major cause of damage and affects the above definition of DI as well.

This method is more involved than many damage criteria and considers several dynamic response characteristics, including the maximum ductility, dissipated hysteretic energy and the number of reversals. Although it does not explicitly refer to each one of

these parameters to estimate the possibility or degree of damage, it does relate these response characteristics through the low-cycle fatigue concept. In this way, DI depicts the safety of the design for any particular material type. If the DI is larger than 1, the failure of the system for the examined earthquake record is assumed eminent. How much smaller or larger from one the index is that would determine the relative degree of safety or the probability of failure for the system designed. Here, the calculated damage indices for S-SDOF systems are presented in the ratio format (S-SDOF/B-SDOF response ratio) so the relative effects of stiffening behavior can be viewed in light of this damage index.

4.3 Equivalent Viscous Damping, ζ_{eq}

Equivalent viscous damping (ζ_{eq}) presents the equivalent viscous hysteretic damping. It is based on the equal area approach that assumes the same amount of energy loss per cycle as applied in experimental tests [Priestley *et al.*, 1996]. The calculation of this factor, when hysteretic loops are symmetric is given in the following equation and also presented in Figure 4-1.

$$\xi_{eq} = \frac{1}{4\pi}\left[\frac{E_d}{E_S}\right] \tag{33}$$

In this equation, E_d is the area within the inelastic force-displacement response curve, which is a measure of the hysteretic damping or energy-dissipating capacity of the structure. Es is the strain energy stored in an equivalent linear elastic system and is shown by hatched area in the Figure 4-1.

In the case of asymmetrical hysteresis response in two loading directions, the average value for this factor will be calculated. This is done by separating the hysteretic loop at force axis into two segments, as shown in Figure 4-1, and calculating different parameters at each segment separately to use in Equation (34).

$$\xi_{eq} = \frac{1}{4\pi}\left[\frac{E_{d1}}{E_{S1}} + \frac{E_{d2}}{E_{S2}}\right] \tag{34}$$

It should be noted that equivalent viscous damping ratio is one of the important inelastic bridge design parameters in some of the more recent displacement-based design methods [Kowalsky, 1997].

4.4 Normalized Effective Stiffness Ratio, n_k

The effective stiffness, K_{eff}, defines the stiffness of an equivalent linear elastic system as shown in Figure 4-1. This stiffness is defined as the ratio of the maximum force to the corresponding maximum displacement responses.

$$K_{eff} = F/\Delta \tag{35}$$

For non-dimensional representation of this factor, the effective stiffness can be divided by initial stiffness value, K_0, as presented in the following equation.

$$n_k = K_{eff}/K_0 \tag{36}$$

In the case of asymmetrical hysteresis response in two loading directions, the average value for this factor will be calculated. This is done by separating the hysteretic

loop at force axis into two segments, as shown in Figure 4-1, and calculating different parameters at each segment separately to use in Equation (37).

$$n_k = \frac{1}{2}\left(\frac{K_{eff1}}{K_{01}} + \frac{K_{eff2}}{K_{02}}\right) \tag{37}$$

It should be noted that effective stiffness is one of the important inelastic bridge design parameters in some of the more recent displacement-based design methods [Kowalsky, 1997] This damage index, unlike other indices, indicates higher damage for lower values.

4.5 Residual Deformation Index, RDI

The residual deformation index, RDI, is representative of inelastic response of the structure and can be used as an index to measure the incurred damage. Any cyclically loaded structure that responds inelastically incurs a permanent residual displacement at the end of loading period, which can be measured at each performance level through experimental tests. The RDI index is a dimensionless ratio, which is calculated by dividing residual displacement by the ideal yield displacement of the system. For a symmetric cyclic loop, this index is calculated according to Equation (38) and Figure 4-1:

$$RDI = \Delta_r / \Delta_y \tag{38}$$

In the case of asymmetrical hysteresis response in two loading directions, the average value for this factor will be calculated. This is done by separating the hysteretic loop at force axis into two segments, as shown in Figure 4-1 and calculating different parameters at each segment separately to use in Equation (39).

$$RDI = \frac{1}{2}\left(\frac{\Delta_{r1}}{\Delta_{y1}} + \frac{\Delta_{r2}}{\Delta_{y2}}\right) \tag{39}$$

4.6 A Note on Quantifying the Response Parameters

Over the past 15 years, based on large-scale tests on different bridge structural components at UCSD, different performance levels are defined both qualitatively and quantitatively for bridge structures [Hose *et al.*, 1999]. The behaviors defined fall into five performance levels, which for the reinforced concrete (RC) bridge members are presented in Table 4-1. The correlation between different visual damage signs and performance levels are the basis for calibrating different response parameters which is done during laboratory tests by measuring the parameters at different stages of the simulated responses.

As a result of such measurements, identification force-displacement curves (i.e., force-displacement curves that are labeled at each performance level) are calculated for three major structural behaviors: Brittle, Strength Degrading, and Ductile. These curves are similar to the identification curves for buildings presented by FEMA 274 and FEMA 306, but each curve is labeled according to the five bridge performance levels that are quantified by different bridge response parameters like RDI, ζ_{eq}, and n_k. Figure 4-2 presents an identification curve for a ductile RC bridge component with corresponding calibrated response parameters.

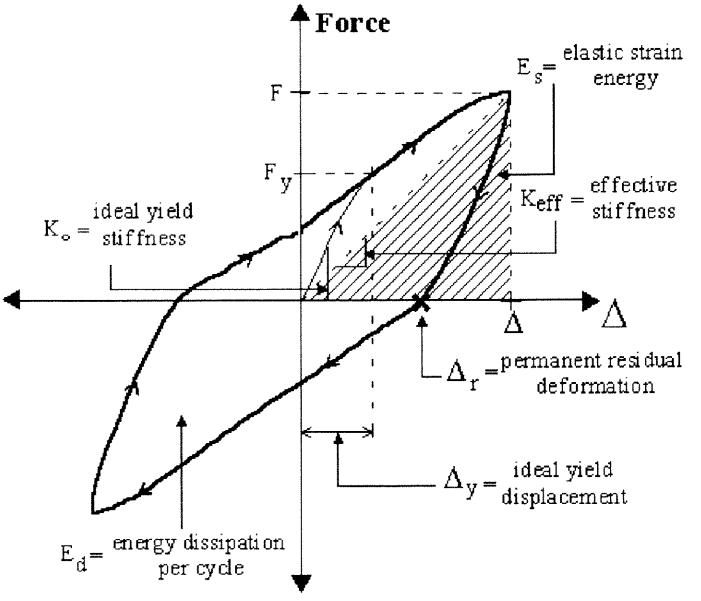

Symmetric Hysteretic Loop

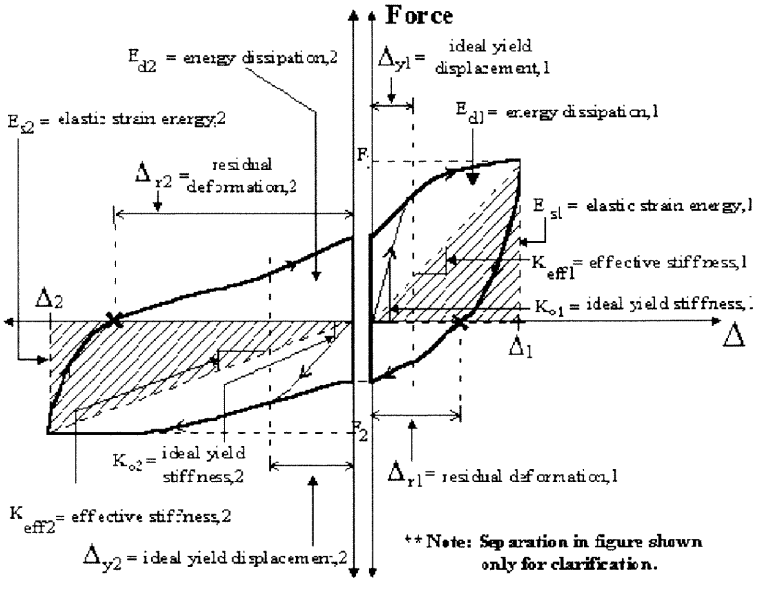

Asymmetric Hysteretic Loop

Figure 4-1 Calculating Different Response Parameters For Symetric and Asymetric Hysteretic Loops [Hose *et al.* 1999]

Table 4-1 Descriptions of the Bridge Performance Levels for Reinforced Concrete Components (Hose *et al.* 1999)

Performance Level	Social-Economical Description	Qualitative Performance Description	Quantitative Performance Description
I	Fully Operational	Onset of Hairline Cracks	Cracks Barely Visible
II	Operational	Theoretical First Yield of Longitudinal Reinforcement	Cracks Widths < 1mm
III	Life Safety	Initiation of Inelastic Deformation, Onset of Concrete Spalling, Development of Diagonal Cracks	Crack Widths 1-2 mm, Length of Spalled Region > 1/10 of Cross-Section Depth
IV	Near Collapse	Wide Crack Widths/Spalling Over Full Local Mechanism Region	Crack Widths > 2mm, Diagonal Cracks Extend Over 2/3 of Cross-Section Depth, Length of Spalled Region > 1/2 of Cross-Section Depth
V	Collapse	Buckling of Main Reinforcement, Rupture of Transverse Reinforcement, Crushing of Core Concrete	Crack Widths > 2 mm in Cocrete Core, Measurable Dilation > 5% of Original Member Dimension

In the next section, in terms of different response parameters and damage indices, the results of the extensive parametric study for simple stiffening systems are presented. The analytical results are given in the form of response ratios (i.e., S-SDOF/B-SDOF), which is useful to capture the relative effects of the IE components on the base component. Correlating damage indices to the state of damage is an ongoing experimental work [UCSD, 1999] and the intention here is to make a relative evaluation.

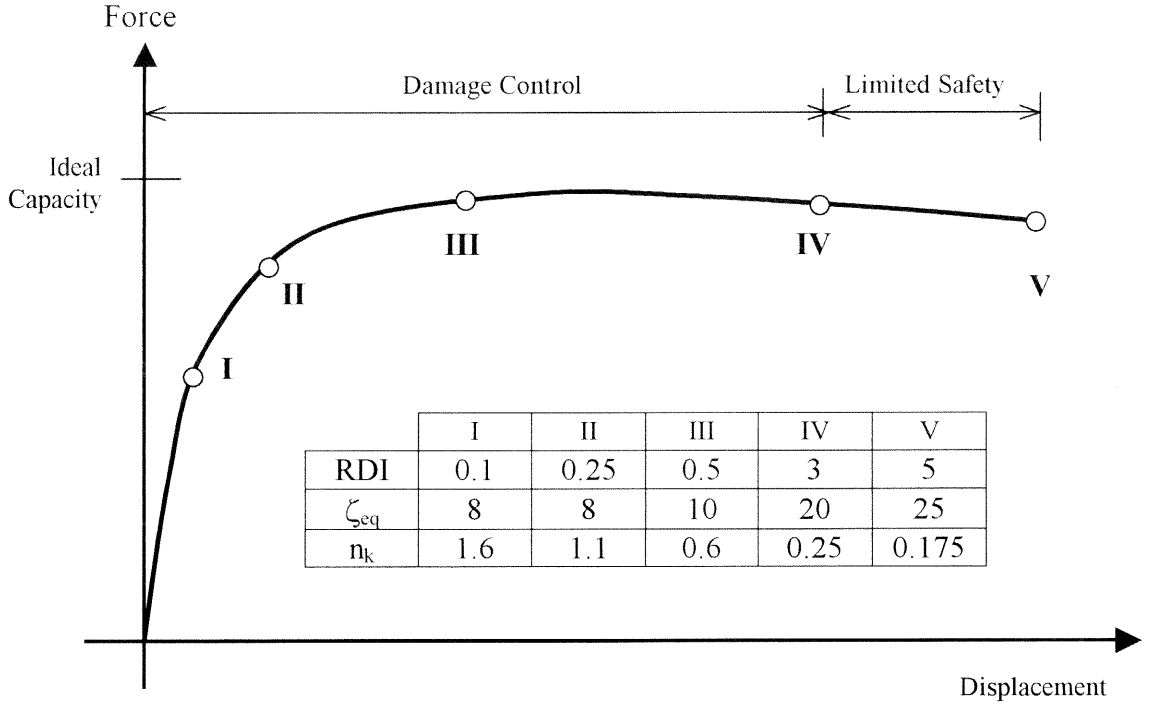

	I	II	III	IV	V
RDI	0.1	0.25	0.5	3	5
ζ_{eq}	8	8	10	20	25
n_k	1.6	1.1	0.6	0.25	0.175

Figure 4-2 Typical Identification Curve for a Ductile Reinforced Concrete Bridge Component [Hose *et al.* 1999]

CHAPTER 5

NONLINEAR RESPONSE OF SIMPLE STIFFENING SYSTEM

Parametric study included 368,795 cases of both S-SDOF and B-SDOF (i.e., 367,360 S-SDOF and 1435 B-SDOF). For each analysis, different response parameters and damage indices are calculated. For design implications and obtaining important statistical values, mean and Mean-Plus-One-Standard-Deviation (MPOSD) responses for the 41 different earthquake records are calculated. These statistical response values are the only ones that are used for discussions to fallow.

In light of the huge amount of data, accessing the database to calculate some useful statistical values or extract the results for a particular stiffening system would be difficult and inefficient if there is no organized mean to manage the requests and process the responses. In this study, a JAVA object oriented program with a simple Graphical User Interface (GUI) front end is developed to build and manage the response database. This program enables the user to make the following requests;

- Response of any particular system

- The maximum, the minimum, mean, MPOSD responses of a group of systems. This group is defined by specifying the range of the attributed parameters.

- Comparison of S-SDOF and B-SDOF responses by obtaining their response ratios

Using this program, it is possible to compare S-SDOF and B-SDOF responses and also investigate the effects of different stiffening parameters on the response of these

systems. The following sections describe the comparisons and present the results that are useful in understanding stiffening systems and also developing new pseudo-static methods for design application, such as seismic analysis of MSSS bridges.

5.1 Comparison of S-SDOF and B-SDOF Responses

Comparison of S-SDOF and B-SDOF (i.e., the base component without surrounding IE) responses show that how an S-SDOF system differs from B-SDOF system in terms of different response parameters (i.e., displacement, energy, damage index, etc.). The comparison is viewed by drawing the maximum, the minimum, mean, and MPOSD curves. Statistically, mean and MPOSD responses are referred to as 50% and 16% chance of exceeding, respectively, and therefore they can be used in a design process that the safety and reliability of the system has to be assured against possible future seismic forces. The minimum and the maximum values give the possible range of response variations for cases considered and present the scattering of the responses.

The comparison is better done when responses are presented in relative term (i.e., S-SDOF/B-SDOF ratio). The ratio format eliminates peak ground acceleration (PGA) as an extra factor and represents the results in a dimensionless format. By this, values greater than one indicate that IE component has increasing (i.e., not restrictive) effect on the base system's response. An exception is for indices such as effective stiffness where smaller values indicate larger damages, therefore the ratio values less than one for such indices would have the same interpretations.

When MPOSD curves are used, the graphs presented in this section can be viewed as design graphs for S-SDOF systems, where stiffening parameters are not well

quantified. In this case, the MPOSD curves will yield the statistical S-SDOF response where there is less than 16% chance of surpassing due to variation of all stiffening parameters within the range considered.

Values for S-SDOF parameters that are not representative of MSSS bridges (i.e. β=0.5, α=0.5) are excluded from the statistical calculations (unless they are drawn in a separate curve for comparison). Also note that elastic S-SDOF systems are associated with the R_y of 0.1.

5.1.1 Displacement Ratio

Displacement response of structural systems is one of the main response parameters that is used in design codes. It is a common belief that stiffening systems will have smaller displacement responses. Although this is correct for the wide range of stiffening systems with different R_y factors, there are exceptions that mostly happen for long period and elastic stiffening systems.

Appendix Figure A.1 to Figure A.4 show displacement response ratios for systems with R_y factors equal to 0.1 (elastic systems), 2, 3, and 5. Considering MPOSD graphs, it can be seen that inelastic stiffening systems mainly have lower displacement responses than B-SDOF systems; the displacement ratios except in the case of R_y=2 (only after 2.2 second period as it is seen in Figure A.2), are always below 1. In elastic systems, stiffening behavior has increasing effect especially after 1.5 second (Figure A.1).

Displacement ratio has an increasing trend as period of the base system increases. The increase is higher when the base system is responding more elastically. In other words, as the Ry factor decreases displacement ratio increases. For example, this can be seen by comparing Figure A.1 and Figure A.4. In Figure A.1, for elastic systems,

displacement ratio on MPOSD curve varies from 0.6 (at 0.3 sec) to 1.5 (at 3.0 sec). In contrast, in Figure A.4 for systems with R_y=5 this variation is in smaller range of 0.2 to 0.85.

Stiffening systems has more disperse displacement response when the base system has smaller Ry factor. For example, in Figure A.1 (i.e., for elastic systems) the difference between the maximum and the minimum responses reaches as high as 1.4, but for R_y=5 (Figure A.4) this difference is at most equal to 0.6.

5.1.2 Dissipated Hysteretic Energy Ratio

The amount of dissipated energy in a structural system is proportional to the extent of damage in that system. Figure A.5 through Figure A.7 show the dissipated energy ratios for stiffening systems with R_y factors of 2, 3 and 5. There is a common trend in all graphs in which the hysteretic energy demands for S-SDOF systems are higher than that for the B-SDOF systems (especially for periods greater that 0.7 second).

The higher energy dissipation demand for stiffening systems is due to the larger number of hysteretic loops and/or the larger displacement demands. In another words, an S-SDOF system with almost the same displacement response as its corresponding B-SDOF system, may have higher number of hysteretic loops than the B-SDOF component. This can be seen in the Figure A.8 and Figure A.9, where hysteretic response loops for an S-SDOF system and its corresponding B-SDOF system are presented. As is seen in the figures, the S-SDOF system has more hysteretic loops, and although both systems have almost the same displacement responses, the S-SDOF system dissipated about twice as much as the B-SDOF system.

By considering MPOSD curves, it can be seen that the energy response ratio increases as the R_y factor decreases. For example, referring to Figure A.5 to Figure A.7, the response ratios for systems with R_y factors equal to 2, 3, and 5 reach as high as 5, 3, and 2, respectively. Dispersion of the responses is higher for lower R_y factors. For example, the difference between the maximum and the minimum response values for R_y=2 (Figure A.5) reaches as high as 9, where as for R_y=5 (Figure A.7), this difference is not more than 2.5.

5.1.3 Other Response Ratios

Other response parameters such as low-cycle fatigue damage index (DI), equivalent viscous damping (ζ_{eq}), normalized effective stiffness ratio (n_k,) and residual deformation index (RDI), are all directly or indirectly related to the displacement and hysteretic energy responses. Therefore, the general trend observed in displacement and hysteretic energy responses could be found in these response parameters as well.

Appendix Figure A.10 to Figure A.12 show the DI response ratios for S-SDOF systems with R_y factors equal to 2, 3, and 5. This index has more or less the same variation and dispersion pattern as the dissipated hysteretic energy ratio to the power of two. For example, for R_y=2 and periods larger than 2 seconds, the maximum DI response ratio is about 10^2 (Figure A.10), where for dissipated hysteretic energy demand this ratio is about 10 (Figure A.5). Other influential parameters on this index is number of reversals (N_{rev}). This number generally increases in S-SDOF systems but numerically the increase is not much in comparison to hysteretic energy increase. For example, in the case of R_y=2, the maximum N_{rev} ratio (S-SDOF/B-SDOF) reaches as high as 2.4 compared to the hysteretic energy response ratio which is 10. Furthermore, referring to the DI formula

N_{rev} ratio will increase the DI by a power of 1.2 in contrast to the hysteretic energy response ratio that increases the DI by a power of 2.

Appendix Figure A.13 to Figure A.15 show the response ratios for equivalent viscous damping ratio (ζ_{eq}) for systems with R_y factors equal to 2, 3, and 5. This damage index is obtained by referring to the envelope hysteresis response of the base component by calculating the areas within the loop (i.e., area within the inelastic force-displacement curve); therefore ζ_{eq} is larger for larger displacement responses and it fallows more or less the displacement response ratio pattern. As is seen in Figure A.13 through Figure A.15, when the R_y factor increases the MPOSD curves tend to become less slanted, indicating less sensitivity of the response ratio to a period change. For example, the response ratios at periods 0.3 and 3 for R_y factor of 2 (Figure A.13) are 0.5 and 1.4, respectively, while at the same periods for R_y factor of 5 (Figure A.15) the response ratios are 0.85 and 1.05.

Referring to MPOSD curves, roughly at periods longer than 1.5 seconds slightly higher damage is predicted by ζ_{eq} index for S-SDOF systems. The possibility of damage increases as R_y factor decreases. As is seen in Figure A.13 through Figure A.15, the response ratios at most reach as high as 1.1, 1.3, and 1.4 for R_y factors equal to 5, 3, and 2, respectively.

Appendix Figure A.16 to Figure A.18 show the normalized effective stiffness (n_k) ratio responses for systems with Ry factors equal to 2, 3, and 5. Based on its definition, this response factor will yield lower values for higher displacement responses, therefore for this index the lower values mean higher damage and instead of MPOSD curves the MMOSD (Mean-Minus-One-Standard-Deviation) curves are presented. As is seen in the

figures, and by referring to MMOSD curves, stiffening systems at periods less than 1.7 seconds have protective effect on their base components. At periods larger than 1.7 seconds, except in the case of R_y factor of 2 where slightly more damage is predicted for S-SDOF systems (as high as 25% more), almost the same damage level is expected for S-SDOF and B-SDOF systems.

Figure A.19 to Figure A.21 show response ratios for residual deformation index (RDI) for systems with Ry factors equal to 2, 3, and 5. This index has similar variations as the displacement response ratios. Referring to MPOSD curves, stiffening systems would suffer more damage in systems with long periods, especially periods longer than 2 seconds. Systems with lower Ry factor also show higher damage. The RDI ratio reaches as high as 1.7, 1.3, and 1.1 at 3 second period for systems with Ry factor equal to 2, 3, and 5, respectively.

In this section, the S-SDOF systems were compared to B-SDOF systems through examining several response ratios and it was shown that S-SDOF systems mostly have less displacement responses and higher dissipated hysteretic energy. Other response parameters and damage indices that are more or less related to the displacement and dissipated hysteretic energy responses show similar patterns. The presented comparison between S-SDOF and B-SDOF systems does not give any information about the sensitivity of the S-SDOF response to various stiffening parameters (i.e., α, β, Rg, and m). To achieve this, there is a need for different types of graphs where S-SDOF response is drawn in terms of separate response parameter values.

5.2 Effects of the Stiffening Parameters Variations on the S-SDOF Responses

The variation of S-SDOF responses per different stiffening parameters (i.e., α, β, R_g, m) is the subject of this section. The variation is shown in terms of response ratios (S-SDOF/B-SDOF) and MPOSD curves. Graphs are plotted only for displacement and dissipated hysteretic energy responses since other response parameters have more or less similar variations. Concluded results are qualitative and comparative and a general pattern of increasing or decreasing of the response ratios with the stiffening parameter values are described. Results are described in terms of percentage changes of response ratios at lower and longer periods, and in systems with different R_y factor.

The graphs presented in this section can be viewed as design graphs for S-SDOF systems where only one stiffening parameter is well quantified (any of α, β, R_g, or **m** parameters) and the rest of the parameters are considered in the range values. By this, the well-quantified parameter can be used to calculate the S-SDOF response with less than 16% chance of exceeding due to the variation of the other stiffening parameters in the ranges considered.

5.2.1 Variation of the Stiffness Ratio (α)

Appendix Figure A.22 to Figure A.27 show the displacement and dissipated hysteretic energy ratio responses for S-SDOF systems with R_y factors equal to 2, 3, and 5. Curves on these figures are for different values of α, presenting the relative effects of the stiffness ratio on the response of S-SDOF systems. It can be seen in the figures, that as α increases, the displacement and dissipated hysteretic energy responses of S-SDOF systems tend to decrease. In another words, as α increases, the stiffening systems have

more restrictive effect (or protective in terms of damage) on the base component responses. This restrictive effect is more obvious at higher periods where response ratio is bigger. At higher periods for systems with different R_y factors, displacement response ratio decreases for about 25% when α increases from 10 to 50. At lower periods, the displacement response ratios for different α values are closer to each other and seem to converge toward a point.

At higher periods when α increases from 10 to 50, dissipated hysteretic energy response decreases by about 50%, 40%, and 27% for systems with R_y factors equal to 2, 3, and 5, respectively. At lower periods, the dissipated energy response ratios for different α values are closer to each other and seem to converge toward a point. For the graphs with α factor equal to 0.5, which is drawn just for comparison, the slope of variations is reverse compared to the other curves. A noticeable difference can be seen in lower periods where displacement and dissipated hysteretic energy response ratios are higher than one and reach as high as 1.7 for displacement and 8 for dissipated hysteretic energy.

The increase in the displacement response of the stiffening cases with α factor of 0.5 is similar to the increase reported by Bejar et al [1992] for bilinear systems with large kinematic strain hardening (i.e. 50% and 75%). Therefore it could be said that an S-SDOF system with small α factor acts more like a bilinear system with large kinematic strain hardening. It should be noted that, since in MSSS bridges for the interaction between pier bents and the surrounding abutments large values for α (larger than 10) are expected, the effects of the smaller values of α on the responses are not investigated here.

5.2.2 Variation of the Strength Ratio (β)

Appendix Figure A.28 to Figure A.33 show the displacement and dissipated hysteretic energy ratios for S-SDOF systems for different values of R_y and β. The strength ratio (β) has a unique and different effect on the response of S-SDOF systems than other parameters. Referring to the figures for displacement ratio responses, it is seen that there is an inflection point at about 1.5 second period. For periods longer than 1.5 second, larger β causes larger displacement response ratio. However, for periods shorter than 1.5 second, the displacement response ratio stay more or less insensitive to the β variation.

Dissipated hysteretic energy response ratio for S-SDOF systems has a clear variation trend with the strength ratio (β). As is seen in the figures, as β increases the energy response ratio increases too. This increase is more for long periods and small R_y factors. For example, at long periods by increasing β from 5 to 20, the dissipated hysteretic energy ratio increases by 160%, 130%, and 90% for systems with Ry factor of 2, 3, and 5, respectively. At lower periods, the dissipated energy response ratios for different β values are closer to each other and seem to converge toward a point.

In contrast to the dissipated hysteretic energy ratio, displacement ratio has not been as much affected by β variations. This leads to an important conclusion that when for a particular IE component the strength ratio (β) changes the S-SDOF displacement response does remain more or less the same (this concept better can be viewed in a pushover analysis procedure). For the graphs with β factor of 0.5 that are just drawn for comparison, the displacement and dissipated hysteresis response ratios have almost stayed the same through out the period range considered (the response ratios are about 0.8 for displacement and about 1.0 for dissipated hysteretic energy).

5.2.3 Variation of the Gap Size Factor (R_g)

Appendix Figure A.34 to Figure A.39 show the displacement and dissipated hysteretic energy response ratios for S-SDOF systems for different values of R_y and R_g. As is seen in the figures, the displacement and dissipated energy response ratios are smaller when gap size is smaller (i.e., larger Rg). Therefore, smaller gap size has protective effects on the S-SDOF component when different damage criteria are considered for comparing S-SDOF and B-SDOF systems. Unlike the other stiffening parameters, response curves per different gap sizes are more or less parallel to each other with the response increasing from lower to higher periods.

When R_g increases from 2 to 20, displacement response ratio decreases for about 50% and 10% at short and long periods, respectively. Similar to the displacement response, dissipated hysteretic energy response ratio decreases with an increase in R_g factor. When R_g increases from 2 to 20, at short and long periods the dissipated hysteretic energy ratio decreases about 90% and 15%, respectively.

5.2.4 Variation of the Mass Ratio (m)

Appendix Figure A.40 to Figure A.45 show the displacement and dissipated hysteretic energy response ratios for S-SDOF systems for different values of R_y and **m**. As is seen in the figures, as **m** increases the displacement and dissipated hysteretic energy responses of S-SDOF systems increase. It should be noted that the case with **m**=0.01 refer to stiffening systems that their IE components are massless (only stiffness). As is seen in the figures, such a massless IE model presents an average response for stiffening systems with different **m** values.

Displacement response ratio increases for about 25% at higher periods when **m** increases from 0.5 to 2. At lower periods, the displacement response ratios for different **m** values are closer to each other and seem to converge toward a point. Dissipated hysteretic energy response increases at higher periods by about 100%, when **m** increases from 0.5 to 2. At lower periods, like the displacement response, the dissipated energy ratios for different values of **m** are close to each other and seem to converge toward a point.

5.3 Pseudo-static Analysis of S-SDOF Systems

A pseudo-static analysis is suitable for any structural system that acts dominantly in its first mode of vibration. Therefore, MSSS bridges that comprised of several SDOF systems can be considered to be analyzed by such method. Currently, pushover analysis for MSSS bridges, as described in FHWA (1995), is made by superposing the AASHTO elastic design RS on the resistance curve of the system. The bridge system is modeled as if all the gaps between pier bents are closed (i.e., compression model). In the model, pier columns are assumed elastic and can respond nonlinearly by interacting with the abutments (stiffness, strength, and the gap size over of the abutment are considered). For such procedure two criticisms can be made; first the pushover curve for MSSS bridge in the longitudinal direction has stiffening characteristics (when pier bents hit the abutment) while the RS employed is for linear elastic systems, and second the non-linearity in pier bents (i.e., plastic hinge at pier bents) is not considered.

A more realistic and reliable pseudo-static analysis for stiffening systems has to be made by superposing an inelastic stiffening design RS in force-displacement coordinates

on resistance curve of the system that includes the nonlinear behavior of the components. So far, no inelastic RS for stiffening systems has been developed. Therefore, in the first step to introduce a pseudo-static analysis method for S-SDOF systems a proper design RS has to be developed. In order to do so, in the following sections the analysis results are viewed and analyzed in force-displacement format.

5.3.1 Design Response Spectra for S-SDOF Systems

Current design codes have procedures to calculate force and displacement demands for different structural systems. When a system acts dominantly in its first mode of vibration, pseudo-static analysis is the fastest way of analyzing the system within an acceptable accuracy. There are different design response spectra developed for linear-elastic and bilinear-inelastic systems, but none for stiffening systems. Although in an attempt to analyze a pier-abutment interaction, which has stiffening characteristics, a design RS for linear-elastic systems was utilized [AASHTO, 1996; FHWA, 1995], the validity of linear-elastic design RS in calculating S-SDOF responses is questionable and there is a need to evaluate accuracy of the procedure and establish a proper design RS for S-SDOF systems.

The database developed for S-SDOF systems can be viewed in force-displacement format per different yield force factor (R_y). Representation of the results in the form of minimum, maximum, mean, and MPOSD curves helps to see the response scattering due to different S-SDOF parameters and to introduce design response spectra for S-SDOF systems accordingly. The important issue is to divide and categorize results in separate groups so that a particular pattern, useful in drawing conclusions, could be observed. For this purpose, graphs are grouped per different R_y and β factors, which are the most

important parameters in determining the force responses. Note that, as is seen in previous sections, the displacement response of S-SDOF systems is not sensitive to the β variations. This fact will be used later to adjust AASHTO RS by a simple force factor (dependant to R_y and β) and leaving the displacement coordinates unchanged.

Appendix Figure A.46 to Figure A.54 show force-displacement response spectra obtained from the parametric study that suits S-SDOF systems with parameter values common to MSSS bridges (i.e., R_y=2, 3, and 5, α= 10, 20 and 50, β=5, 10, and 20, R_g=2, 3, 5, and 20, **m**=0.01, 0.5, 1, and 2). In these figures, response graphs are the minimum, the maximum, mean, and MPOSD curves. As seen on the figures, based on the results the elastic AASHTO RS is adjusted (as will be described in the next section) for the S-SDOF systems and are plotted as well. For systems with R_y of 2, Figure A.46, Figure A.47 and Figure A.48 show S-SDOF RS for systems with β values of 20, 10, and 5, respectively. For systems with R_y of 3, Figure A.49, Figure A.50, and Figure A.51 show S-SDOF RS for systems with β values of 20, 10, and 5, respectively. For systems with R_y of 5, Figure A.52, Figure A.53, and Figure A.54 show S-SDOF RS for systems with β values of 20, 10, and 5, respectively.

Referring to the figures, it can be seen that there is a common pattern where at higher periods curves are merging to each other and at lower periods they diverge. Despite of the diverging pattern at lower periods, caused by different force responses, the displacement responses have little differences when different response curves between the minimum and the maximum are utilized. This is because of the high stiffness of the S-SDOF systems at low periods, where the high-sloped resistance curve would cross

different response curves at considerably different force levels but almost similar displacement values.

One measurement for the scatter of responses, is simply the difference between the maximum and the minimum response curves. This measurement is simple and does not include all the response values in the calculation. The other measurement for the scatter, which is more involved than the previous one, is the difference between mean and MPOSD values. If the responses are more populated around mean then the mean and MPOSD curves are close to each other. For such situation, the MPOSD curves beside their statistical meaning, present closer response values to the real response of the most cases.

As is seen in the figures, the scatter of responses (considering both measurements) is increased for larger β and smaller R_y and also for lower periods especially less than 1 second. For example as shown in Figure A.46, for the most scatter case with the lowest R_y of 2 and the highest β of 20, the force factor varies from 4 to 16, whereas for the largest R_y (5) and the smallest β (5) (Figure A.54), this variation is from 0.5 to 4. However, even for the most scattered region, the mean and MPOSD curves have relatively stayed close to each other. This can be seen in the Figure A.46, where despite of the large variation range of 4 to 16 for the force factor, the difference between mean and MPOSD at most reaches to 4. Therefore, MPOSD curves could yield close results for the most systems and meanwhile present the responses that have 16% chance of exceeding.

It should be noted that the MPOSD curves have to be extracted from the database either for a particular system (i.e., with specified stiffening parameters) or for a range of

S-SDOF systems (i.e., a range for different stiffening parameters). In the first case, the MPOSD curve is calculated for different earthquake responses. However, if a range for S-SDOF systems were indicated, the MPOSD computation additionally includes a range of responses for the specified stiffening systems. Therefore, the MPOSD curves computed, beside representing 16% statistical chance of exceeding due to earthquake records also represent 16% chance of exceeding due to the stiffening parameters variations (i.e., variations in α, β, R_y, R_g, and **m**).

5.3.2 Adjusting AASHTO RS for S-SDOF Systems

The response curves including MPOSD graphs have more or less the same shape as the AASHTO RS (ARS) but placed at upper force levels. By close inspection of the results, it appears that AASHTO RS can be adjusted to become an S-SDOF RS by a simple force factor (i.e., to be multiplied to the force coordinate response only) as is stated in Equation (40).

$$\text{Adjusting Force Factor} = (\beta+1) / R_y$$

$$2 \leq \beta \leq 20 \text{ and } 2 \leq Ry \leq 5 \qquad (40)$$

(other parameter ranges are stated in Table 3-1)

In this scheme, there is no need to adjust the displacement coordinate of the AASHTO RS, since based on the results obtained the S-SDOF displacement response is not sensitive to β variations (Figure A.28 through Figure A.33). It should be noted that the validity of the Equation (40) is only verified in the range considered within the parametric study (see Table 3-1).

Adjusted AASHTO response spectra are compared with MPOSD curves in Figure A.55, Figure A.56 and Figure A.57 for systems with Ry equal to 2, 3, and 5, respectively. Adjusted AASHTO RS with different R_y and β factors are presented by AASHTO_R_y_β notation and referred as AASHTO stiffening RS (ASRS). As is seen in the figures, ASRS has a good agreement with MPOSD curves especially at higher periods. At lower periods, new upper force limit factors are set for ASRS. These limits are set according to the MPOSD curves and presented in Table 5-1. It can be seen in the table, that the original upper force factor of 2.5A is multiplied by $(\beta+1) / R_y$, but in cases that this will over-estimate the responses by diverging from the calculated MPOSD graph the upper limit is reduced accordingly.

Using ASRS in calculating the displacement response of S-SDOF systems, is more reliable than using a linear RS where the stiffening behavior is not part of its definition. Comparing the AASHTO RS and ASRS, although both have a common trend of predicting lower responses for S-SDOF systems in comparison to B-SDOF systems, the ASRS will yield higher force and displacement responses. This will identify the AASHTO RS as an un-conservative RS for analyzing S-SDOF systems.

Table 5-1 Force Factor Upper Limits for the S-SDOF AASHTO Response Spectrum

Ry	β	Force Factor Upper Limit
2	5	$2.5*A*(\beta+1) / R_y = 7.5A$
	10	$\mathbf{1.6}*A*(\beta+1) / R_y = 8.8A$
	20	$\mathbf{1.3}*A*(\beta+1) / R_y = 13.7A$
3	5	$2.5*A*(\beta+1) / R_y = 5.0A$
	10	$2.5*A*(\beta+1) / R_y = 9.2A$
	20	$\mathbf{1.6}*A*(\beta+1) / R_y = 11.2A$
5	5	$2.5*A*(\beta+1) / R_y = 3.0A$
	10	$2.5*A*(\beta+1) / R_y = 5.5A$
	20	$\mathbf{1.9}*A*(\beta+1) / R_y = 8.0A$

5.3.3 Practical Application of the S-SDOF Response Spectrum

As it was mentioned before, an MSSS bridge consists of several components including pier bents and abutments interacting with each other. In the longitudinal direction of MSSS bride, each pier bent can be considered as a S-SDOF system surrounded by interacting environment (IE) consisted of adjacent pier bents and abutments. Considering these facts, one appropriate way to transform a pier bent to an equivalent S-SDOF system would be to combine the surrounding components at each side, including each abutment, into one IE component with gap size, mass, stiffness, and strength equal to the sum of the values in the surrounding components. By this, the IE component is placed at the maximum possible distance (sum of gap sizes) from the base component.

Using the proposed approach, the Clements Bridge (Bridge #1) pier bents in the medium stiff soil (G_S = 4ksi) are analyzed under PGA of 0.4g, using different stiffening

response spectra. The stiffening response spectra used are ASRS and MPOSD curves. The pseudo-static analyses (pushover) are shown in Figure A.58 and Figure A.59. It should be noted that since in this bridge the properties of IE components at each side is not the same, displacement direction (displacement to the left or to the right) would be a factor in determining an equivalent symmetric S-SDOF system. As is seen in these figures, there are two capacity diagrams for each pier as well as two S-SDOF design response spectra. It also can be seen that ASRS has very good coincidence with S-SDOF RS obtained directly from the database. This is another indication that in determining S-SDOF RS, the Ry and β factors are the most influential parameters and that the proposed adjustment for AASHTO RS yields a reliable and accurate S-SDOF RS.

The properties of the equivalent stiffening systems that are used in calculating S-SDOF RS from the response database are shown in Table 5-2. It should be noted that the values presented are the closest available parameters in the response database to the real parameter values of the pier bents. For instance, the real "α" and "β" values for the pier-2 when it is pushed to the right are 78.4 and 11.1. However, values of 50 and 10, which are the closest match in the database are used, respectively. For any bridge stiffening parameter value, that is within the database range but is not close to one of the values used, two surrounding values in the database are considered in calculating the average responses.

5.3.4 AASHTO/FHWA's Approach vs. Proposed Method for the Pseudo-Static Analysis of MSSS Bridges

Based on AASHTO and FHWA guidelines, there are two approaches to calculate MSSS bridge displacement responses. In both methods pier bents are considered elastic. In the

first method, based on the tension model, all the gaps between different components are assumed to be open and no interaction among them considered. Such method is usually used for first run analysis where the displacement responses are used to determine whether pier bents respond into the nonlinear range by interacting with the abutments.

The second method, based on the compression model, all the gaps are assumed to be closed and whole bridge acted as a unite. Based on the comression model there are two approaches to calculate the demands. The first approach is a try and error method; guess stiffness (firs to start with the combined stiffnesses), determine force and displacement responses, and revise stiffness if the abutment's strength is surpassed by the demand. The second approach is a direct solution by plotting the spectral force vs. displacement.

The direct approach for the compression model solution can be referred as the pushover analysis. In this analysis, the displacement response is crossing point of the AASHTO elastic RS in the force-displacement format and the resistance curve. The resistance curve is drawn for a bridge system where the pier bents combined into one unite and is pushed toward the abutment where its strength, stiffness, and gap distance to the pier bents are considered.

Figure A.60 shows the pushover analysis of the Bridge #1 using the FHWA/AASHTO and proposed methods. Based on the current guidelines, the AASHTO RS is calculated for the total weight of the bridge (piers 1 and 2 combined) and only the gap size between the abutment and the adjacent pier bent is considered (i.e., 762 mm). In the contrast, the proposed method considers the bilinear property of each pier bent and abutment and also their interaction to the surrounding components with different gap

distances, stiffnesses, and strengths. The calculated FHWA/AASHTO response is less than those calculated by the proposed method. This marks the FHWA/AASHTO compression method as an un-conservative approach for pseudo-static analysis of MSSS bridges if the pier bents respond into nonlinear range by interacting with the abutments.

The same result can be obtained again by reviewing an example, presented in one of the FHWA publications [FHWA, 1997]. Figure A.61 presents the direct solution approach to the compression model of the example bridge. The results of the analysis are compared to the proposed method in Figure A.62. As is seen in the figure, consistent with the previous example for the Pier-1 of Bridge #1, the proposed method yields higher displacement demand.

Table 5-2 Equivalent Stiffening Systems for the Bridge #1 in the Longitudinal Direction (G_S = 27.6 Mpa, PGA = 0.4g)

Stiffening Parameter	Pier 1		Pier 2	
	To Left	To Right	To Left	To Right
α	50	50	50	50
β	5	10	5	10
m	0.5	2.0	1	0.5
R_g	2.5	2	3	4.7
R_y	2.7		3.7	
Base System Period (sec)	1.4		2.27	

5.4 Conclusions

In this section, by referring to the extreme values and MPOSD curves of different response ratios, the general behavior of S-SDOF systems in comparison to the B-SDOF systems were explained. The summery of the results are as follow.

- Inelastic stiffening systems, despite of few cases, mostly have smaller displacement responses in comparison to B-SDOF systems.

- Elastic S-SDOF systems at periods longer than 1.5 seconds have mostly larger displacement responses. For these systems, on MPOSD curves, the displacement response reaches a value as high as 1.5 of that for B-SDOF system.

- Inelastic S-SDOF systems have higher dissipated hysteretic energy demand, especially at periods longer than 0.7 second. The dissipated energy ratio is higher for systems with lower strengths (i.e., smaller R_y factor). On MPOSD curves the response ratios reach as high as 5, 3, and 2 for stiffening systems with R_y factors of 2, 3, and 5, respectively.

- Other damage index ratios have similar variation patterns as displacement response ratios or dissipated hysteretic energy response ratios. All of these damage indices predict higher damage for S-SDOF systems at long periods with smaller R_y factor.

- In descending order and by referring to MPOSD curves, following are the damage criteria that predict higher damage for S-SDOF systems: DI (as high as 35 after 0.7 sec. period), dissipated hysteretic energy (as high as 5 after 0.7 sec period), RDI for

inelastic systems (as high as 1.7, after 1.7 period), displacement for elastic systems (as high as 1.5 after 1.5 sec period)

- Referring to MPOSD curves, the following are damage criteria that predict no more damage or at most slightly higher damage for S-SDOF systems: ζ_{eq} (as high as 1.4 after 1.7 sec period), $1/n_k$ (as high as 1.25 after 1.7 period), and displacement for inelastic systems with R_y=2 (as high as 1.15 after 2.25 sec period).

- It was shown that the displacement and hysteretic energy response of S-SDOF systems decreases by larger stiffness ratio (α) and smaller gap size (or R_g) and smaller mass ratio (**m**). Variation of the strength ratio (β) has negligible effect on the displacement response ratios. But S-SDOF systems dissipate higher hysteretic energy as strength ratio increases.

- In determining force and displacement responses of S-SDOF systems, the R_y and β factors are the most important parameters. Based on this fact, the AASHTO RS can be adjusted for S-SDOF systems by multiplying the force coordinate by (β+1) / R_y factor and setting upper force limits as stated in Table 5-2. It should be noted that this adjusted spectrum is valid for stiffening systems that have stiffening parameters within the range considered (Table 3-1)

CHAPTER 6

SUMMARY AND CONCLUSIONS

Placing some parts of the United States (including New Jersey) in higher seismic zones by the 1988 NEHRP maps has raised attention to the earthquake response of MSSS bridges that originally designed for carrying gravity loads. Due to the large number of MSSS bridges on the targeted region, the evaluation of the bridges relies on the simplified and routine standard procedures and guidelines [FHWA, 1995] that also include pseudo-static earthquake analysis methods.

For investigating the seismic behavior of MSSS bridges, three cases located in New Jersey with 2, 3, and 4 spans were studied analytically. This is done by detailed computer simulations and nonlinear time history analyses and presenting their particular nonlinear response characteristics. It was shown that the soil-structure interaction and the impact between bridge components are among the most important factors affecting the nonlinear response. It was found MSSS bridges behave in stiffening fashion when gaps among pier bents and abutments in longitudinal direction close and system gains more stiffness (a pushover diagram better presents this behavior).

Current pseudo-static methods for MSSS bridges do not employ especial design response spectrum (RS) for stiffening systems and might lead to unreliable analysis results. To develop a stiffening design RS, an extensive parametric study on simple stiffening models was required. Therefore, through evaluation of different MSSS bridge components including pier columns, abutments, and backfill soils, geometrical ranges as well as capacity and stiffness ranges for these components are determined and used both

in defining simple stiffening systems (Figure 3-1) and performing an extensive parametric analysis.

Furthermore, in investigating stiffening systems different damage criteria useful in performance-based seismic engineering are employed in an extensive parametric study that had more than 367,000 analysis cases for simple stiffening models. In the parametric study, for considering variety of seismic events and frequency contents, 41 different strong motion records representing different sites were used. To narrow down the scatter of the responses and reaching to a higher confidence band, a scaling method that uses the AASHTO RS as its target, were employed. The analysis results were stored and managed in a database where the response characteristics investigated through Mean-Plus-One-Standard-Deviation (MPOSD) response values.

In the parametric study, the S-SDOF systems (i.e., the base component with surrounding interacting environments) were compared to B-SDOF systems (i.e., base component without interacting environment) and shown that how variations in stiffening parameters (i.e., strength, stiffness, gap size, and mass) affect the S-SDOF behavior in terms of different damage indices and response parameters. The Results were presented in response ratio format (i.e., S-SDOF/B-SDOF) for better comparison of B-SDOF and S-SDOF systems. It was shown that although S-SDOF systems generally have smaller displacement response compared to B-SDOF systems, they dissipate much higher hysteretic energy (as much as 5 times more) especially at periods larger than 0.7 second. Other response parameters and damage indices are more or less related to the displacement or dissipated hysteretic energy and mostly show higher damages for S-SDOF systems especially at higher period ranges.

In developing pseudo-static analysis methods for stiffening systems, a stiffening design response spectrum was needed. For obtaining such RS, the response database was viewed in force-displacement format per different R_y (i.e., yield force factor) and β (i.e., strength ratio) values. The results showed that by multiplying a factor (Equation (40) to the force coordinate of the AASHTO RS (ARS) and setting new upper force limits (Table 5-1), a stiffening response spectrum (ASRS) that has a good agreement with database results and MPOSD curves would be obtained. It was shown that for MSSS bridges in longitudinal direction, provided that their stiffening parameter values exist in the range considered (Table 3-1), ASRS is a more accurate response spectrum compared to ARS. At the end, the practical application of stiffening RS was demonstrated by analyzing one of the bridges in the longitudinal direction (Figure A.58 and Figure A.59).

6.1 Conclusions

By performing MSSS bridge case studies and extensive parametric analysis of S-SDOF systems, their general behavior and nonlinear seismic response characteristics are explained and investigated. The summary of the results is as follow:

- Seismic response of MSSS bridges is complicated by the potential impact between adjacent spans. Generally, impact reduces displacements, however it significantly increases the level of forces in the bearings. Due to impact forces, bearing failure is quite possible even under low level of peak ground acceleration. Assuming a post-failure behavior at the bearings characterized by stable Coulomb friction, bearing failure over pier bents will act like a fuse and reduces the demand

on the pier bents. Should the bearing remain elastic (not fail), shear failure of pier columns with low lateral reinforcement is likely, even under low levels of PGAs.

- Seismic response of MSSS bridges is sensitive to soil-structure interaction and should be considered in dynamic analysis of this type of bridges. This was recognized and investigated in the S-SDOF parametric study by considering various values for the strength, the stiffness, and the mass of IE components. It was shown that within the range considered, the displacement and hysteretic energy responses of S-SDOF systems decrease by larger stiffness ratio (α), smaller gap size, and smaller mass ratio (**m**). Displacement response of S-SDOF systems was not sensitive to the "variation" of the strength ratio (β) within the range considered, but dissipated hysteretic energy response increased for larger strength ratios.

- In comparison to B-SDOF systems, inelastic S-SDOF systems have smaller displacement responses and at periods longer than 0.7 second, dissipate larger hysteretic energy. The dissipated energy ratio is higher for systems with lower strengths (i.e., smaller R_y factor). On MPOSD curves the response ratio reaches to as high as 5, 3, and 2 for stiffening systems with R_y factor equal to 2, 3, and 5, respectively. All other damage indices in general predict higher damage for S-SDOF systems at long periods with smaller R_y factor.

- The AASHTO RS (ARS) can be adjusted by multiplying the force coordinate by "$(\beta+1) / R_y$" factor and setting upper force limits as stated in Table 5-1 to obtain the AASHTO Stiffening RS (ASRS). The ASRS has a good agreement with the MPOSD values determined from the response database.

6.2 Future Work

The analytical study of stiffening systems through simplified S-SDOF modeling can be expanded in several ways:

- Adding asymmetric stiffening parameters to the developed analytical model. This can be done by defining different IE components at each side of the base system and even considering several (more than 2) IE components. Such a model would be more similar to the real asymmetric situations seen in MSSS bridges.

- Calculating comparable analytical response parameters and damage indices to the test results. This can be done through studying hysteretic loops for different materials and cross sectional details and trying to analytically implement them into the simple stiffening models. Such advanced stiffening models can be used directly in a performance-based analysis procedure.

- Considering more discrete values and stiffening modeling options in the parametric study to expand the response. The developed database can be linked to an interface program so it can be accessed locally and over the network connection. By doing so, there would be an instant access to the responses of any particular stiffening system and its design response spectrum. Such interface connection can be used by practicing engineers to evaluate different stiffening systems in a performance-based analysis procedure.

APPENDIX

FIGURES

The following figures (explained in chapter 5) present; the comparison of the responses for S-SDOF and B-SDOF systems, the effects of the stiffening parameters on the response ratios (S-SDOF/B-SDOF), response spectra for S-SDOF systems, and the pushover analysis for stiffening systems (MSSS Bridges).

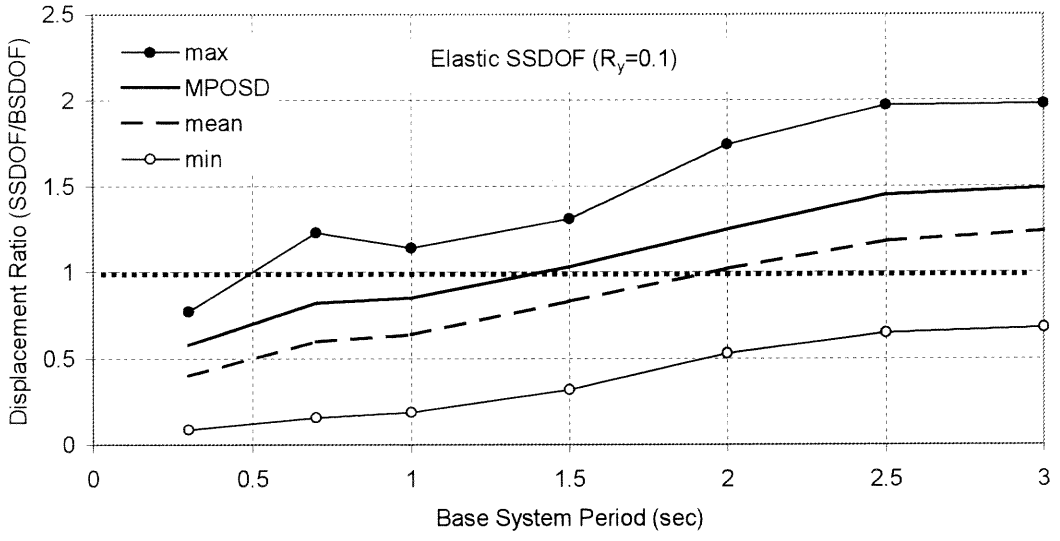

Figure A.1 Displacement Ratios for Elastic Stiffening Systems (Ry=0.1)

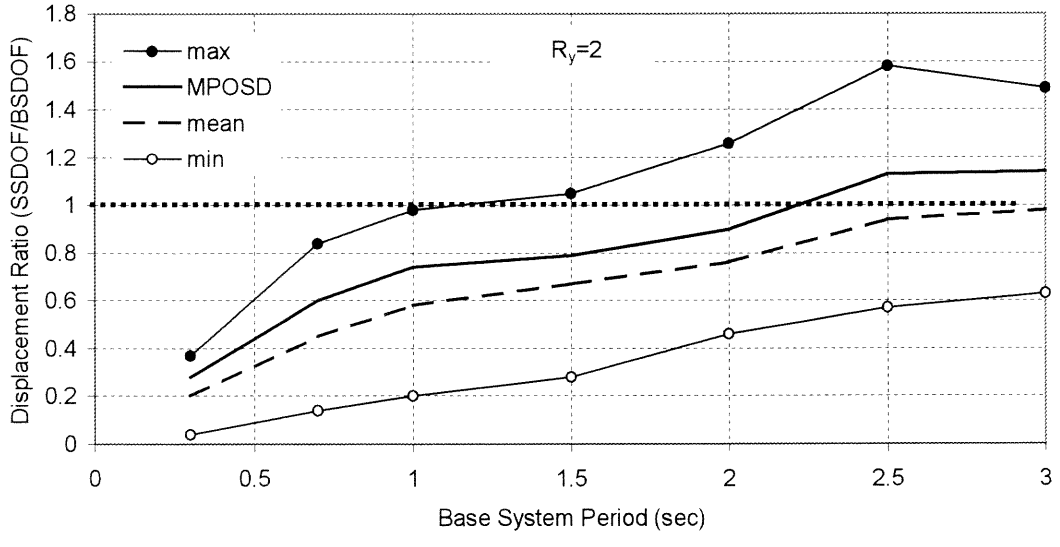

Figure A.2 Displacement Ratios for Stiffening Systems with Ry Factor of 2

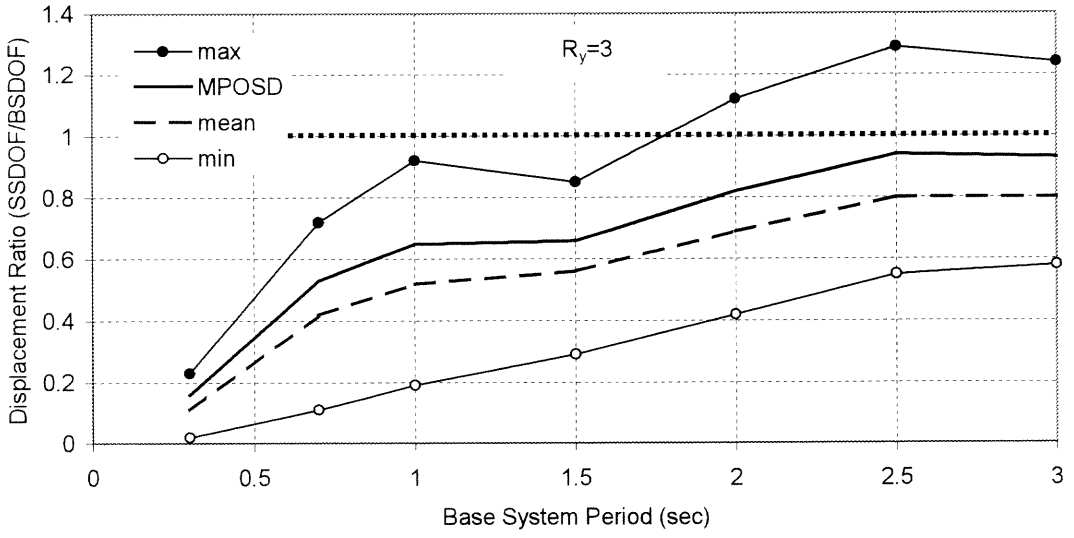

Figure A.3 Displacement Ratios for Stiffening Systems with Ry of 3

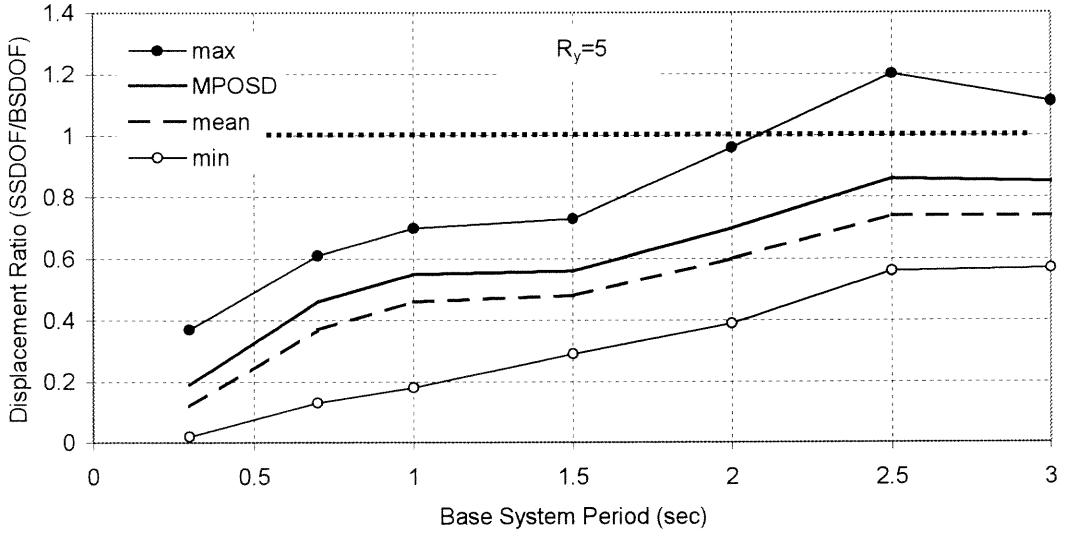

Figure A.4 Displacement Ratios for Stiffening Systems with Ry Factor of 5

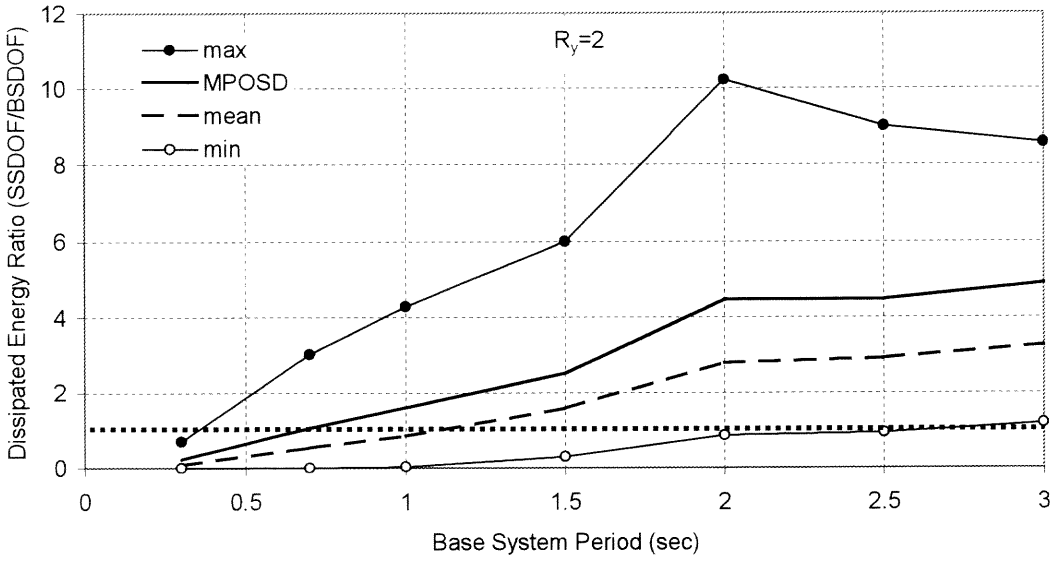

Figure A.5 Dissipated Hysteretic Energy Response Ratios for Stiffening Systems with Ry Factor of 2

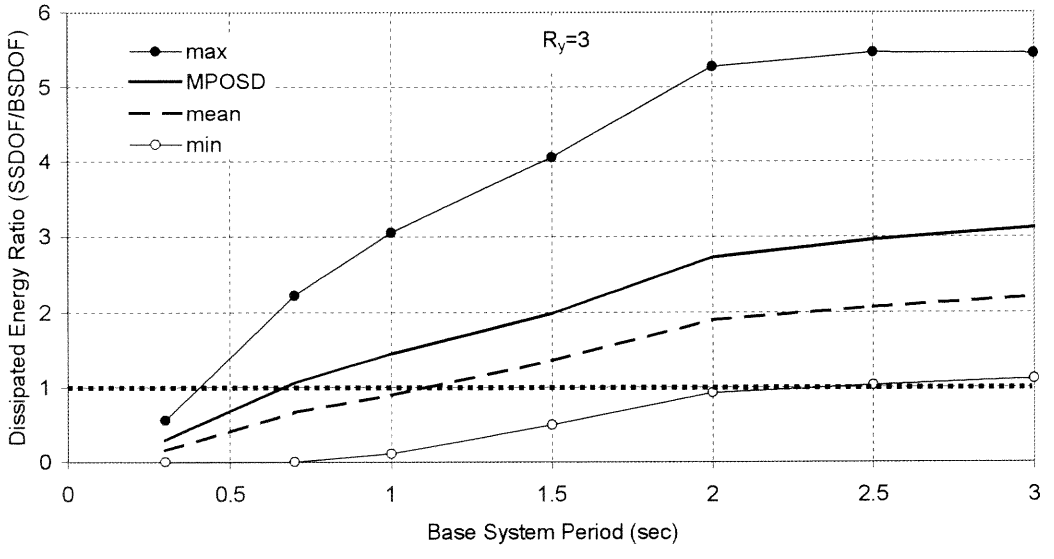

Figure A.6 Dissipated Hysteretic Energy Response Ratios for Stiffening Systems with Ry Factor of 3

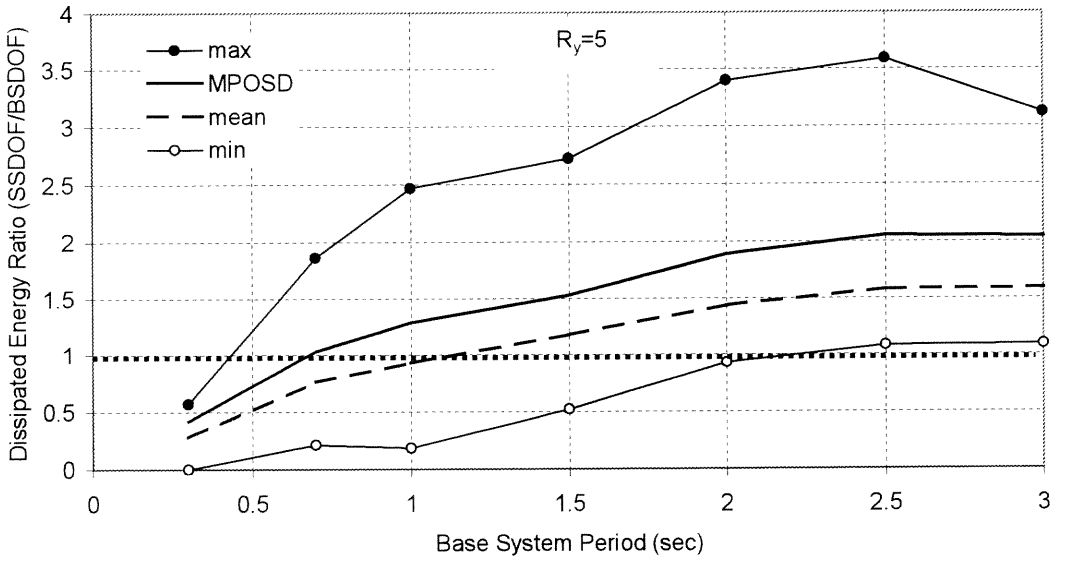

Figure A.7 Dissipated Hysteretic Energy Response Ratios for Stiffening Systems with Ry Factor of 5

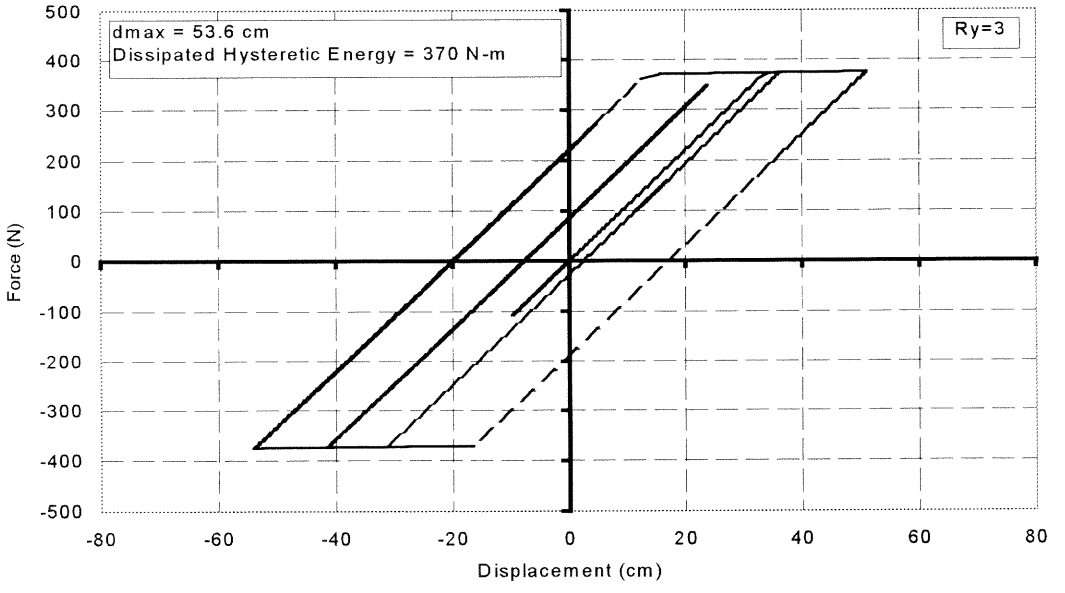

Figure A.8 Hysteretic Force-Displacement Response of a B-SDOF System (T=2.5 sec, Ry=3)

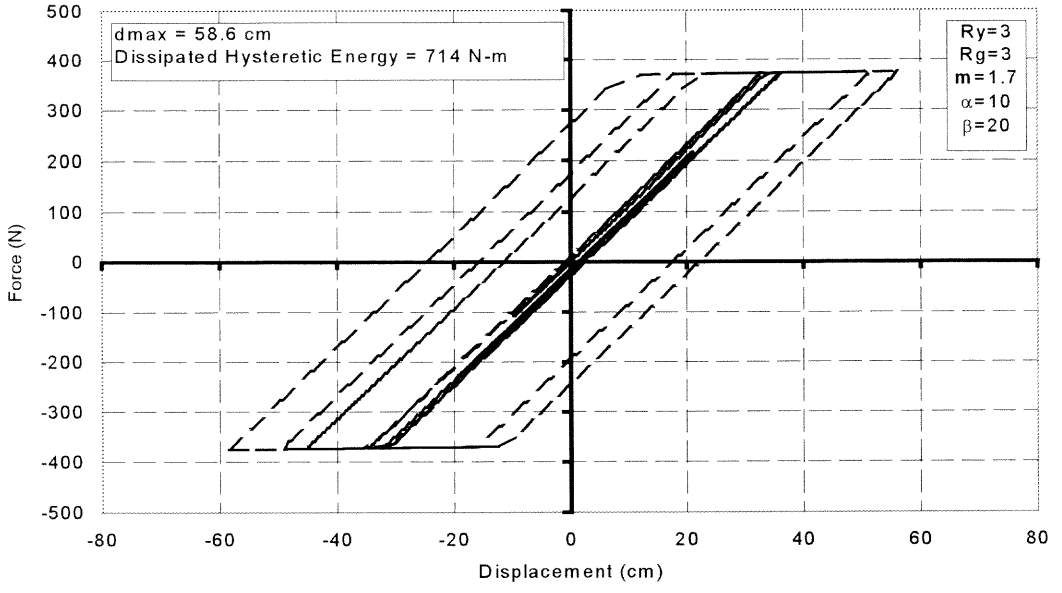

Figure A.9 Hysteretic Force-Displacement Response of an S-SDOF System (T=2.5 sec, Ry=3, Rg=3, α=10, β=20, **m**=1.7)

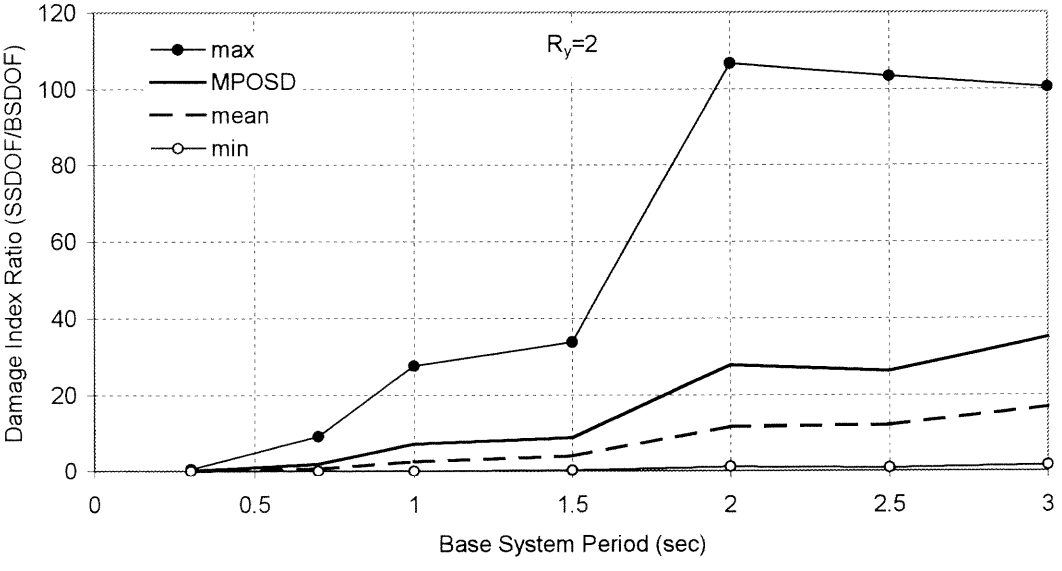

Figure A.10 DI Ratios for Stiffening Systems with Ry Factor of 2

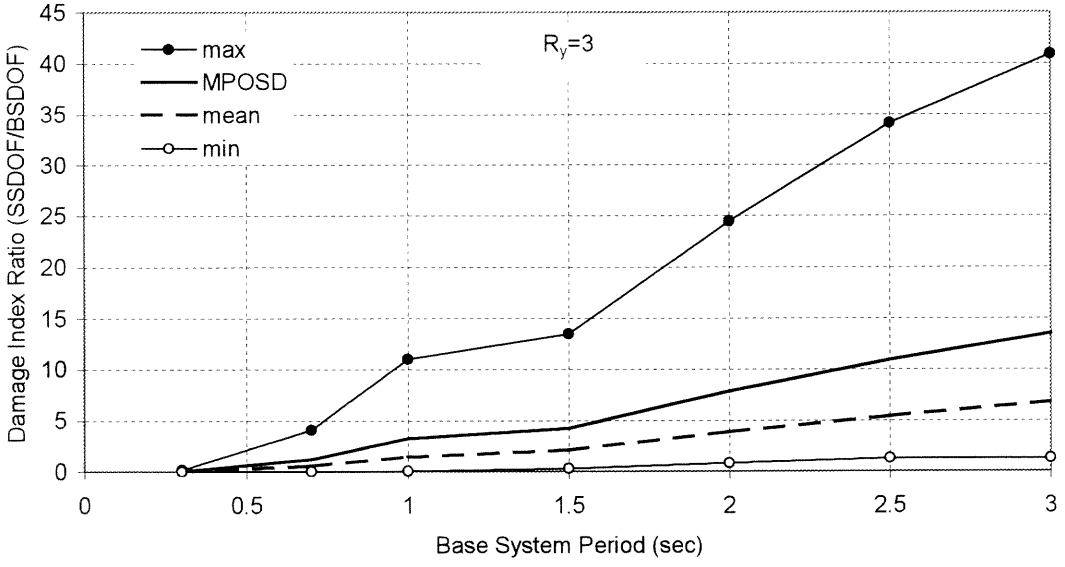

Figure A.11 DI Ratios for Stiffening Systems with Ry Factor of 3

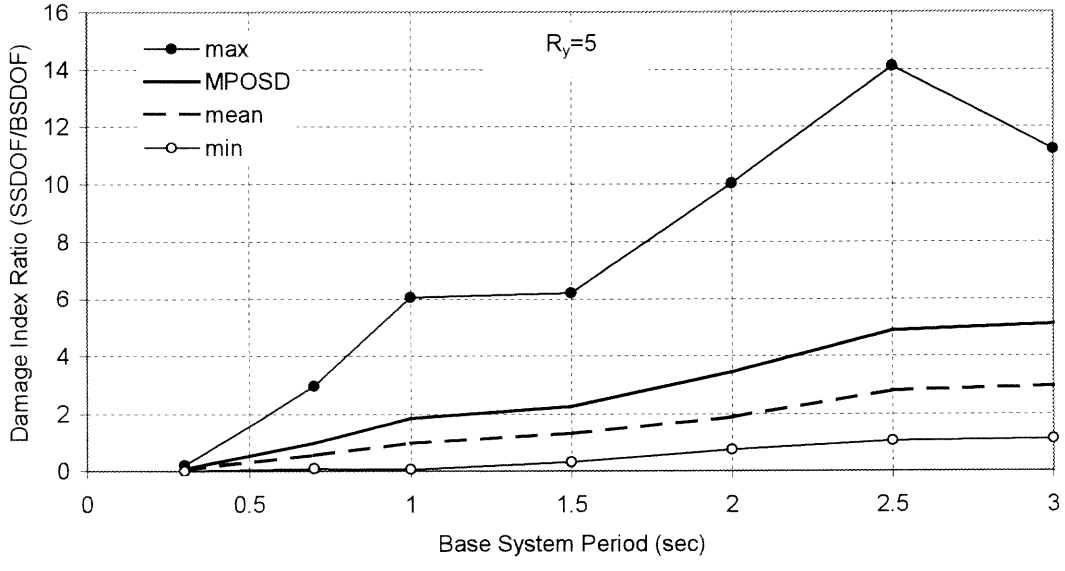

Figure A.12 DI Ratios for Stiffening Systems with Ry Factor of 5

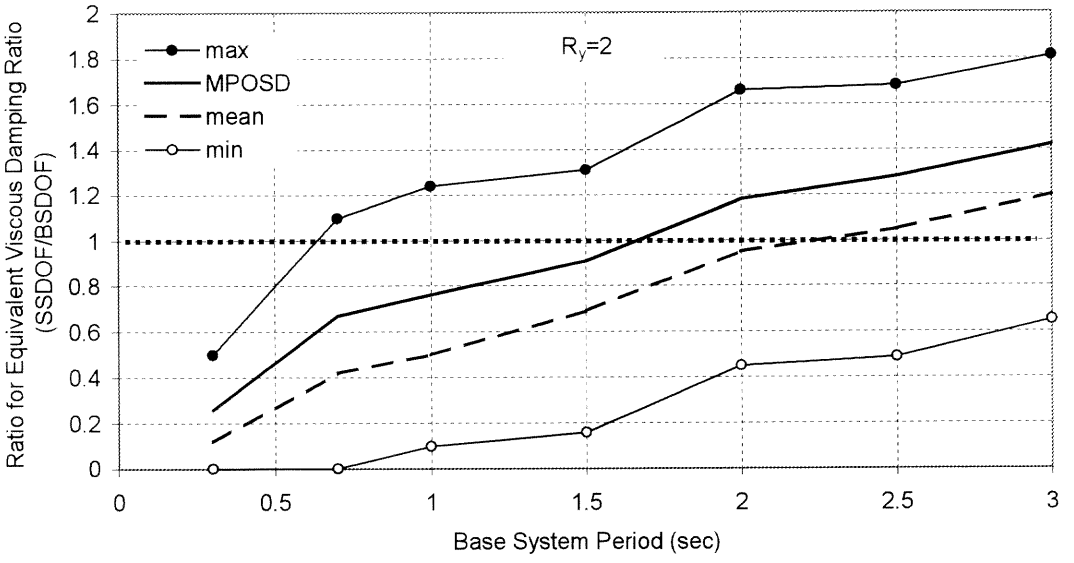

Figure A.13 ζ_{eq} Ratios for Stiffening Systems with Ry Factor of 2

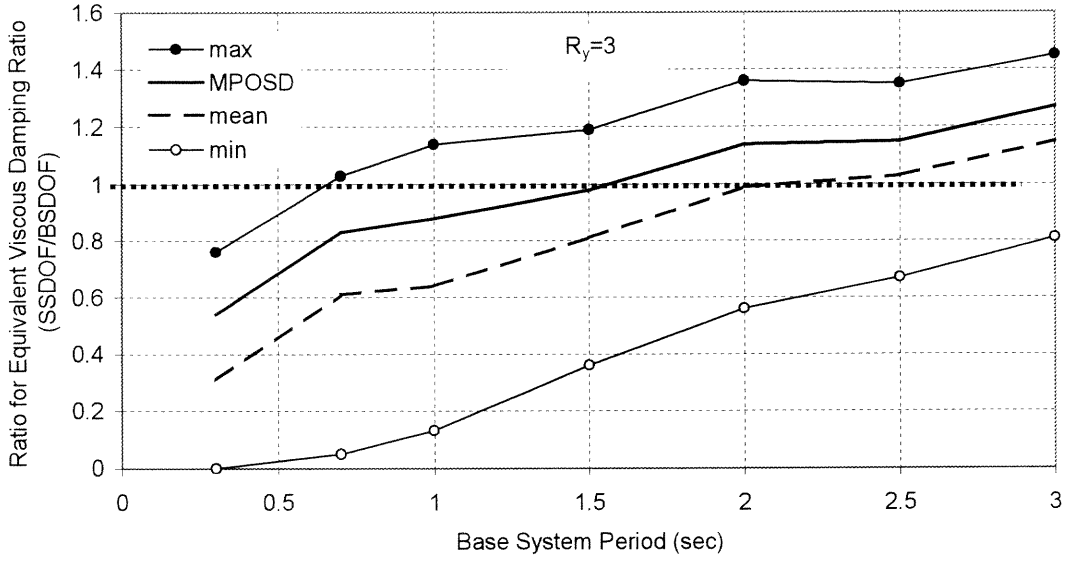

Figure A.14 ζ_{eq} Ratios for Stiffening Systems with Ry Factor of 3

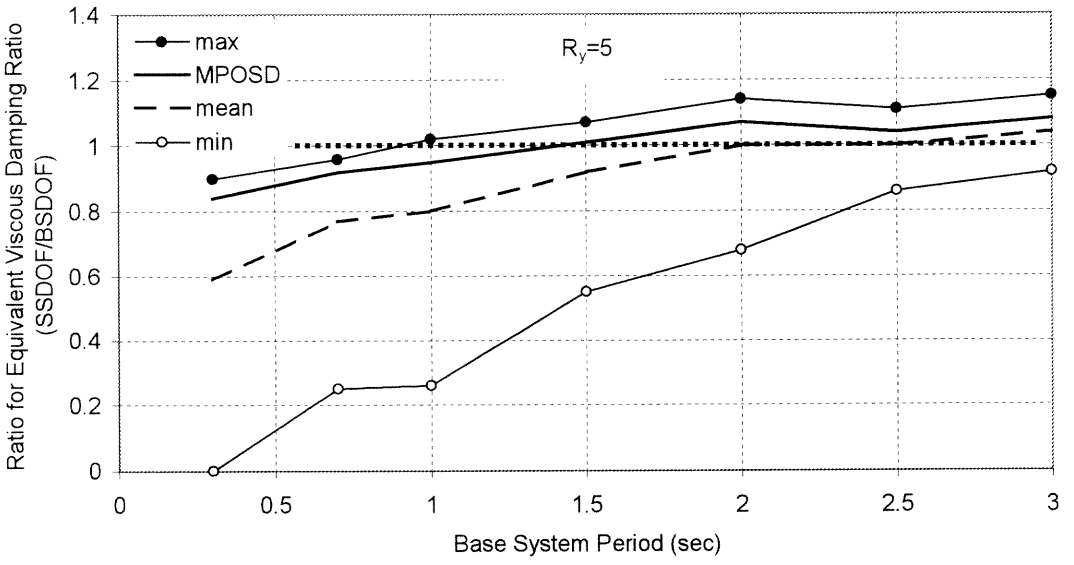

Figure A.15 ζ_{eq} Ratios for Stiffening Systems with Ry Factor of 5

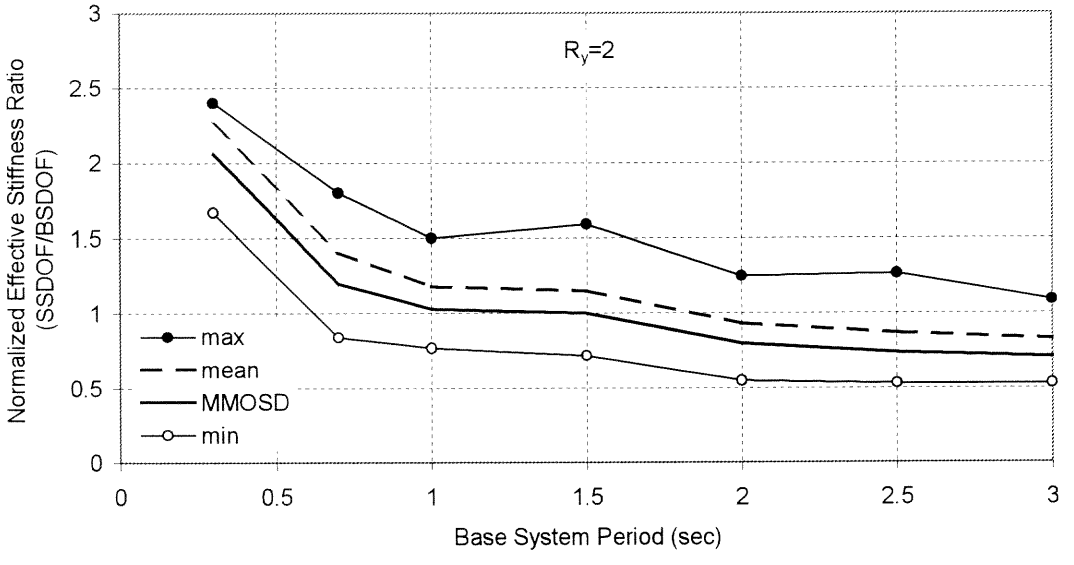

Figure A.16 n_k Ratios for Stiffening Systems with Ry Factor of 2

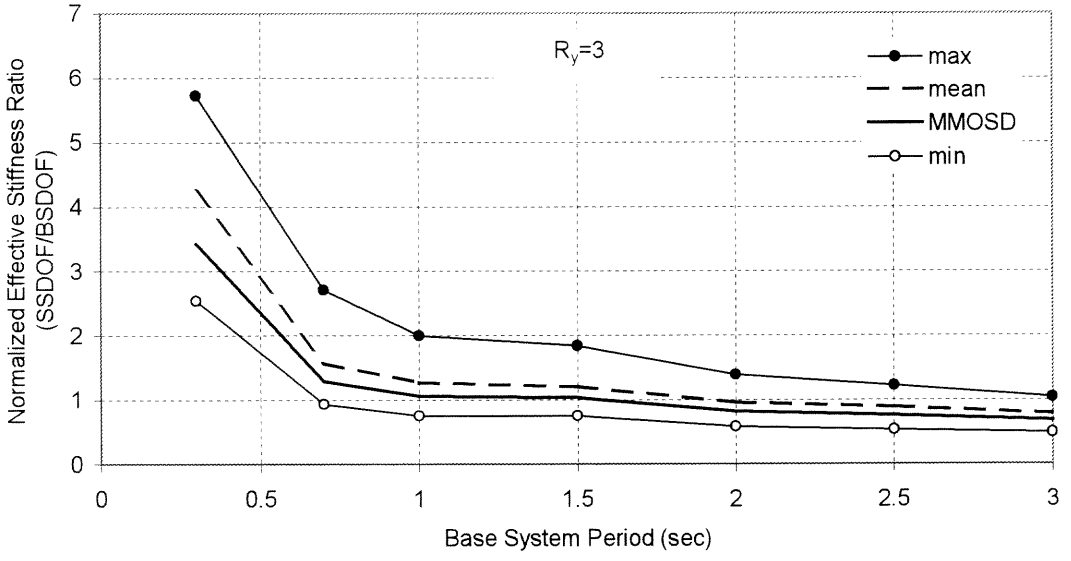

Figure A.17 n_k Ratios for Stiffening Systems with Ry Factor of 3

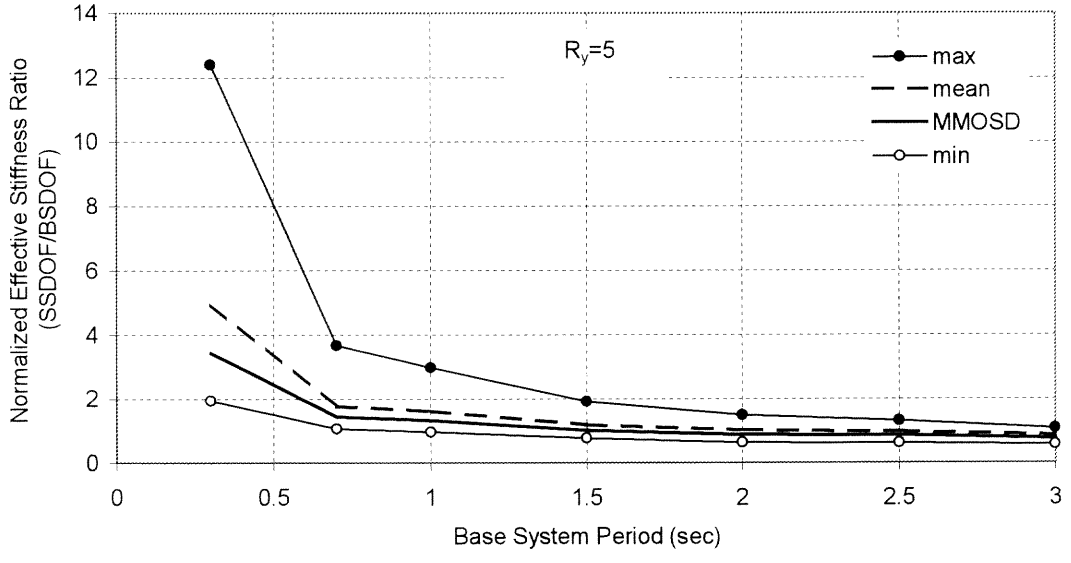

Figure A.18 n_k Ratios for Stiffening Systems with Ry Factor of 5

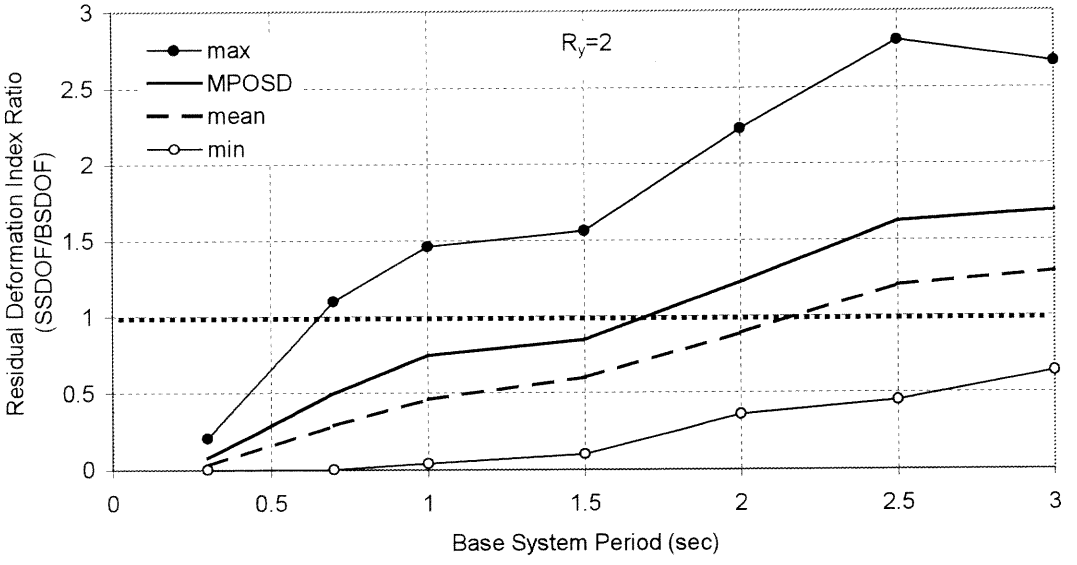

Figure A.19 RDI Ratios for Stiffening Systems with Ry Factor of 2

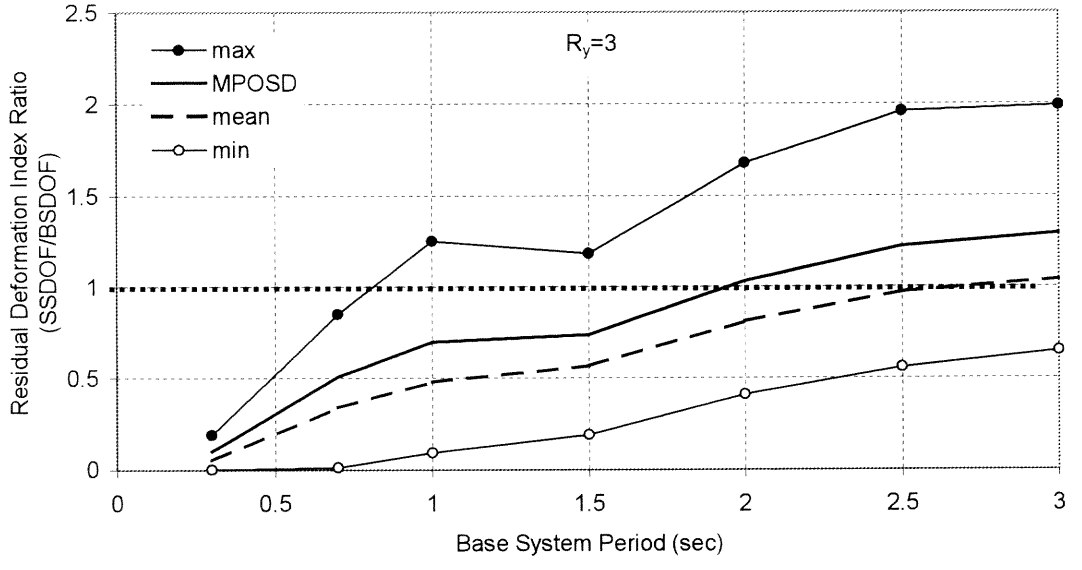

Figure A.20 RDI Ratios for Stiffening Systems with Ry Factor of 3

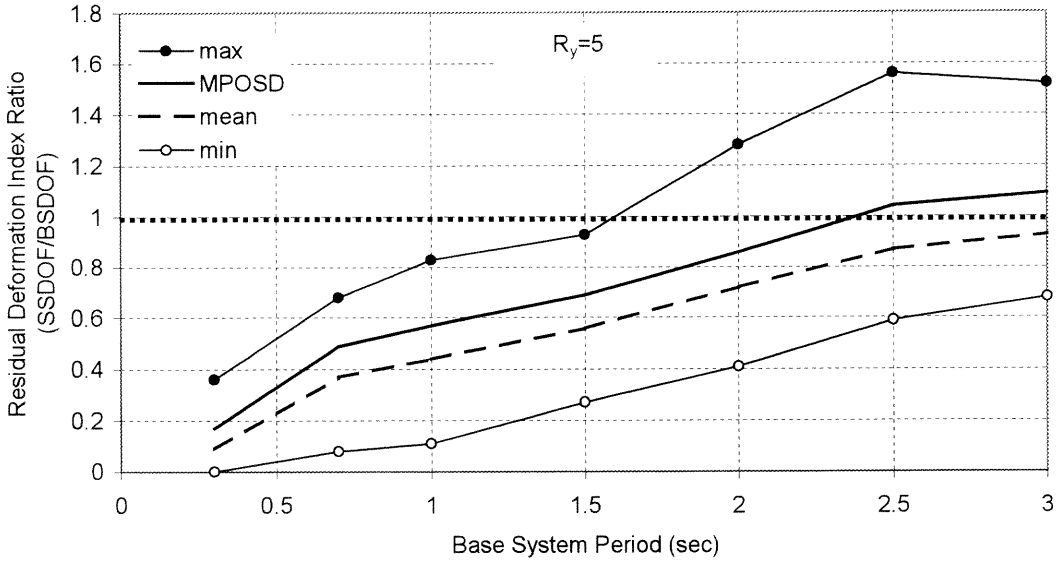

Figure A.21 RDI Ratios for Stiffening Systems with Ry Factor of 5

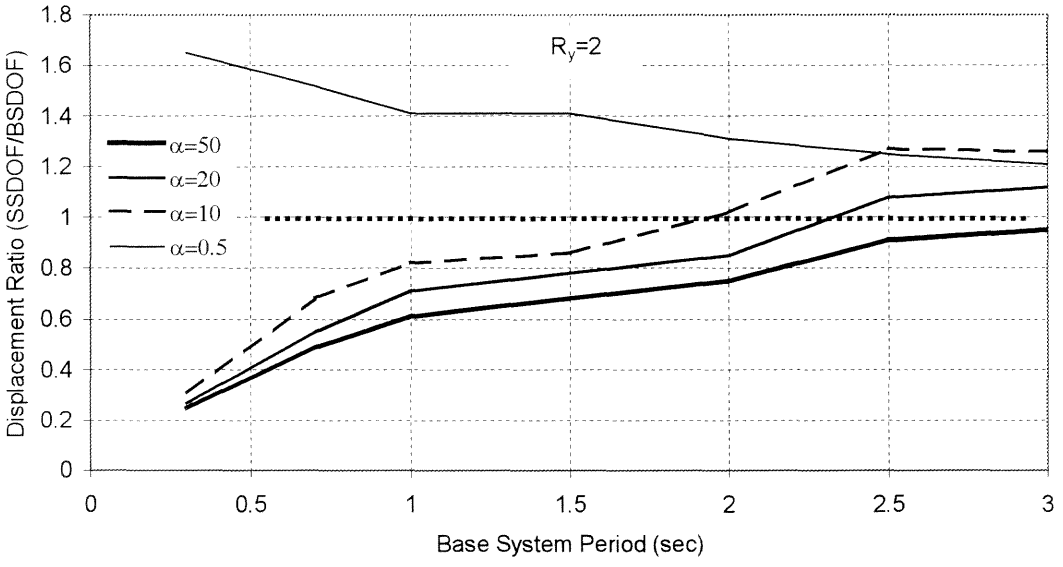

Figure A.22 Effect of α on the Displacement Response of S-SDOF Systems with Ry Factor of 2

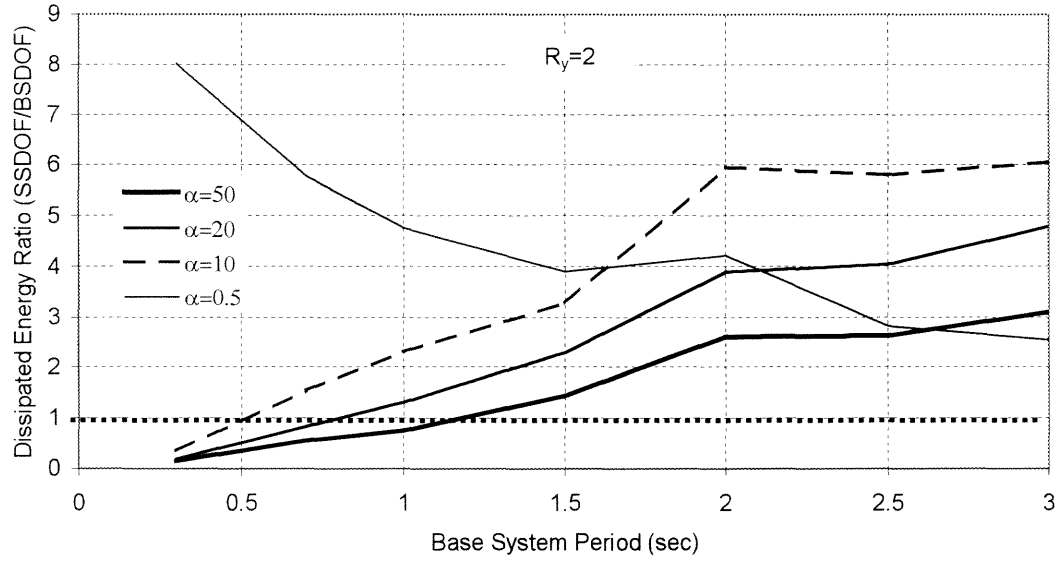

Figure A.23 Effect of α on the Dissipated Hysteretic Energy Response of S-SDOF Systems with Ry Factor of 2

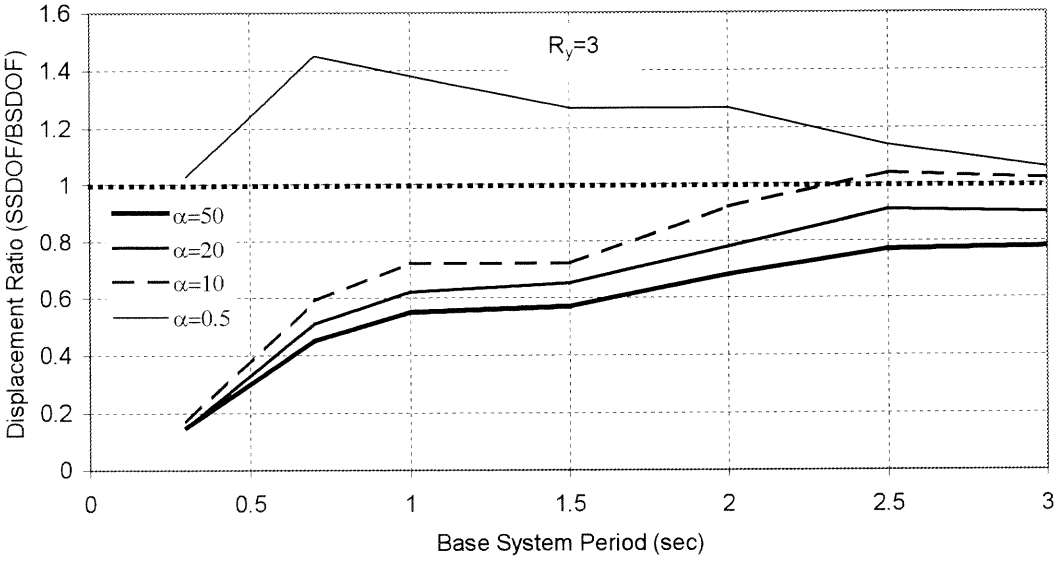

Figure A.24 Effect of α on the Displacement Response of S-SDOF Systems with Ry Factor of 3

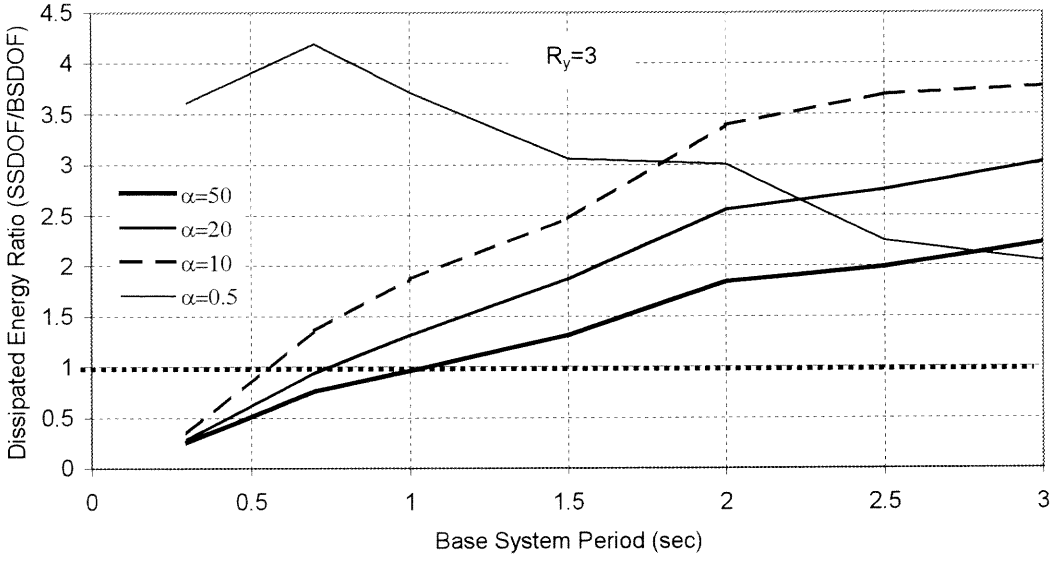

Figure A.25 Effect of α on the Dissipated Hysteretic Energy Response of S-SDOF Systems with Ry Factor of 3

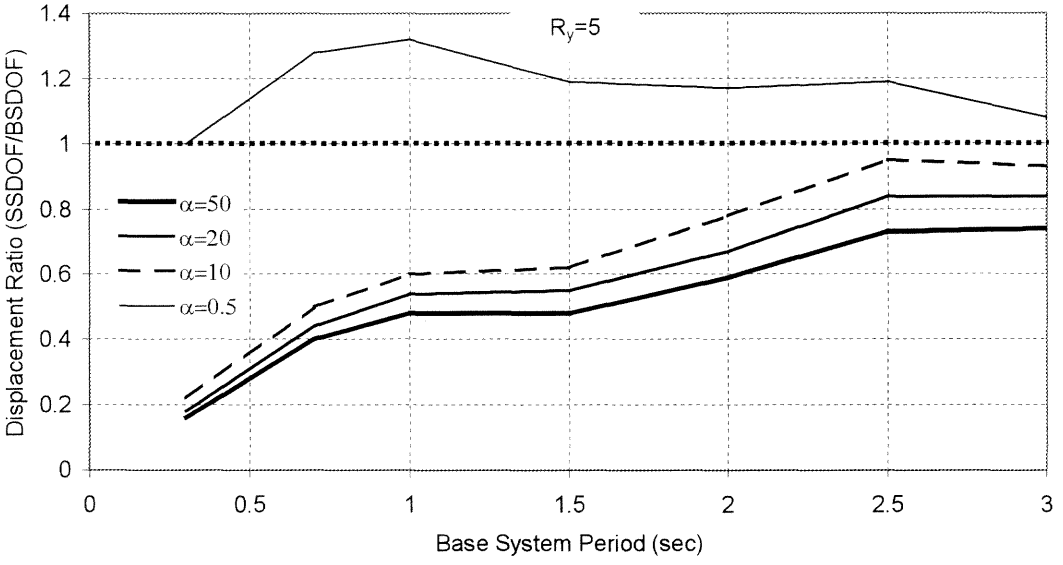

Figure A.26 Effect of α on the Displacement Response of S-SDOF Systems with Ry Factor of 5

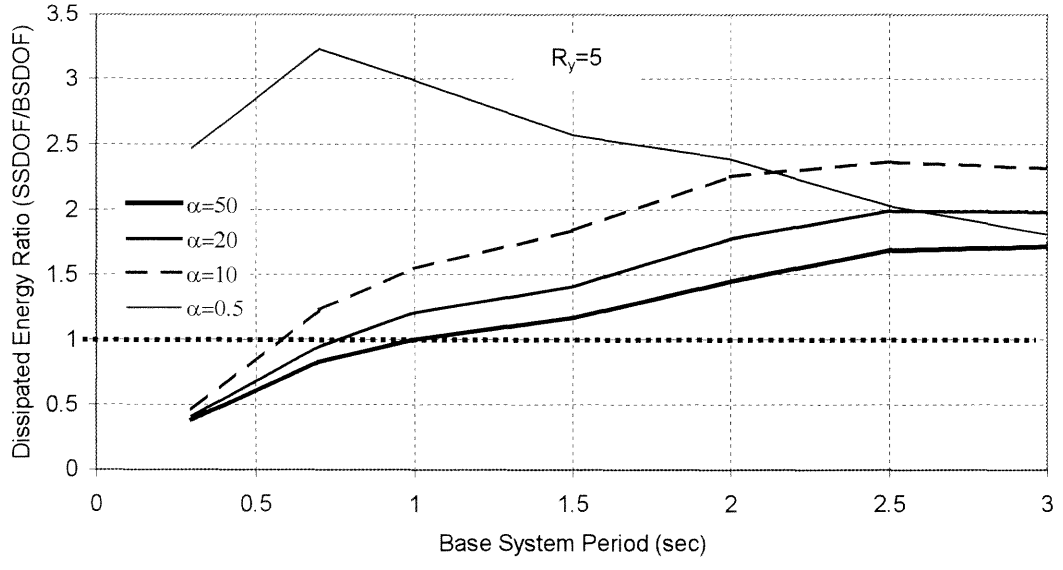

Figure A.27 Effect of α on the Dissipated Hysteretic Energy Response of S-SDOF Systems with Ry Factor of 5

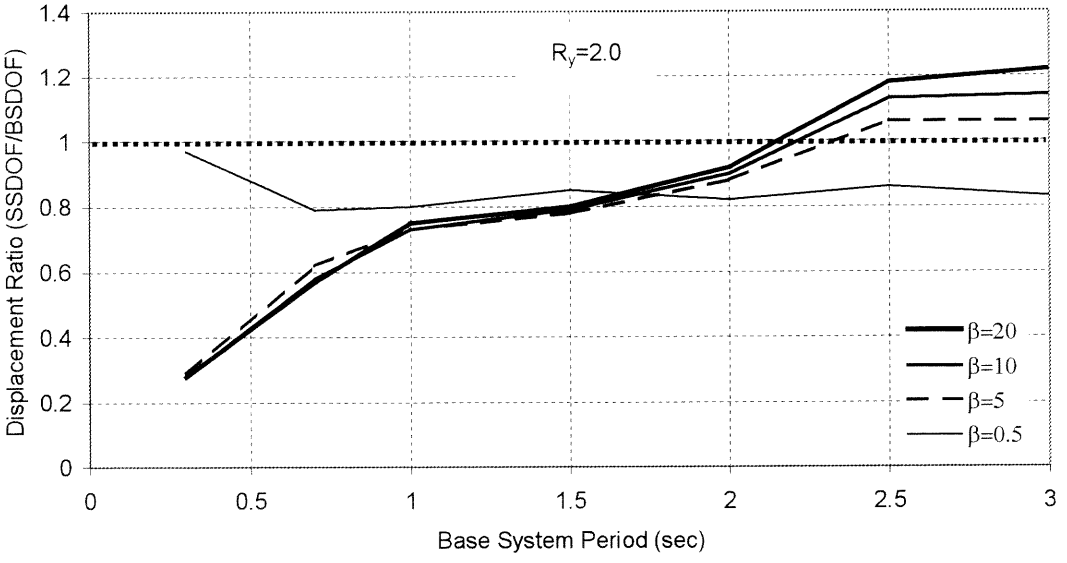

Figure A.28 Effect of β on the Displacement Response of S-SDOF Systems with Ry Factor of 2

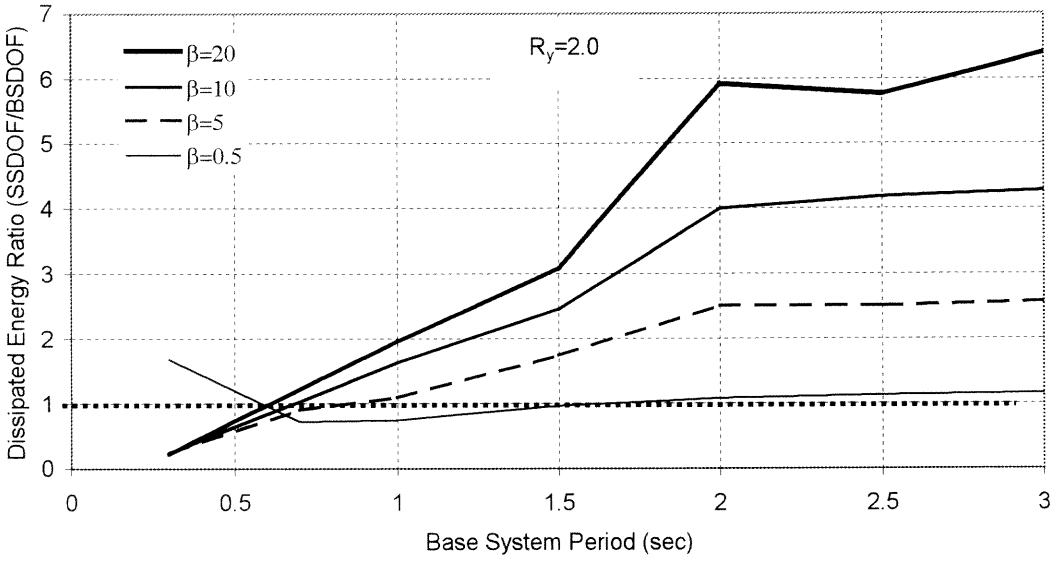

Figure A.29 Effect of β on the Dissipated Hysteretic Energy Response of S-SDOF Systems with Ry Factor of 2

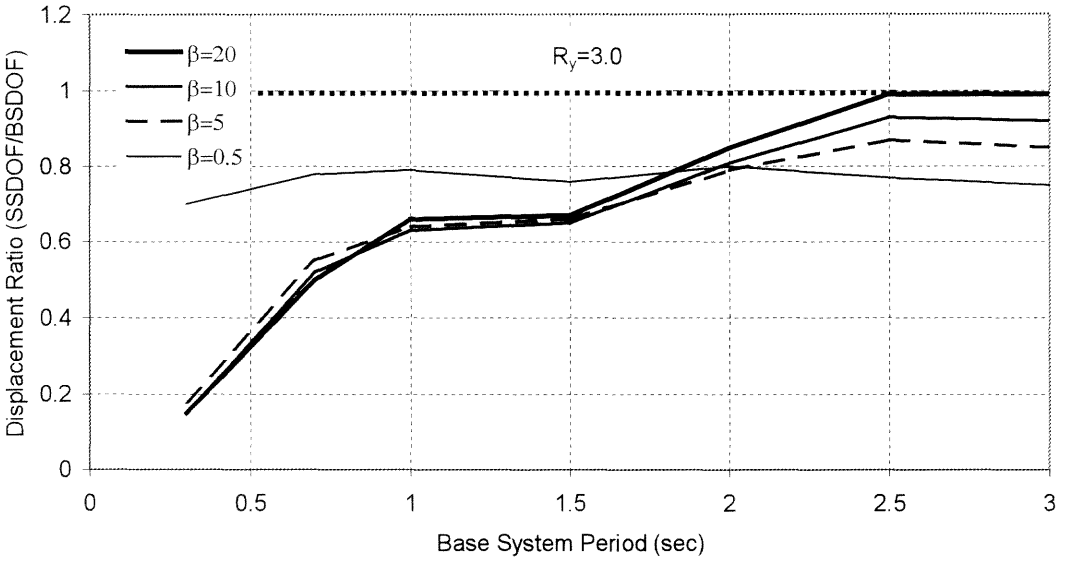

Figure A.30 Effect of β on the Displacement Response of S-SDOF Systems with Ry Factor of 3

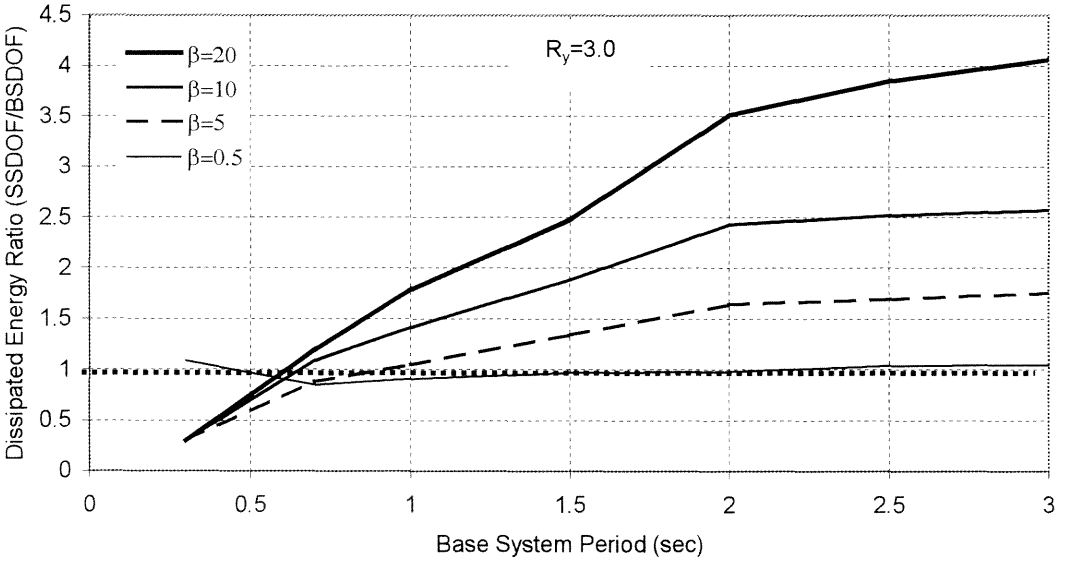

Figure A.31 Effect of β on the Dissipated Hysteretic Energy Response of S-SDOF Systems with Ry Factor of 3

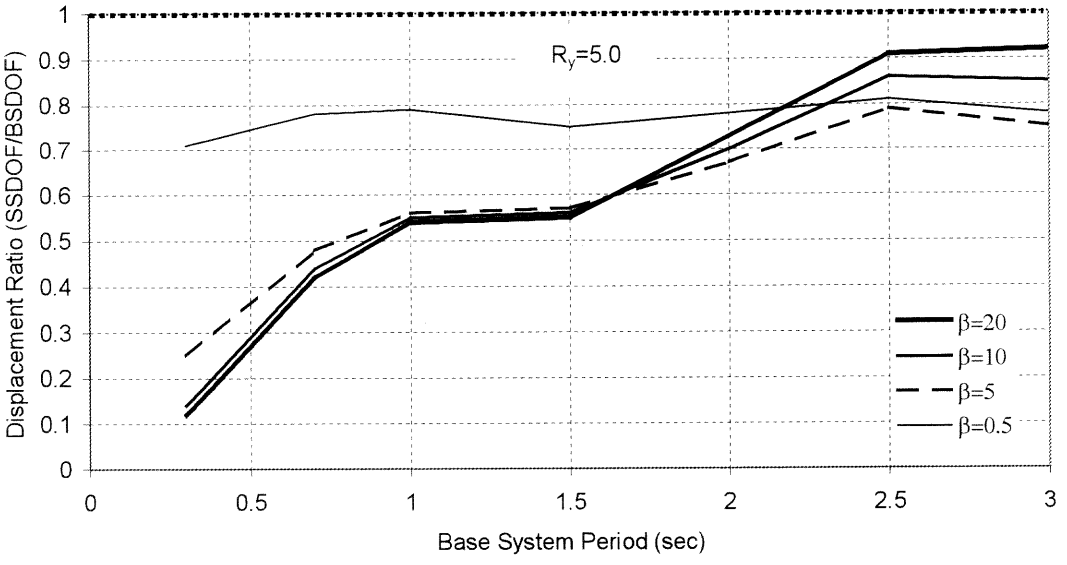

Figure A.32 Effect of β on the Displacement Response of S-SDOF Systems with Ry Factor of 5

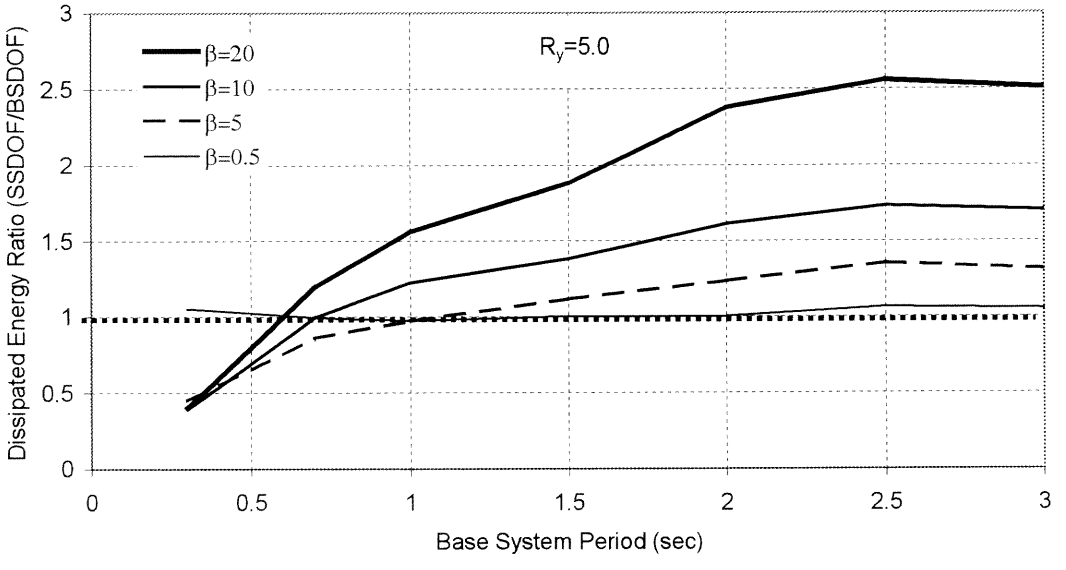

Figure A.33 Effect of β on the Dissipated Hysteretic Energy Response of S-SDOF Systems with Ry Factor of 5

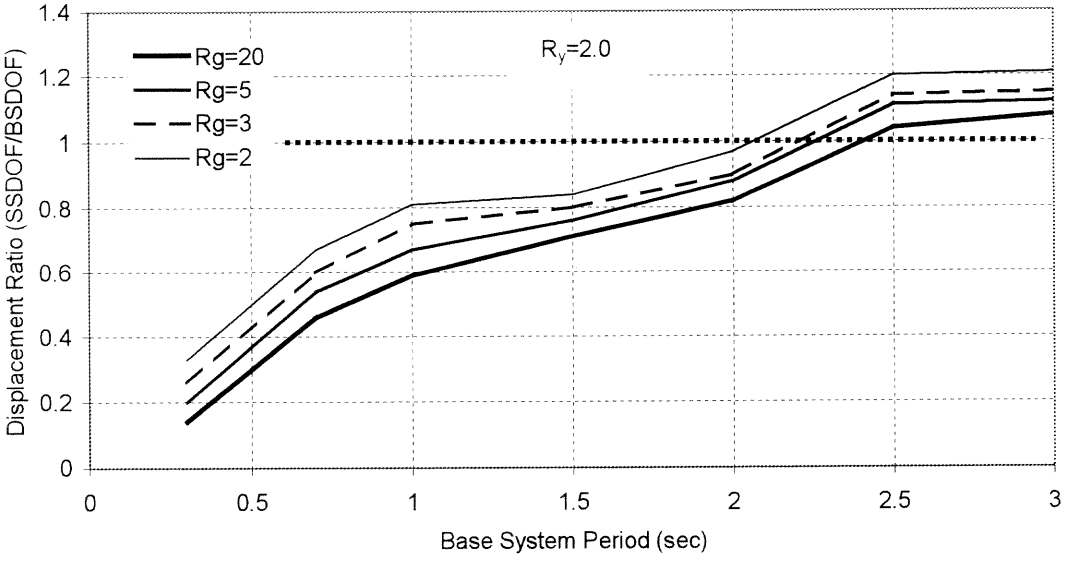

Figure A.34 Effect of Rg on the Displacement Response of S-SDOF Systems with Ry Factor of 2

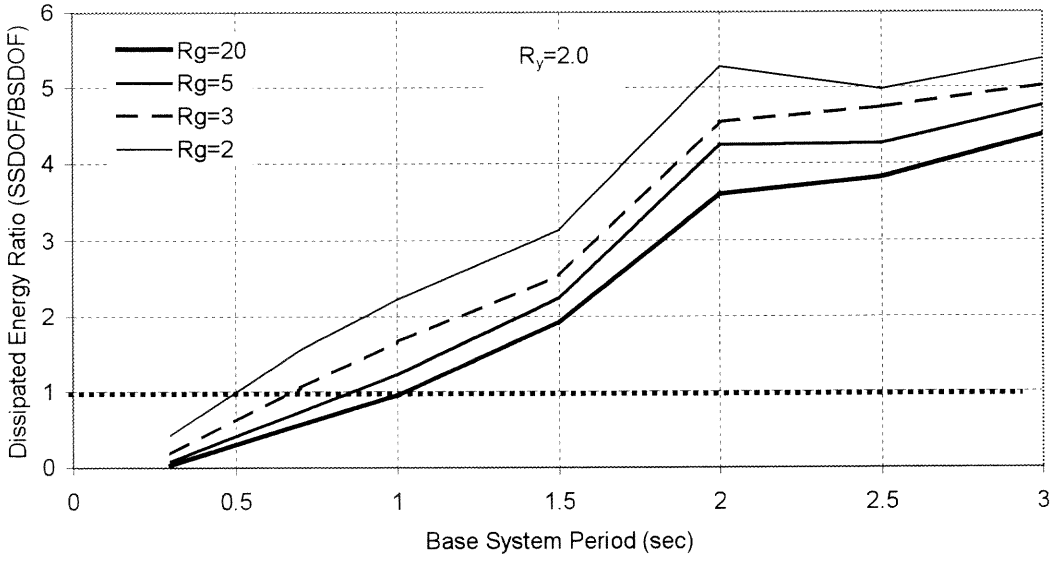

Figure A.35 Effect of Rg on the Dissipated Hysteretic Energy Response of S-SDOF Systems with Ry Factor of 2

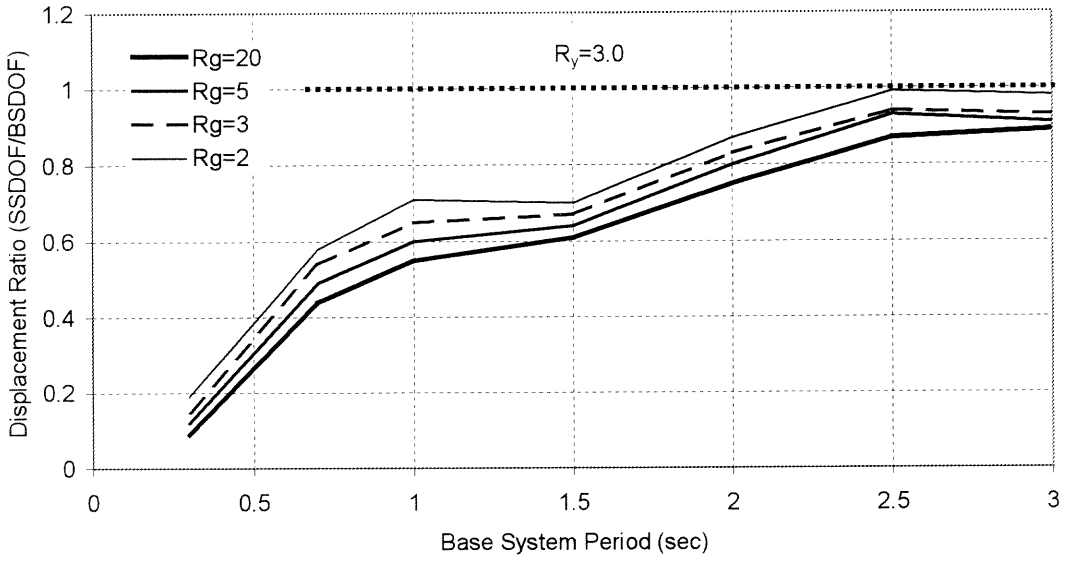

Figure A.36 Effect of Rg on the Displacement Response of S-SDOF Systems with Ry Factor of 3

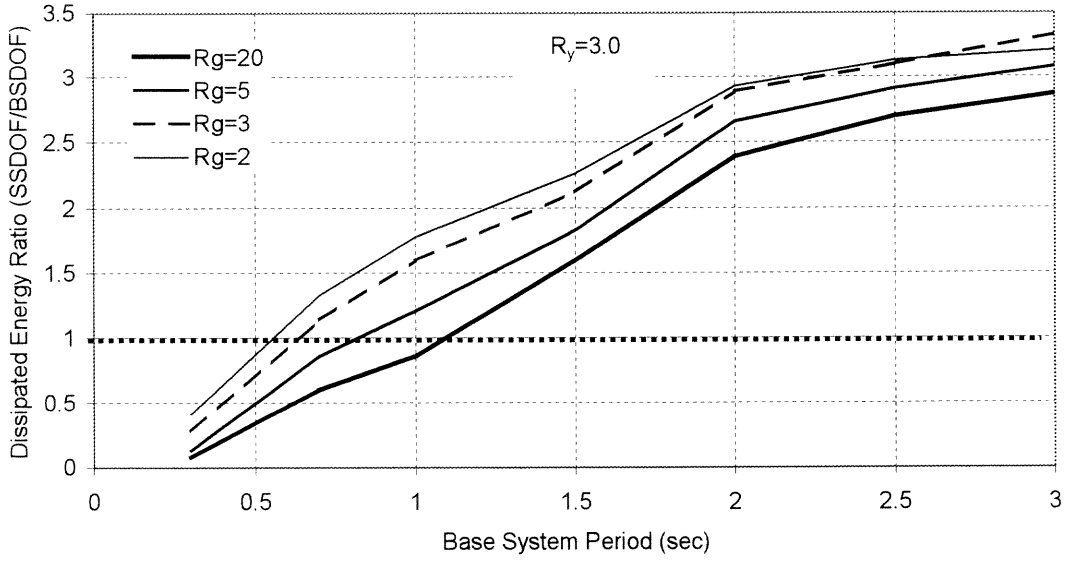

Figure A.37 Effect of Rg on the Dissipated Hysteretic Energy Response of S-SDOF Systems with Ry Factor of 3

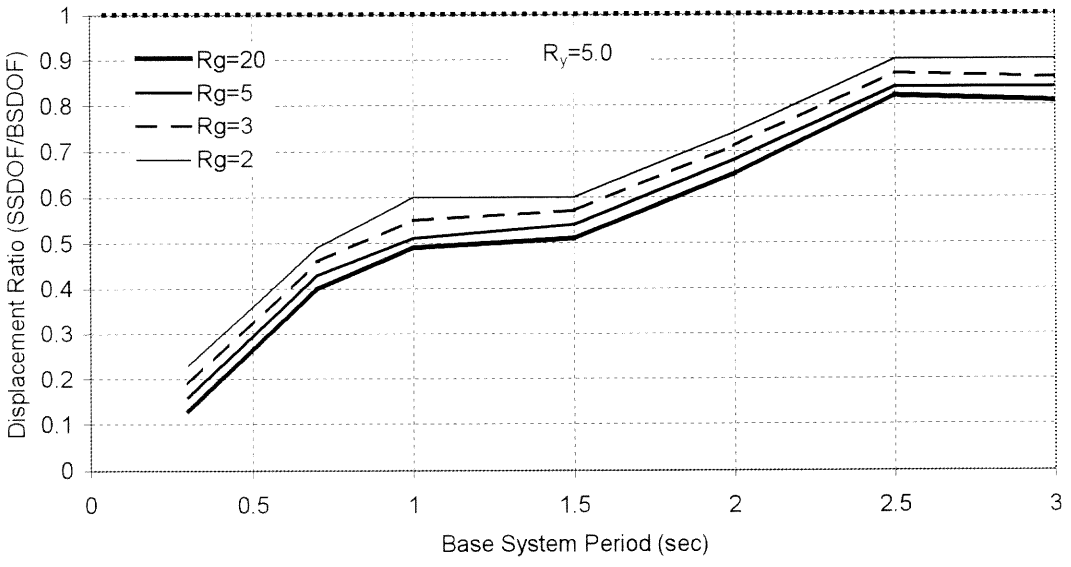

Figure A.38 Effect of Rg on the Displacement Response of S-SDOF Systems with Ry Factor of 5

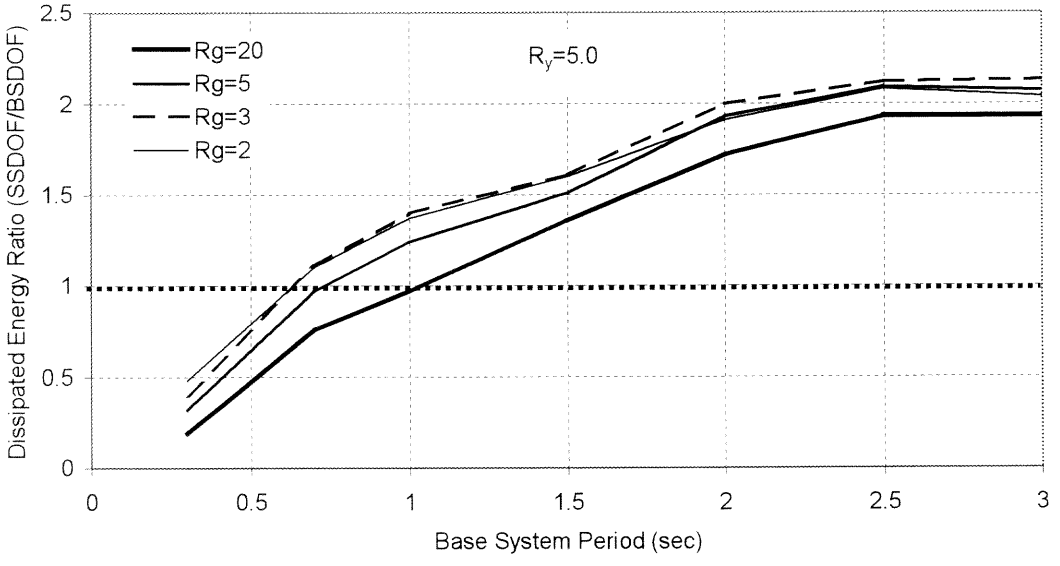

Figure A.39 Effect of Rg on the Dissipated Hysteretic Energy Response of S-SDOF Systems with Ry Factor of 5

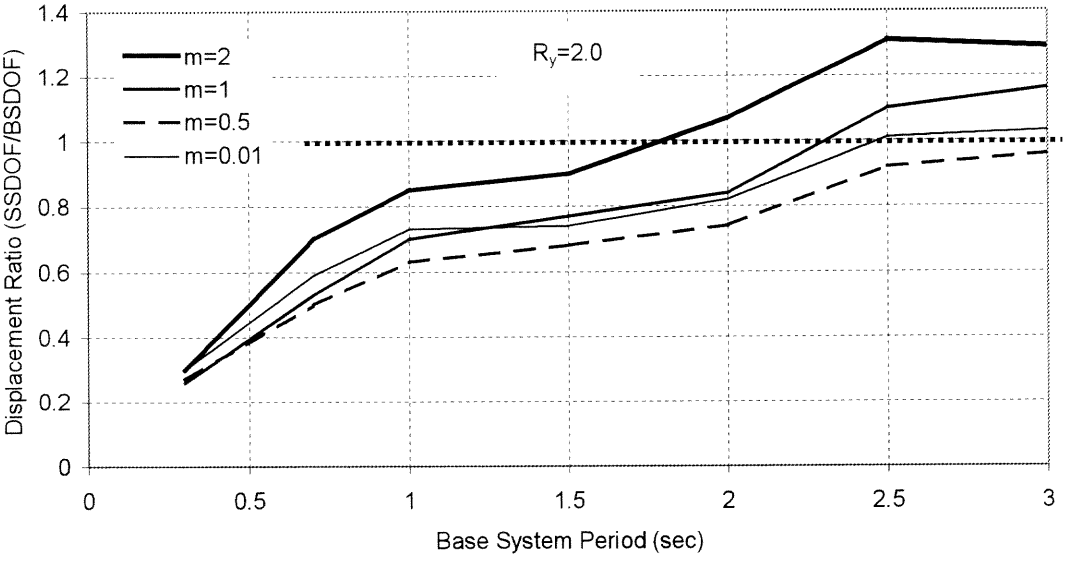

Figure A.40 Effect of **m** on the Displacement Response of S-SDOF Systems with Ry Factor of 2

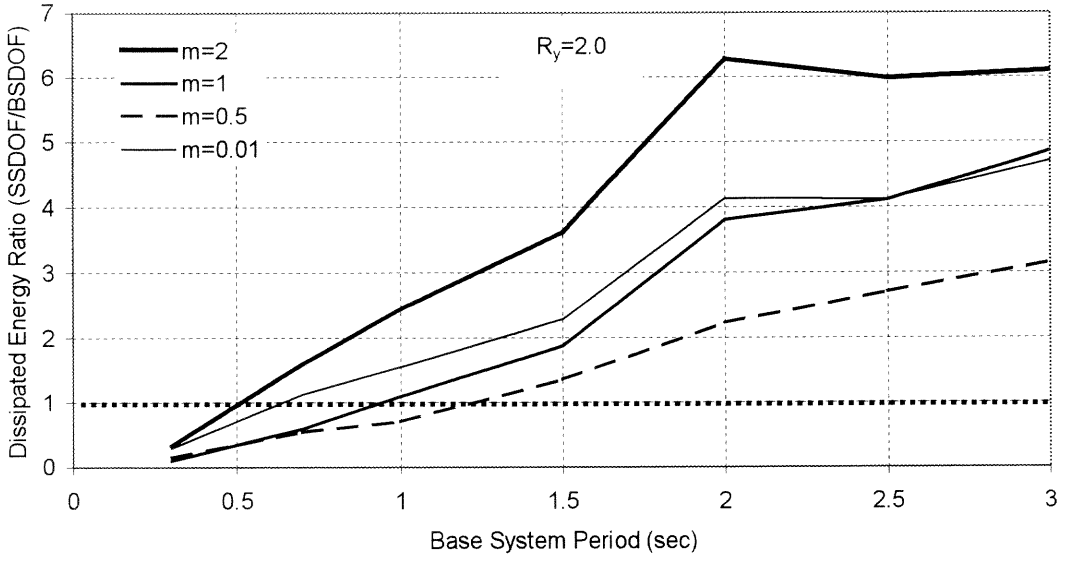

Figure A.41 Effect of **m** on the Dissipated Hysteretic Energy Response of S-SDOF Systems with Ry Factor of 2

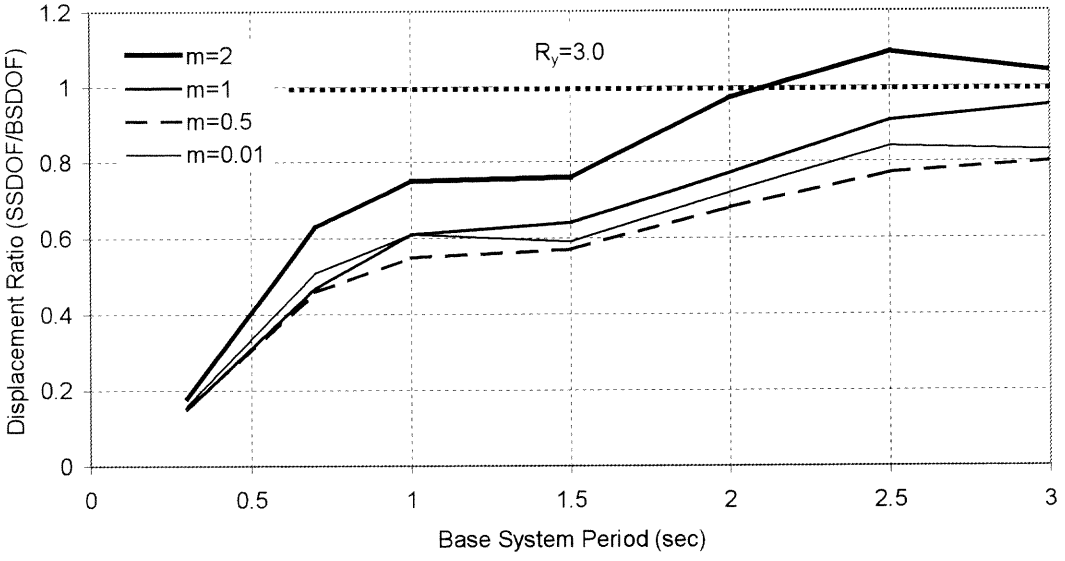

Figure A.42 Effect of **m** on the Displacement Response of S-SDOF Systems with Ry Factor of 3

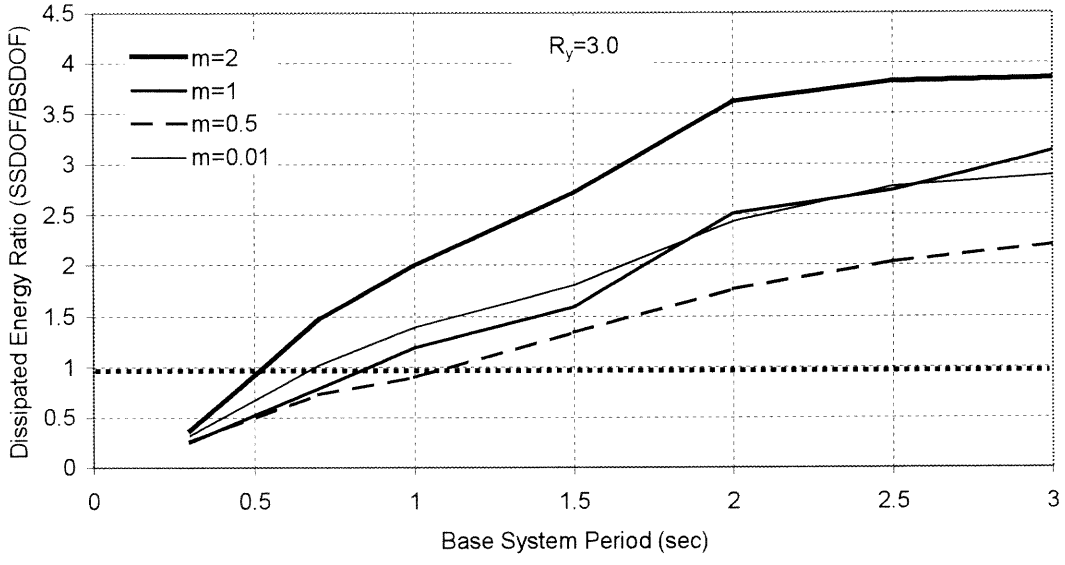

Figure A.43 Effect of **m** on the Dissipated Hysteretic Energy Response of S-SDOF Systems with Ry Factor of 3

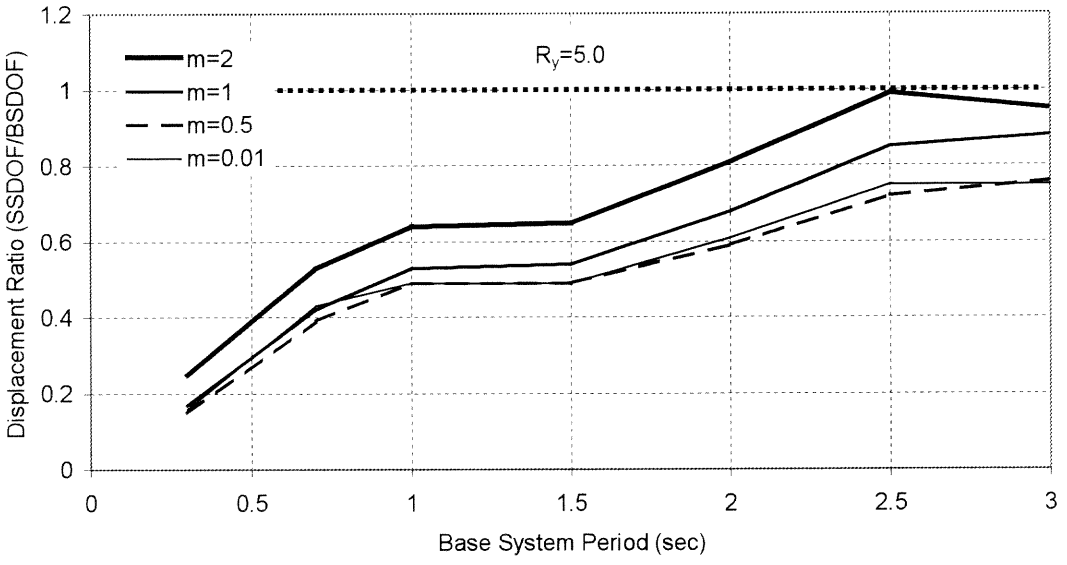

Figure A.44 Effect of **m** on the Displacement Response of S-SDOF Systems with Ry Factor of 5

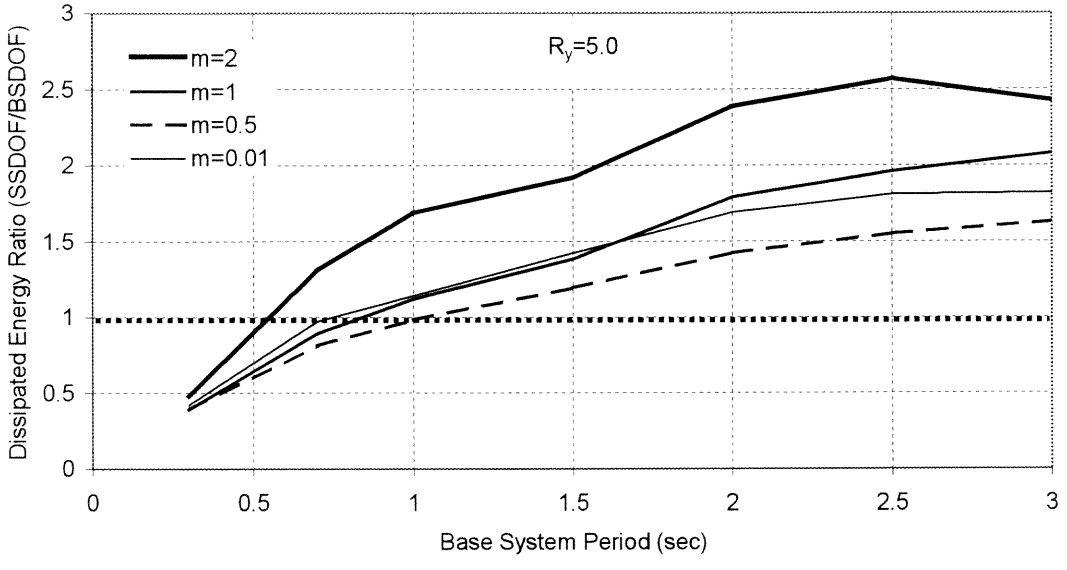

Figure A.45 Effect of **m** on the Dissipated Hysteretic Energy Response of S-SDOF Systems with Ry Factor of 5

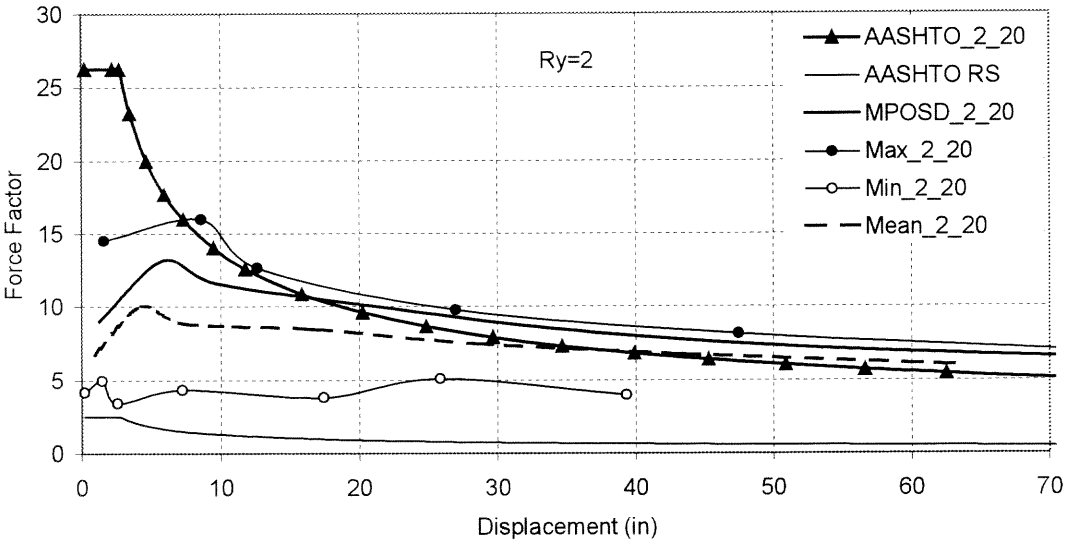

Figure A.46 S-SDOF Response Spectra for Ry=2 and β=20

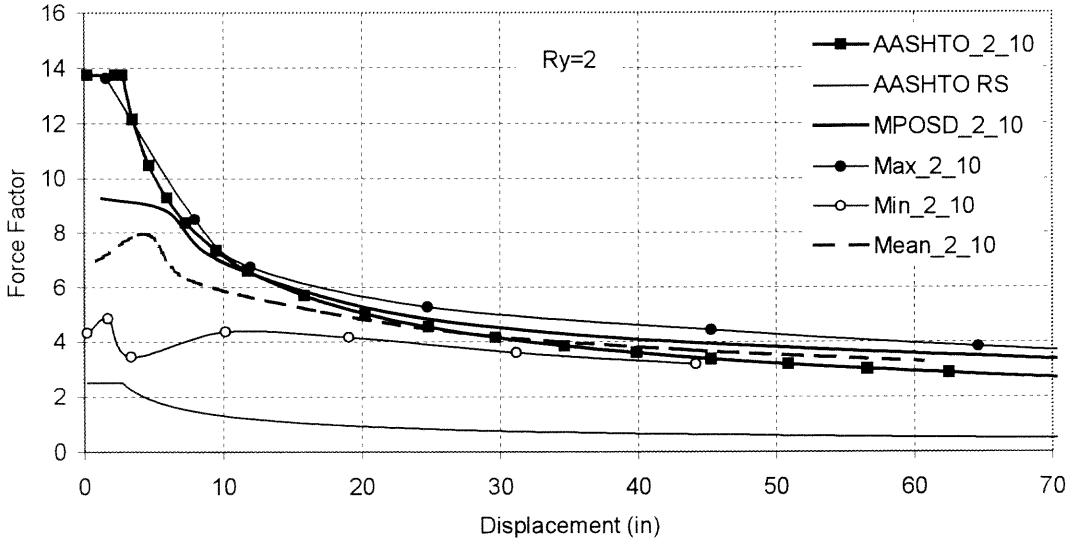

Figure A.47 S-SDOF Response Spectra for Ry=2 and β=10

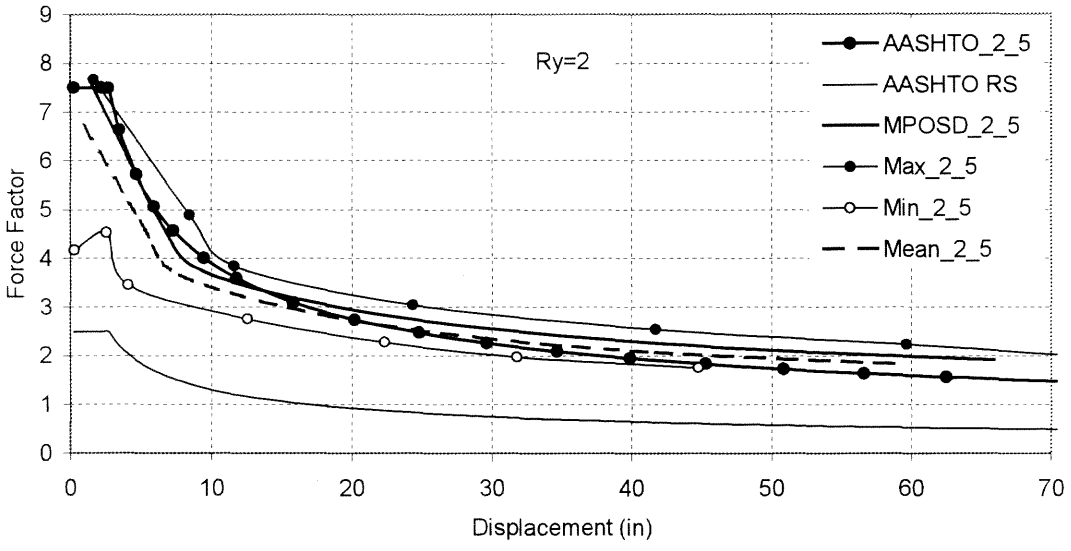

Figure A.48 S-SDOF Response Spectra for Ry=2 and β=5

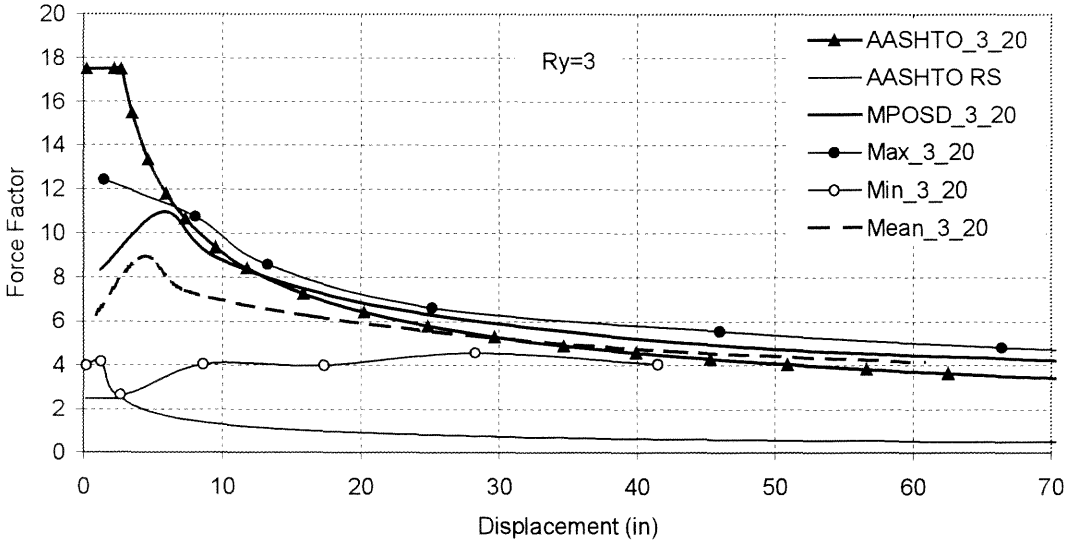

Figure A.49 S-SDOF Response Spectra for Ry=3 and β=20

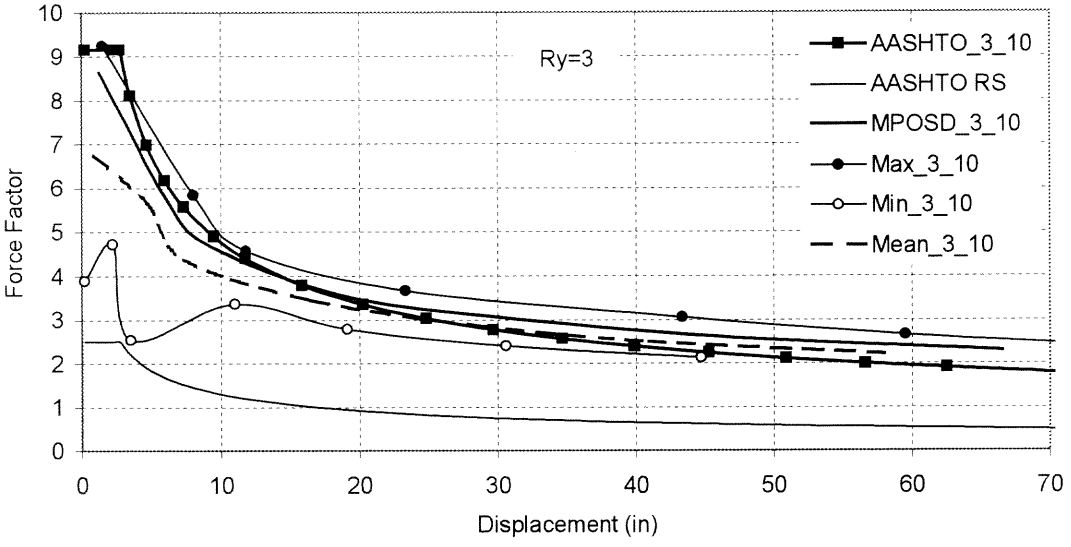

Figure A.50 S-SDOF Response Spectra for Ry=3 and β=10

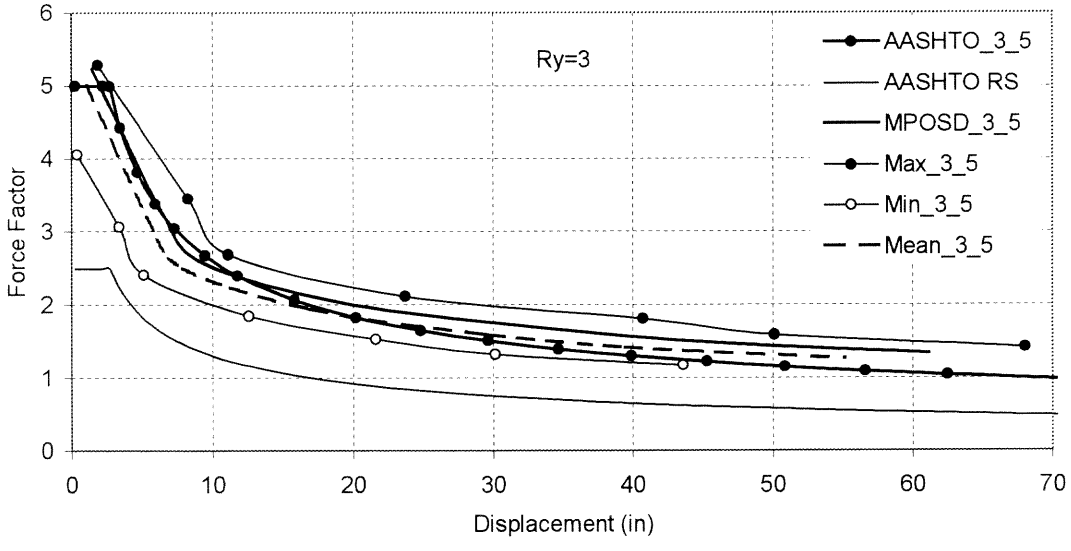

Figure A.51 S-SDOF Response Spectra for Ry=3 and β=5

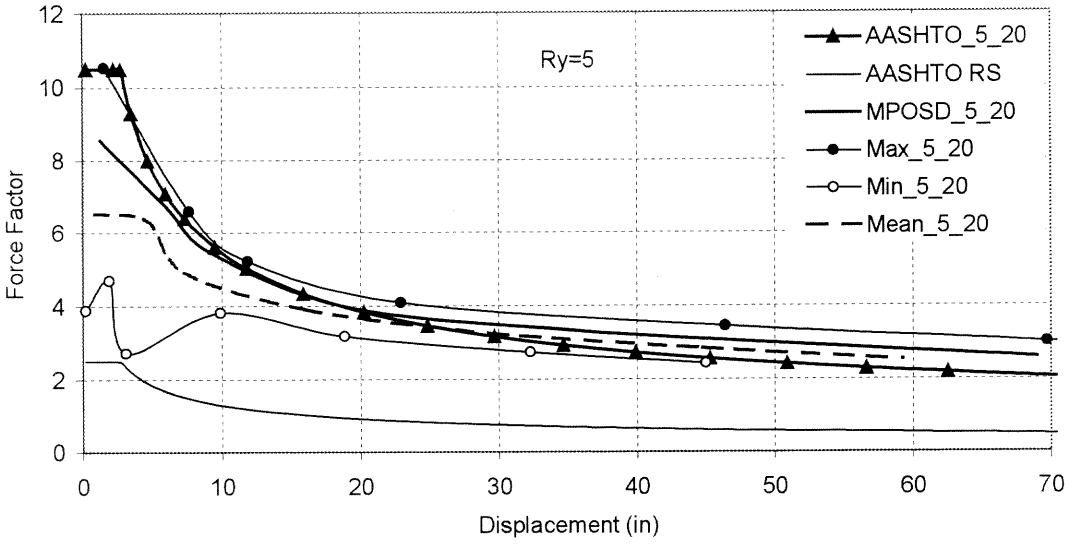

Figure A.52 S-SDOF Response Spectra for Ry=5 and β=20

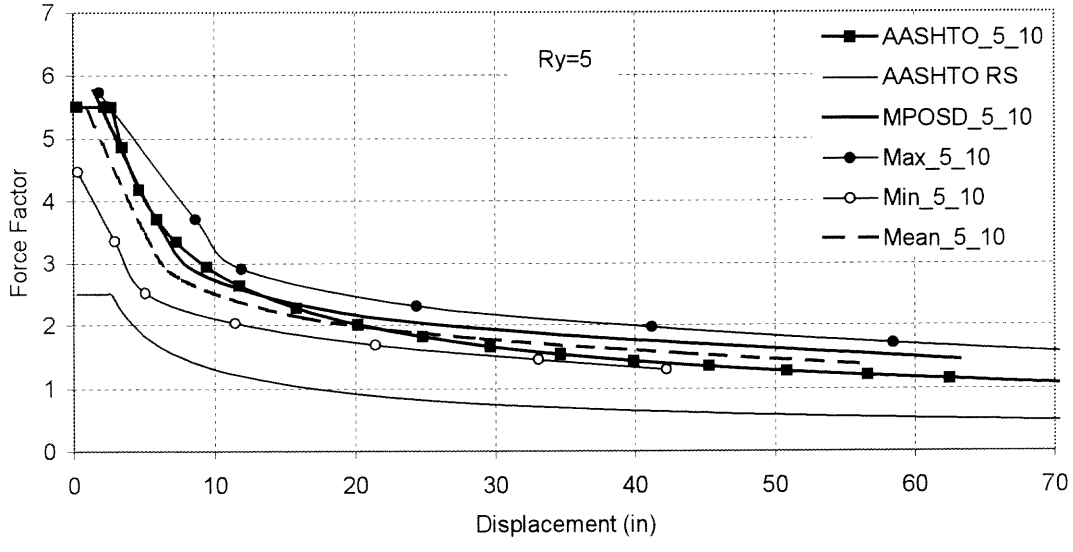

Figure A.53 S-SDOF Response Spectra for Ry=5 and β=10

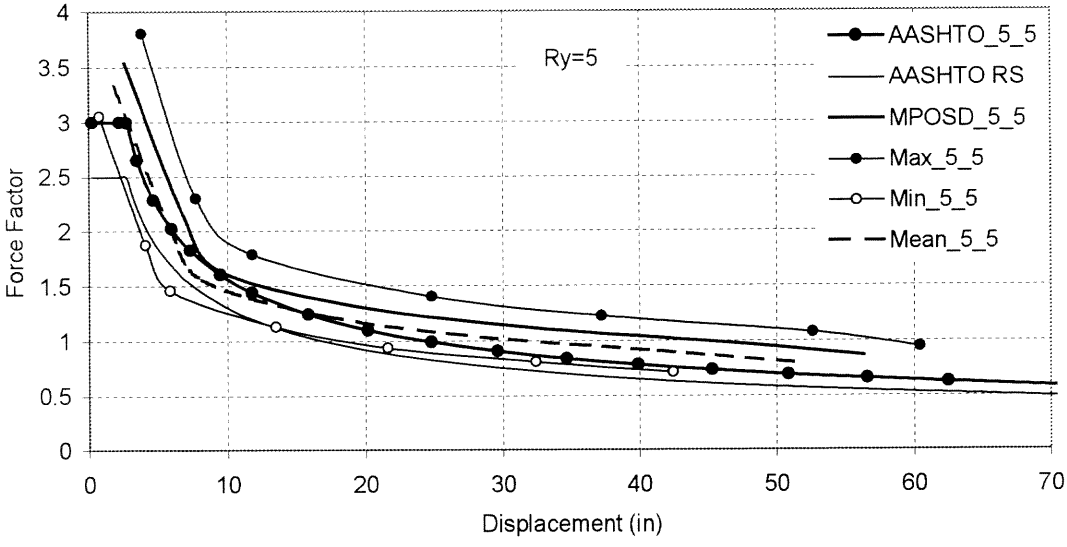

Figure A.54 S-SDOF Response Spectra for Ry=5 and β=5

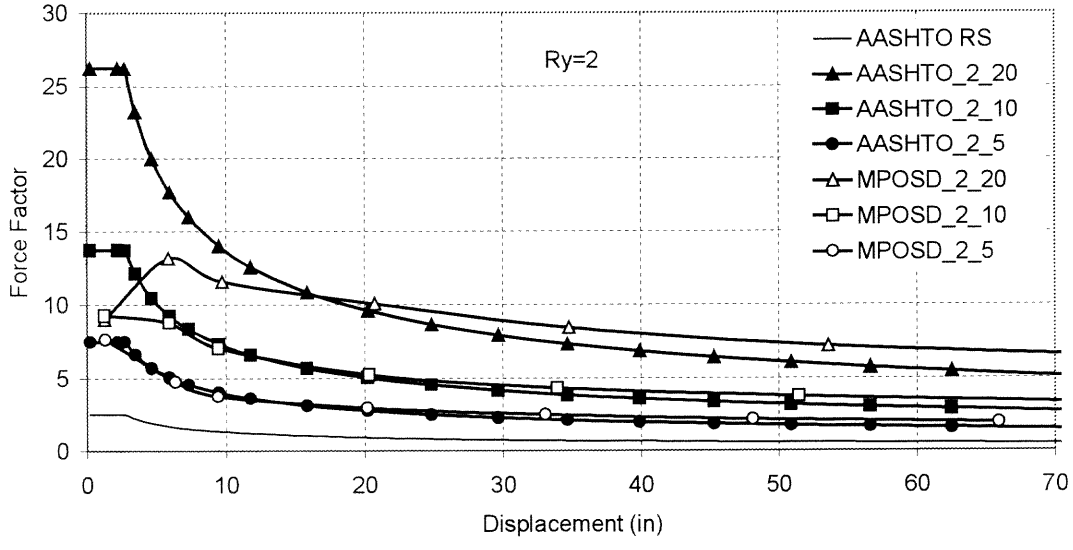

Figure A.55 Design S-SDOF Response Spectra for Ry=2; MPOSD and ASRS

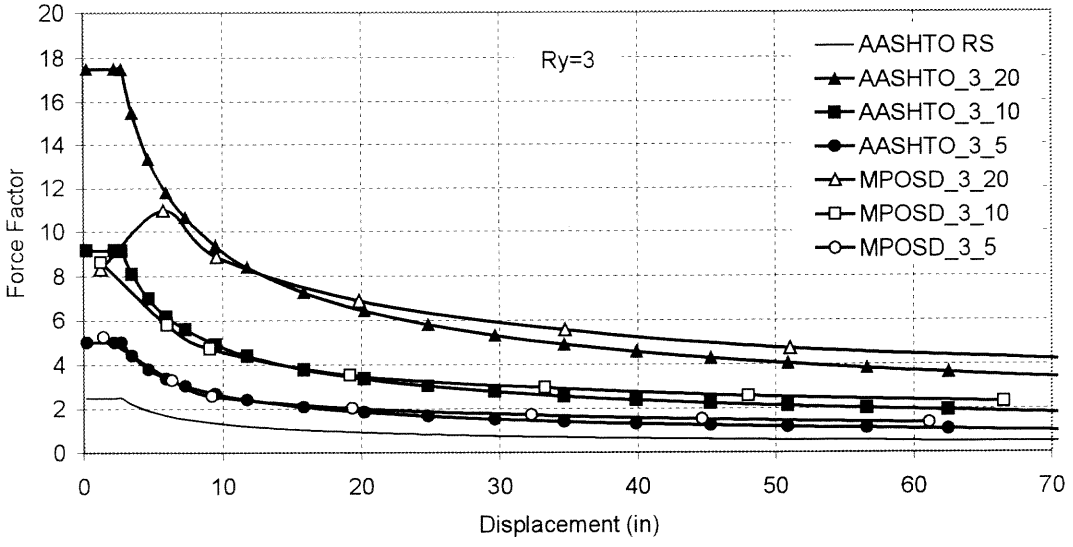

Figure A.56 Design S-SDOF Response Spectra for Ry=3; MPOSD and ASRS

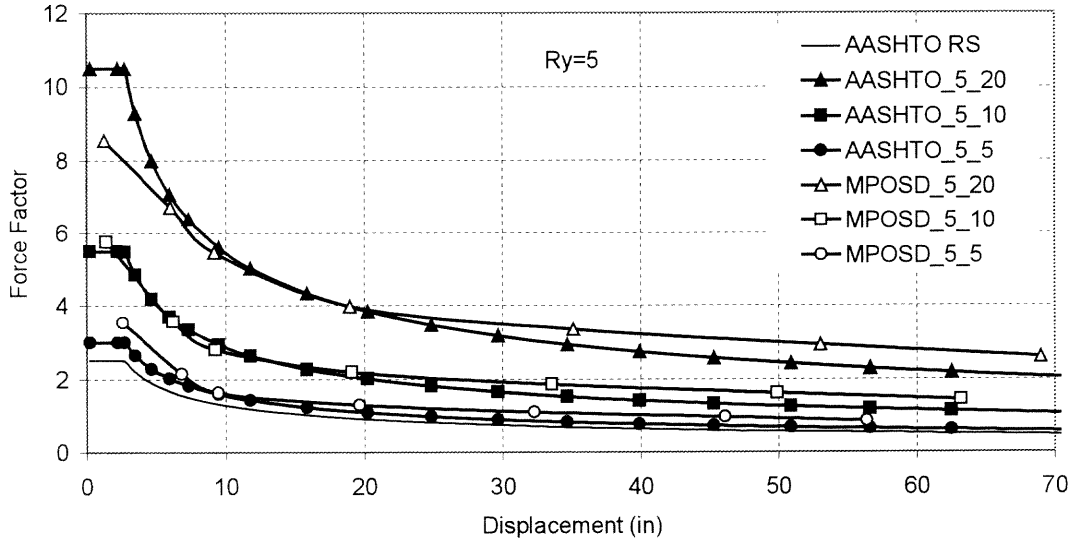

Figure A.57 Design S-SDOF Response Spectra for Ry=5; MPOSD and ASRS

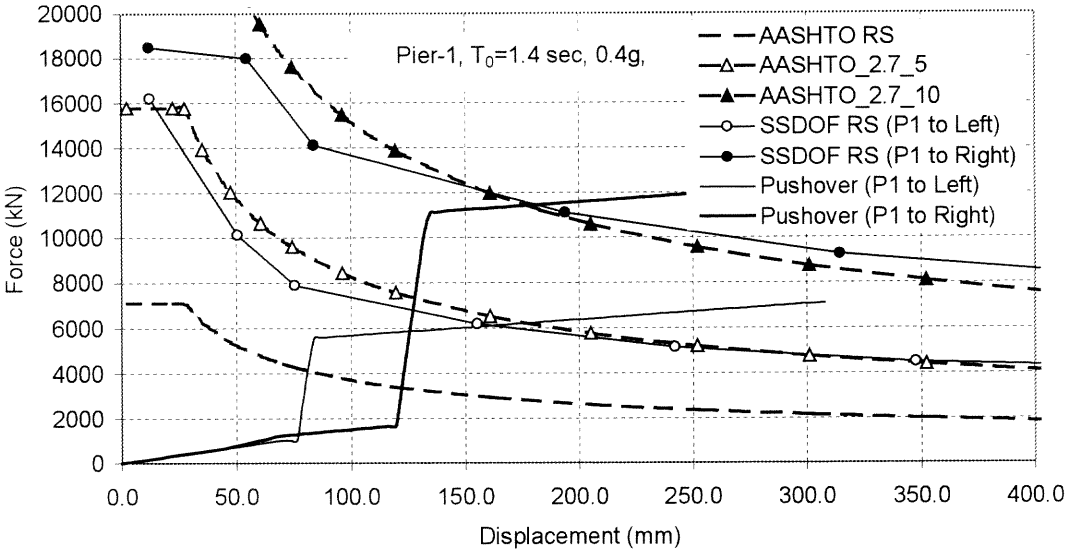

Figure A.58 Pushover Analysis for Pier-1 in Bridge #1 (PGA of 0.4g)

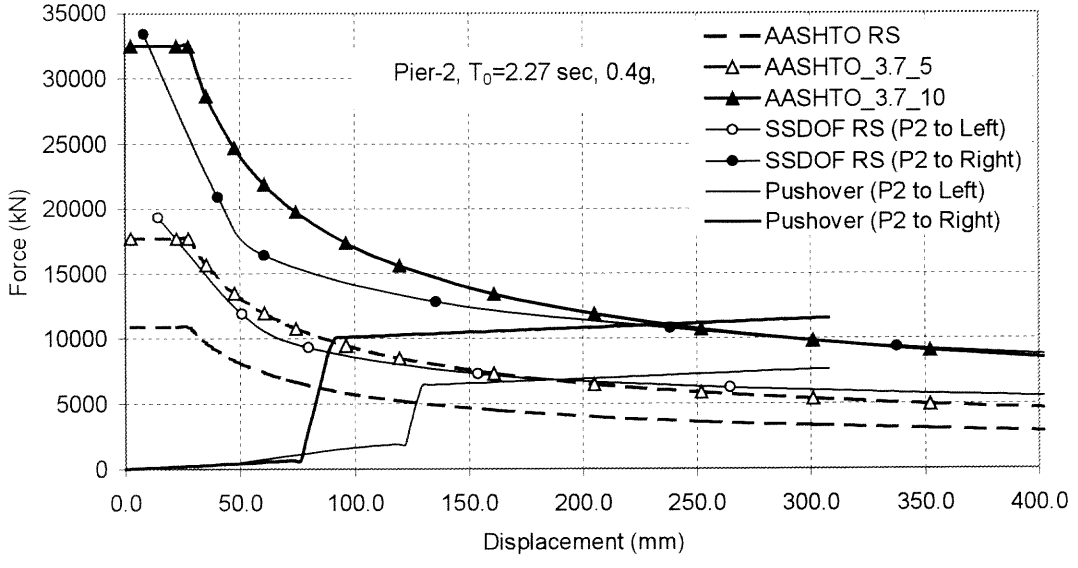

Figure A.59 Pushover Analysis for Pier-2 in Bridge #1 (PGA of 0.4g)

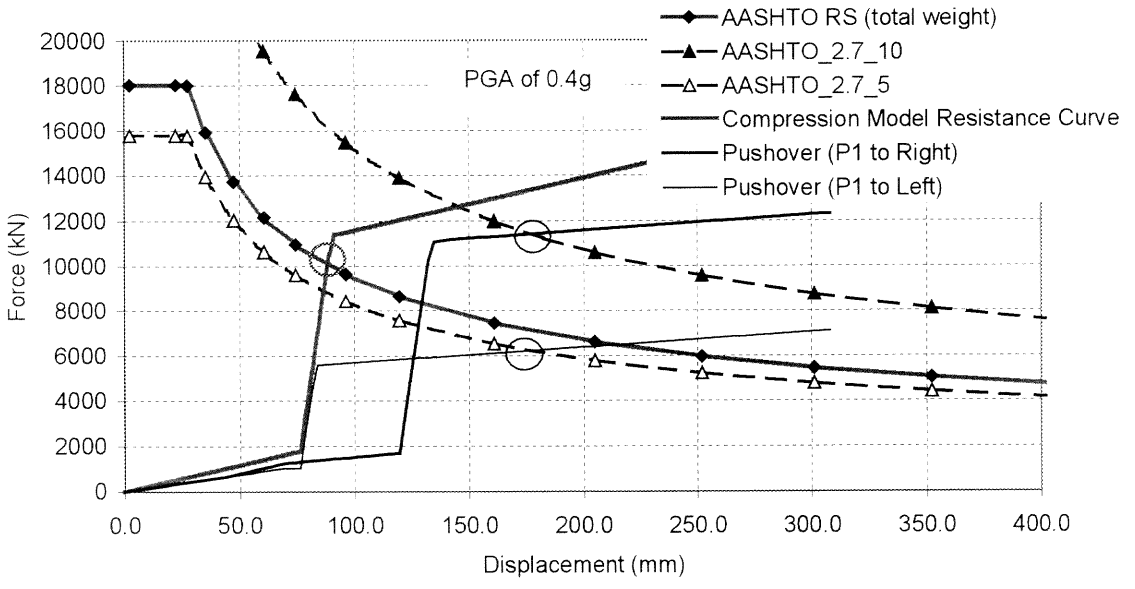

Figure A.60 Comparison of the AASHTO/FHWA Compression Model Solution to the Proposed Method (Pier-1 in Bridge #1, PGA of 0.4g)

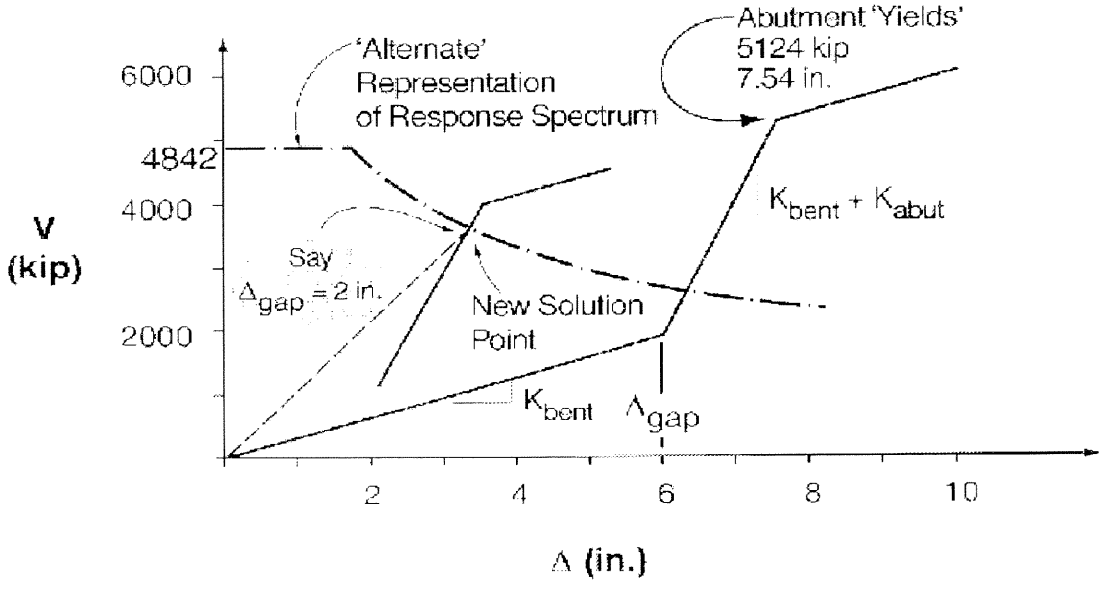

Figure A.61 Direct Solution for the Compression Model (FHWA Practice Problem 1 [1996], PGA of 0.4g)

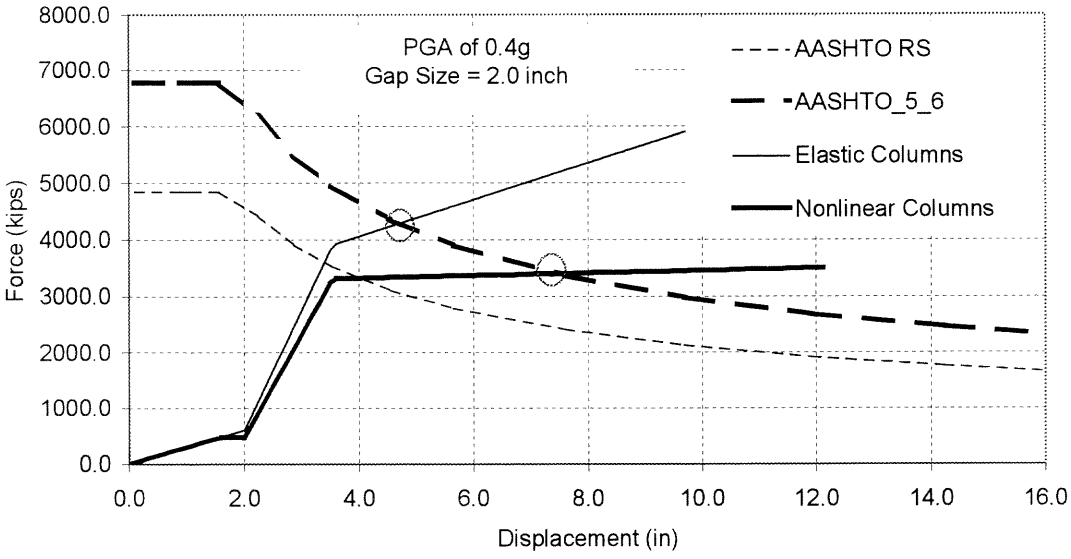

Figure A.62 Comparison of the AASHTO/FHWA Compression Model Solution to the Proposed Method (FHWA Practice Problem 1 [1996], PGA of 0.4g)

REFERENCES

Applied Technology Council, "Seismic Evaluation and Retrofit of Concrete Buildings," Report ATC-40, November 1996.

AASHTO, AASHTO LRFD Bridge Design Specifications, 2st Edition, Washington, D.C., 1998

AASHTO, AASHTO Standard Specifications for Highway Bridges, 16th Edition, Washington, D.C., 1996

Bejar, L.A. de, and K. Ganapathi, "A Note on Inelastic Response Spectra for Systems with Bilinear Spring Force and Kinematic Strain-Hardening," Earthquake Spectra, Vol. 8, No. 2, 1992.

CALTRANS, Bridge Design Aids 14-1, California Department of Transportation, Sacramento, CA, October 1989.

Chai, Y. H., K. M. Romstad, and S. M. Bird, "Energy-Based Linear Damage Model for High-Intensity Seismic Loading," Journal of Structural Engineering, Vol. 121, No. 5, pp. 857-864, May 1995

Chen, Ma-Chi, and J. Penzien, "Analytical Investigations of Seismic Response of Short, Single, or Multiple-Span Highway Bridges," Earthquake Engineering Research Center, College of Engineering, University of California, Berkeley, California, Report No. EERC 75-4, January 1975.

Chopra, Anil K., and Rakesh K. Goel, "Direct Displacement-Based Design: Use of Inelastic vs. Elastic Design Spectra," Earthquake Spectra, Vol. 17, No. 1, February 2001.

Chopra, Anil K., and Rakesh K. Goel, "Capacity-Demand-Diagram Methods for Estimating Seismic Deformation of Buildings," Earthquake Spectra, Vol. 15, No. 4, pp 637-656, November 1999.

Dicleli, Murat, and Michel Bruneau, "An Energy Approach to Sliding of Single-Span Simply Supported Slab-on-Girder Steel Highway Bridges With Damaged Bearings," Earthquake Engineering and Structural Dynamics, Volume 24, 1995

Dicleli, Murat, and Michel Bruneau, "Seismic Performance of Multispan Simply Supported Slab-on-Girder Steel Highway Bridges," Engineering Structures, Volume 17, Number 1, 1995

Federal Emergency Management Agency, "Evaluation of Earthquake Damaged Concrete and Masonary Wall Buildings: Basic Procedures Manual," FEMA 306, May 1999.

Federal Emergency Management Agency, "NEHRP Guidelines for the Seismic Rehabilitation of Buildings," FEMA 273; and NEHRP Commentary on the Guidelines for the Seismic Rehabilitation of Buildings, FEMA 274, Washington, D.C., October 1997

Federal Highway Administration, "Seismic Design of Highway Bridge Foundations Vol. II: Design Procedures and Guidelines," Report No. FHWA/RD-86/102, June 1986.

Federal Highway Administration, "Seismic Retrofitting Manual for Highway Bridges," Publication No. FHWA-RD-94-052, May 1995.

Federal Highway Administration, "Seismic Bridge Design Applications," Part Two, Publication No. FHWA-SA-97-018, July 1996.

Goel, Rakesh K., and A. K. Chopra, "Evaluation of Bridge Abutment Capacity and Stiffness during Earthquakes," Earthquake Spectra, Volume 13, No. 1, pp. 1-23, February 1997.

Hose, Yael D., P. Silva, and F. Seible, Performance Library of Concrete Bridge Components, Sub-Assemblages, and Systems Under Simulated Seismic Loads, Sstructural Systems Research Program, SSRP 99/08, University of California, San Diego, La Jolla, January 1999.

Kim, Sang-Hyo, Sang-Woo Lee, and Ho-Seong Mha, "Dynamic Behaviors of the bridge considering pounding and friction effects under seismic excitations," Structural Engineering and Mechanics, Vol. 10, No. 6, 2000

Kowalsky, M. J., Direct displacement-based design: a seismic design methodology and its application to concrete bridges, Dissertation submitted in partial satisfaction of the requirements in Structural Engineering, University of California, San Diego, La Jolla, 427 pp., 1997

Krawinkler, H., "New Trends in Seismic Design Methodology," 10th European conference on earthquake engineering, Rotterdam, 2, pp 821-830, 1995.

Mander, J. B., F. D. Panthaki, and M. T. Chaudhary, "Evaluation of Seismic Vulnerability of Highway Bridges in the Eastern United States," Proceedings of Lifeline Earthquake Engineering in the Central and Eastern US, ASCE National Convention in New York, September 1992.

Maragakis, Emmanuel, Bruce Douglas, and Spiros Vrontinos, "Classical Formulation of the Impact Between Bridge Deck and Abutments During Strong Earthquakes," 6th Canadian Conference on Earthquake Engineering, Toronto, 1991.

Maragakis, Emmanuel, Raj Siddharthan, and Greg Thornton, "Nonlinear Interaction Models for the Evaluation on the Response of Bridge Structures," Proceedings on Ninth World Conference on Earthquake Engineering, Vol VI, Tokyo-Kyoto, Japan, August 2-9, 1988.

Maroney, B., B. Kutter, K. Romstad, Y. H. Chai, and E. Vanderbilt, "Interpretation of large scale bridge abutment test results," Proceedings of 3rd Annual Seismic Research Workshop, California Department of transportation, Sacramento, Calif., 1994.

Martinez-Rueda, and Juan Enrique, "Scaling Procedure for Natural Accelerograms Based on a System of Spectrum Intensity Scales," Earthquake Spectra, Vol. 14, No. 1, pp. 135-152, February 1998.

Mast, Robert, L. Marsh, C. Spry, S. Johnson, R. Griebenow, J. Guarre, and W. Wilson, "Seismic Bridge Design Applications, Part 2", Federal Highway Administration, Report No. FHWA-SA-97-018, July 1996.

McCabe, S. L., and W. J. Hall, "Assessment of Seismic Structural Damage," Journal of Structural Engineering, Vol. 115, No. 9, p 2166-2183, September 1989.

Pantelides, C. P., and X. Ma, "Linear and Nonlinear Pounding of Structural Systems," Computers & Structures Vol. 66, No. 1, pp 79-92, 1998

Powell, G. H., and S. Campbell, "DRAIN-3DX Element Description and User Guide," Report No. UCB/SEMM-94/08, Dept. of Civil Engineering., Univ. of California, Berkeley, CA, Dec 1994.

Priestly, M. J. N., F. Seible, and G. M. Calvi, Seismic Design and Retrofit of Bridges, First edition, John Wiley & Sons, Inc., New York, 686 pp, 1996.

Prakash, V., G. H. Powell, D. D. Campbell, and F. C. Filippou, "DRAIN-2DX Preliminary Element User Guide," Dept. of Civil Engineering, University of California at Berkeley, CA, Dec. 1992.

Saadeghvaziri, M. Ala, and A. Yazdani Motlagh, "Nonlinear Response of MSSS Bridges under Earthquake Ground Motions: Case Studies," Report No. FHWA/NJ-99-026-7270, Federal Highway Administration, October 1999.

Saadeghvaziri, M. Ala, A. R. Yazdani-Motlagh, and S. Rashidi, "Effects of Soil-Structure Interaction on Longitudinal Seismic Response of MSSS Bridges," Soil Dynamics and Earthquake Engineering, Vol. 20, Issue 1-4, December 1999.

Saadeghvaziri, M. Ala, and S. Rashidi, "Seismic Retrofit and Design Issues for Bridges in New Jersey," Transportation Research Records, No. 1594, November 1997.

Saadeghvaziri, M. Ala, and S. Rashidi, "Effect of Steel Bearings on Seismic Response of Bridges in Eastern United States," Proceedings Of the 6th US National Conf. On Earthquake Engineering, Seattle, 1998.

Shome, N., C. A. Cornell, P. Bazzurro, and J. E. Carballo, "Earthquakes, Records, and Nonlinear Responses," Earthquake Spectra, Vol. 14, No. 3, pp. 469-500, August 1998.

SEAOC, Appendix B: conceptual framework for performance-based seismic design, Vision 2000, Structural Engineers Association of California, 393-416, 1996.

Tseng, W. S., and J. Penzien, "Analytical Investigations of the Seismic Response of Long Multiple-Span Highway Bridges," Earthquake Engineering Research Center, College of Engineering, University of California, Berkeley, California, Report No. EERC 73-12, 1973.

University of California, San Diego, The UCSD/PEER Performance Library for Concrete Bridge Components, Sub-Assemblages, and Systems under Simulated Seismic Loads, http://www.structures.ucsd.edu/PEER/Capacity_Catalog/Capacity_Catalog.html, 1999.

Veletsos, A. S., and N. M. Newmark, "Effect of Inelastic Behavior on the Response of Simple System to Earthquake Motion", Proc. 2nd World Conf. On Earthquake Engineering, pp 895-912, 1960.

Wilson, J., and B. S. Tan, "Bridge Abutments: Formulation of Simple Model for Earthquake Response Analysis," Journal of Engineering. Mech., ASCE, Vol. 116, No. 8, August 1990.

Yazdani Motlagh, A., M. Ala Saadeghvaziri, "Nonlinear Seismic Response of Stiffening SDOF Systems," Engineering Structures, The Journal of Earthquake, Wind and Ocean engineering, Vol. 23, No. 10, Oct. 2001

Zahra, T. F., W. J. Hall, "Seismic Energy Absorption in Simple Structures," Report No. UILU-ENG-82-2011, University of Illinois at Urbana-Champaign, Urbana, Illinois, July 1982.

Zimmerman, R. M., and R. D. Brittain, "Seismic Response of Multi-Simple Span Highway Bridges," Proceedings of the 3rd Canadian Conf. on Earthquake Engineering, Montreal, 1979.